2007-03-21

Rectification of 2-D to 3-D Finite Element Analysis in Buried Concrete Arches Under Discrete Loading

Adam D. Aagard
Brigham Young University - Provo

RECTIFICATION OF 2-D TO 3-D FINITE ELEMENT ANALYSIS OF BURIED CONCRETE ARCHES UNDER DISCRETE LOADING

by

Adam D. Aagard

A thesis submitted to the faculty of

Brigham Young University

in partial fulfillment of the requirements for the degree of

Master of Science

Department of Civil and Environmental Engineering

Brigham Young University

April 2007

BRIGHAM YOUNG UNIVERSITY

GRADUATE COMMITTEE APPROVAL

of a thesis submitted by

Adam D. Aagard

This thesis has been read by each member of the following graduate committee and by majority vote has been found to be satisfactory.

Date	Kyle M. Rollins, Chair
Date	Richard J. Balling
Date	Fernando S. Fonseca

BRIGHAM YOUNG UNIVERSITY

As chair of the candidate's graduate committee, I have read the thesis of Adam D. Aagard in its final form and have found that (1) its format, citations, and bibliographical style are consistent and acceptable and fulfill university and department style requirements; (2) its illustrative materials including figures, tables, and charts are in place; and (3) the final manuscript is satisfactory to the graduate committee and is ready for submission to the university library.

Date

Kyle M. Rollins
Chair, Graduate Committee

Accepted for the Department

Steven E. Benzley
Department Chair

Accepted for the College

Alan R. Parkinson
Dean, Ira A. Fulton
College of Engineering and Technology

ABSTRACT

RECTIFICATION OF 2-D TO 3-D FINITE ELEMENT ANALYSIS OF BURIED CONCRETE ARCHES UNDER DISCRETE LOADING

Adam D. Aagard

Department of Civil and Environmental Engineering

Master of Science

Construction of tunnels and small- to medium-span bridges is a $12 billion per year industry in the United States, with a significant portion going into buried arch structures. Notwithstanding such expenditure, modern arch design and construction, in many cases, is highly conservative. This is because the closed-form solutions used by most designers today do not correctly account for soil-structure interaction. In fact, soil-structure interaction makes a closed form solution impossible. With the advent of high power computers in recent years, some designers have turned to finite element (FE) modeling as the main vehicle of analysis. Such numerical procedures provide an accurate approximation of physical behavior. Practices using FE analysis for buried arch design almost exclusively use two-dimensional models because they are faster to set up and analyze than three-dimensional models and cost substantially less. However, 2-D models fail to account for the stiffness of the structure and spread of discrete loads in the third-

dimension. Both the 1996 and 1998 AASHTO-LRFD Bridge Design Specifications address this problem, providing methods of load reduction. Much of the current reduction, however, is based on research done on concrete bridge decks, and does not account for continuous elastic support or the geometry of the structure. This results in a conservative analysis at low fill covers (<10') and/or increasing spans (>20').

This research provides a method to rectify the discrepancy that arises in discrete loading of 2-D FE models of semi-flexible buried concrete arch bridge, culvert, and tunnel systems due to the plane-strain assumption. Rectification is accomplished by providing a correlation between the deflection of a beam-on-elastic-foundation analysis and a distribution length by which the load in 2-D analysis is reduced. Distribution lengths are derived using bending energy ratios. The correlation considers structural geometry, overburden height, and base soil stiffness. Reduction of the 2-D design load by the proposed distribution length results in shear forces and bending moments nearly equivalent to those obtained from 3-D analysis in the plane of discrete load application transverse to the structure. Less conservative results are also obtained for axial forces. These results are intended for use on structures that are four times the span in length, or longer.

ACKNOWLEDGMENTS

I would like to thank the following individuals and entities: Jason South, for his expertise in the field of buried arches and his devising this thesis topic and providing suggestions and input into this research; Kyle Rollins, for his encouragement and well educated suggestions; Engineering System Solutions, for funding, supplementary data collection, and a drive to continue improving the field; Hydro-Arch, Inc., for funding this work and substantiating design.

TABLE OF CONTENTS

LIST OF TABLES ..... **ix**

LIST OF FIGURES ..... **xi**

1 Introduction **1**

2 History of Analysis, Design, and Construction **3**

2.1 Early Arch History 3

2.2 Modern Arch History 10

2.3 Arches Today 17

3 Design Theory and Tools **21**

3.1 Simplified Equations 21

3.2 Finite Element (FE) Analysis 23

4 Current Analysis Methods and Limitations **27**

4.1 A Brief Explanation of Design Procedure Using FE Analysis 30

4.2 AASHTO Code Allowances 31

5 Research Methods and Results **35**

5.1 3-D Finite Element Analysis 36

5.2 Determination of Distribution Length 43

5.3 Beam-on-Elastic-Foundation (BOEF) Analysis 54

5.4 BOEF and FE Analysis Correlations 57

5.5 Example of Obtaining Distribution Length Using BOEF Analysis 74

6 Conclusions and Recommendations **79**

6.1 Implementation of Results 80
6.2 Recommendations for Future Studies 81
References 83
Appendix A. Moment Dissipation and Magnitude Differences 85
Appendix B. Effects of Fill Height on AASHTO Conservatism 89
Appendix C. Conservatism of AASHTO Provisions 95
Appendix D. Critical Deflection Ratios 97
Appendix E. Conservatism of Prediction Equations 103
Appendix F. Under-Prediction of Axial Forces 107
Appendix G. Design Examples Using Current and Proposed Methods 111

LIST OF TABLES

Table 5-1 – Outline of arch model section properties used in FE analyses 39

Table 5-2 – Summary of HL-93 loading applied above the arch crown at mid-length 42

Table 5-3 – Distribution lengths from the bending energy method and AASHTO provisions 51

Table 5-4 – Representative arch model values used in BOEF analyses 55

Table 5-5 – Critical deflection ratios for BOEF models 60

Table 5-6 – Critical deflection ratios obtained from prediction equations 62

Table 5-7 – Average variation of data from prediction model 63

Table 5-8 – Distribution lengths predicted by recommended method 66

Table 5-9 – Example BOEF deflection values and deflection ratios 75

Table 5-10 – Example interpolation values for determining distribution lengths 76

Table 5-11 – Conservatism of distribution length values for example arch 77

Table 6-1 – Recommended use of distribution lengths for load reduction 81

Table G-1 – Summary of design requirements using current and proposed methods 111

LIST OF FIGURES

Figure 2-1 – Common arch types are a) semicircular, b) segmental, and c) elliptical 4

Figure 2-2 – Arch terminology 5

Figure 2-3 – The Pont du Gard in Nimes, France 6

Figure 2-4 – The Anji Bridge in the Hebei Province of China 7

Figure 2-5 – The Sounding Arch Bridge in Maidenhead, England 7

Figure 2-6 – A sewer tunnel in Paris, France 8

Figure 2-7 – a) arches and pendentives in Notre Dame de Paris and b) a dome on arches with pendentives 9

Figure 2-8 – A 1926 Luten bridge in Washington County, Arkansas 11

Figure 2-9 – Soil mobilization caused by structural deformations 14

Figure 2-10 – Load redistribution through soil arching 15

Figure 2-11 – Force transfer through interface friction 16

Figure 2-12 – A Hydro-Arch bridge in Las Vegas, Nevada 18

Figure 3-1 – Typical arch a) bending moment and b) shear and c) axial force diagrams obtained from FE analysis in the loading plane 24

Figure 4-1 – 18’ span arch and plate models used for comparison of moment dissipation and magnitude at mid-span as a function of longitude 28

Figure 4-2 – Percent of maximum moment at the crown/mid-span as a function of longitude for an 18' span arch ring with one foot of fill and a similar plate with no fill 28

Figure 4-3 – Moment magnitude at the crown/mid-span as a function of longitude for an 18' span arch ring with one foot of fill and a similar plate with no fill 29

Figure 4-4 – Load distribution by a) soil spread and b) structure spread 32

Figure 4-5 – Comparison of 2-D and 3-D moment results in the plane of loading for an 18' span arch ring with one foot of fill 33

Figure 4-6 – Comparison of 2-D and 3-D moment results in the plane of loading for an 18' span arch invert with one foot of fill 34

Figure 5-1 – Spatial representation of arch models used in this research 36

Figure 5-2 – Arch models used in Plaxis: a) 6’ Model, b) 11’ Model, c) 13’ Model, and d) 18’ Model 37

Figure 5-3 – Arch models used in Plaxis: a) 24’ Model, b) 26’ Model, c) 34’ Model, and d) 35’ Model 38

Figure 5-4 – 36’ span arch model used in Plaxis 39

Figure 5-5 – Properties used for soil models in FE analyses 40

Figure 5-6 – 2-D and 3-D finite element models for an 11’ span arch with three feet of fill 41

Figure 5-7 – Elastic-perfectly plastic behavior of a Mohr-Coulomb soil model 43

Figure 5-8 – Effect of fill height on percent of total strain energy by type for an 18' span arch ring 44

Figure 5-9 – Load magnitudes resulting in equivalent structural forces for a) 2-D, b) continuous, and c) discrete loads in the plane of loading 45

Figure 5-10 – Illustration of equivalent positive bending energy volumes 46

Figure 5-11 – Length-to-span ratio effects on distribution length for an 11' span arch with three feet of fill 49

Figure 5-12 – Sample bending energy method calculations for an 11’ span arch with one foot of fill 50

Figure 5-13 – Conservatism of AASHTO computed distribution lengths for positive moment for varying fill covers as a function of span 52

Figure 5-14 – Conservatism of AASHTO computed distribution lengths for positive moment for varying spans as a function of fill cover 52

Figure 5-15 – Conservatism of AASHTO computed distribution lengths for invert moment for varying fill covers as a function of span 53

Figure 5-16 – Conservatism of AASHTO computed distribution lengths for invert moment for varying spans as a function of fill cover 53

Figure 5-17 – Similarities between buried arch and beam-on-elastic-foundation models 55

Figure 5-18 – Comparison of BOEF and FE analysis deflections at the ring/invert connection point for an 18' span model with three feet of fill 57

Figure 5-19 – Deflection ratios for 24’ span BOEF and FE models with three feet of fill 58

Figure 5-20 – Critical deflection ratios for positive moment distribution length for 24’ span BOEF and FE models as a function of fill height 59

Figure 5-21 – Critical deflection ratios for positive moment distribution lengths for BOEF models as a function of fill height 60

Figure 5-22 – Conservatism of predicted to actual distribution lengths for positive moment as a function of fill height 65

Figure 5-23 – Conservatism of predicted to actual distribution lengths for positive moment as a function of span 65

Figure 5-24 – Bending moment comparison for an 18' span arch ring with three feet of fill using various reduction methods 67

Figure 5-25 – Shear force comparison for an 18' span arch ring with three feet of fill using various reduction methods 67

Figure 5-26 – Axial force comparison for an 18' span arch ring with three feet of fill using various reduction methods 68

Figure 5-27 – Effects of axial force on moment capacity 69

Figure 5-28 – Axial force comparison for an 18' span arch ring with ten feet of fill using proposed distribution length for positive moment and 3-D FE analysis 71

Figure 5-29 – Axial force as a function of 2-D/continuous load magnitude for an 18' span arch ring with three feet of fill 71

Figure 5-30 - Bending moment comparison for an 18' span invert with three feet of fill using various reduction methods 72

Figure 5-31 – Shear force comparison for an 18' span invert with three feet of fill using various reduction methods 73

Figure 5-32 – Axial force comparison for an 18' span invert with three feet of fill using various reduction methods 74

Figure A-1 – Percent of maximum moment at the crown/mid-span as a function of longitude for an 11' span arch ring with one foot of fill and a similar plate with no fill....86

Figure A-2 – Percent of maximum moment at the crown/mid-span as a function of longitude for a 24' span arch ring with one foot of fill and a similar plate with no fill....86

Figure A-3 – Moment magnitude at the crown/mid-span as a function of longitude for an 11' span arch ring with one foot of fill and a similar plate with no fill....87

Figure A-4 – Moment magnitude at the crown/mid-span as a function of longitude for a 24' span arch ring with one foot of fill and a similar plate with no fill....87

Figure B-1 – Comparison of 2-D and 3-D moment results in the plane of loading for an 18' span arch ring with two feet of fill....90

Figure B-2 – Comparison of 2-D and 3-D moment results in the plane of loading for an 18' span arch ring with three feet of fill....90

Figure B-3 – Comparison of 2-D and 3-D moment results in the plane of loading for an 18' span arch ring with five feet of fill....91

Figure B-4 – Comparison of 2-D and 3-D moment results in the plane of loading an 18' span arch ring with ten feet of fill....91

Figure B-5 – Comparison of 2-D and 3-D moment results in the plane of loading for an 18' span arch invert with two feet of fill....92

Figure B-6 – Comparison of 2-D and 3-D moment results in the plane of loading for an 18' span arch invert with three feet of fill....92

Figure B-7 – Comparison of 2-D and 3-D moment results in the plane of loading for an 18' span arch invert with five feet of fill....93

Figure B-8 – Comparison of 2-D and 3-D moment results in the plane of loading for an 18' span arch invert with ten feet of fill....93

Figure C-1 – Conservatism of AASHTO computed distribution lengths for negative moment for varying fill covers as a function of span....96

Figure C-2 – Conservatism of AASHTO computed distribution lengths for negative moment for varying spans as a function of fill cover....96

Figure D-1 – Deflection ratios for 24’ span BOEF and FE models with one foot of fill....98

Figure D-2 – Deflection ratios for 24’ span BOEF and FE models with two feet of fill....98

Figure D-3 – Deflection ratios for 24’ span BOEF and FE models with five feet of fill....99

Figure D-4 – Deflection ratios for 24’ span BOEF and FE models with ten feet of fill....99

Figure D-5 – Critical deflection ratios for positive moment distribution lengths for 11’ span BOEF and FE models as a function of fill height....100

Figure D-6 – Critical deflection ratios for positive moment distribution lengths for 18’ span BOEF and FE models as a function of fill height....100

Figure D-7 – Critical deflection ratios for negative moment distribution lengths for 18’ span BOEF and FE models as a function of fill height....101

Figure D-8 – Critical deflection ratios for invert moment distribution lengths for 18’ span BOEF and FE models as a function of fill height....101

Figure D-9 – Critical deflection ratios for negative moment distribution lengths for BOEF models....102

Figure D-10 – Critical deflection ratios for invert moment distribution lengths for BOEF models....102

Figure E-1 – Conservatism of predicted to actual distribution length for negative moment as a function of fill height....104

Figure E-2 – Conservatism of predicted to actual distribution length for invert moment as a function of fill height....104

Figure E-3 – Conservatism of predicted to actual distribution length for negative moment as a function of span....105

Figure E-4 – Conservatism of predicted to actual distribution length for invert moment as a function of span....105

Figure F-1 – Axial force comparison for an 18' span arch ring with one foot of fill using proposed distribution length for positive moment and 3-D FE analysis....107

Figure F-2 – Axial force comparison for an 18' span arch ring with two feet of fill using proposed distribution length for positive moment and 3-D FE analysis....108

Figure F-3 – Axial force comparison for an 18' span arch ring with three feet of fill using proposed distribution length for positive moment and 3-D FE analysis....108

Figure F-4 – Axial force comparison for an 18' span arch ring with five feet of fill using proposed distribution length for positive moment and 3-D FE analysis....109

1 Introduction

The objective of this research is to provide a method by which point loads can be transformed to effective line loads for two-dimensional finite element analysis of buried concrete arches. Currently there are several methods available to analyze buried concrete arches. These include: empirical or simplified closed-form equations and two- and three-dimensional finite element analysis. Engineers will often choose to use the finite element (FE) method over other available tools because it provides the most accurate results. Discrete loading is inherently a three-dimensional problem; yet, two-dimensional modeling is typically done, because it is cheaper, much faster, and requires less user input than three-dimensional modeling. However, due to the assumptions made in developing its mathematical base, 2-D model space fails to capture the true behavior of a system under discrete loading, such as wheel loads. For example, longitudinal stiffness and longitudinal load dissipation are not accounted for, leading to a more compliant structure and higher load concentrations than actually exist.

Design codes, such as the AASHTO-LRFD Bridge Design Specifications, allow for reductions in the load's magnitude to account for these limitations. However, much of the research supporting these reductions is based on tests performed on concrete bridge decks, which are not affected by soil-structure interaction and do not have significant geometric variation. In the cases of low fill height or larger span, using these reductions

in 2-D analysis still results in design forces that are substantially greater than they are in a real 3-D situation. In this research, a method is developed to accurately account for the effects of longitudinal stiffness, geometric variation, and discrete loading in a 2-D finite element model. Using this method in 2-D FE analysis of buried arches results in structural forces that are nearly equivalent to those produced in a 3-D FE model under discrete loading. Further, this research develops a correlation with beam-on-elastic-foundation (BOEF) analysis to predict this reduction factor, known as the distribution length, and prescribes a procedure of implementation. This research is specifically developed for structures that are four times the span in length, or longer.

Currently there is very little research with this specific aim, necessitating its further development. Included in the literature reviewed by the Author are the following two studies attempting to determine distribution lengths for buried structures:

- Simpson Grumpertz & Heger, Inc. (2001) suggests that the distribution length, l, for buried concrete arches should be $l = 1.15H + 3.33ft$, where H is the depth of fill cover in ft. This recommendation does not account for variations in geometry or continuous elastic support and was not the main purpose of the research.
- McGrath, *et al*. (2005) have done research on distribution lengths for box culverts, essentially concluding that the 1996 AASHTO provisions are correct. This study did not include determination of distribution lengths for buried concrete arches, but suggested they be developed.

2 History of Analysis, Design, and Construction

For more than two millennia, arches have been an important and ubiquitous structural form in buildings, tunnels, and bridges. Notwithstanding their antiquity, in many applications their governing mechanics are can be very complex and difficult to quantify analytically, even with today's advances in mathematics and structural analysis. A shift to rigorous mathematical design requirements at both a state and federal level, initiated in the Bureau of Public Roads, lead to a period in the early twentieth century where there was substantial resistance to the use of arches because of the lack of practical analytical solutions. Only recently, with increasing computational power and finite element (FE) analysis, has arch construction been on the rise. This research will focus on semi-flexible small- to medium-span soil-structure arch bridge, culvert, and tunnel systems and the internal forces caused by discrete loads (vehicle or otherwise).

2.1 Early Arch History

An arch behaves much like a catenary, or hanging cable. Because the cable is unable to resist bending moments it takes a form that will result purely in tensile forces under an applied load. An efficient arch follows the same principle; inverting this shape to result in pure compression. Unreinforced masonry and concrete are very weak in tension, and therefore, are able to withstand only minimal bending moments under

loading. A well designed arch will be shaped such that the majority of the force is carried by compressive forces in the arch ring.

To minimize the tensile forces in an arch ring due to bending, it must have a relatively low span-to-rise ratio; on the order of 5:1, or less. This low ratio ensures that the ring will act like a strut rather than a beam (*i.e*. resist forces through axial, rather than bending forces). Three common shapes are used to achieve this ratio: semicircular, segmental, and elliptical (see Figure 2-1).

Figure 2-1 – Common arch types are a) semicircular, b) segmental, and c) elliptical

Arches consist of up to three main components: the ring, invert or abutments, and the spandrel (see Figure 2-2). The ring, or barrel, is the arch part of the arch. Most old arch rings are composed of stone or brick segments called voussoirs, while newer models are composed of reinforced, prestressed, or post-tensioned concrete. The ring serves as the main force-resisting element of the structure. Arches are supported either by abutments at both ends of the ring or an invert connecting both ends together. Because the ring has a tendency to flatten under loading, the abutments or invert must support large horizontal forces, called thrust, as well as vertical forces. The magnitude of these horizontal forces varies depending on the geometry of the ring. Thrust is greatest in segmental shapes and least in semicircular. In the case of an invert, considerable amounts of tension and flexure develop under loading. The structure is raised to grade by

the spandrel, which can be composed entirely of stone, masonry, or concrete or it may consist of two or more walls in-filled with soil. The spandrel and fill add significantly to the overall strength of a structure.

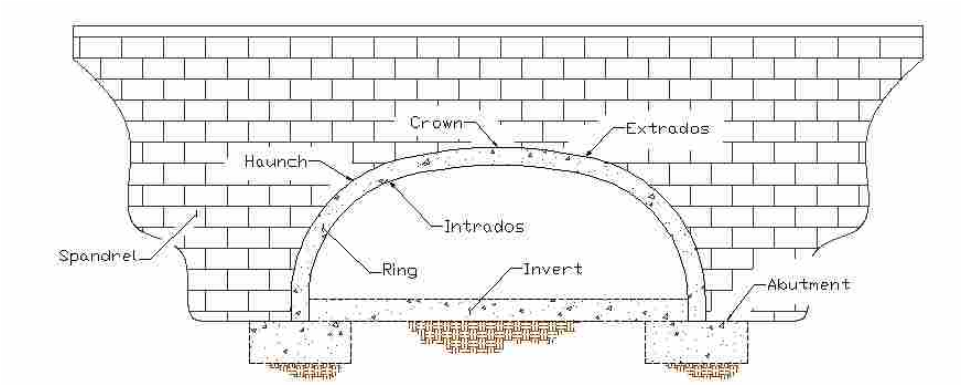

Figure 2-2 – Arch terminology

Some of the most famous historic structural sites in the world are, in full or in part, renowned because of their use of the arch. In fact, most owe their very longevity to the fact that they were built using arches.

The Romans were famous for their usage of arches in construction. The Pont du Gard, in Nimes, is one of the most frequented tourist stops in France (see Figure 2-3). The exact date of construction is debated among archaeologists, but recent studies place it sometime near the middle of the first century, AD. Built by Marcus Vipsanius Agrippa, it stands as a classical example of early semicircular arch construction.

The multiple tiers of arches carry the Roman aqueduct over the Gardon River. The Pont du Gard is constructed without mortar. Instead, its voussoirs are secured together by metal clamps. In 1998 major flooding occurred on the river, causing

substantial damage to many upriver structures. This iconic structure, however, remained intact and sustained only trivial damages.

Figure 2-3 – The Pont du Gard in Nimes, France

In the case of multiple equal spans, such as the Pont du Gard, the thrust generated by each contingent arch pair cancels out. The remaining vertical component of the load is supported by piers.

A famous example of early segmental arch construction is the Anji Bridge, in the Hebei Province of China (see Figure 2-4). The Anji Bridge was built by Li Chun between the years of 595 – 610 AD. The open spandrel construction reduces the overall weight of the bridge and also allows water to flow past more easily in times of flooding. The open spandrel design was an important contribution to bridge building. Its stone voussoirs are connected together by iron dovetails which allow it to flex, rather than crack, under abutment movements. It is the oldest and most well preserved open spandrel arch bridge in the world and is still in service today.

Figure 2-4 – The Anji Bridge in the Hebei Province of China

The Sounding Arch Bridge in Maidenhead, England is one of the most laudable accomplishments of early elliptical arch construction (see Figure 2-5). This bridge is particularly inspiring because it has the largest span-to-height ratio of any masonry voussoir bridge in the world – 5.3:1. It is built of unreinforced brick, and at the time of its construction in 1838, I.K. Brunel, its designer, was heavily criticized and the structure was predicted to fail by most engineers. Contemptuously, however, it remains in heavy use as a railway bridge to this day.

Figure 2-5 – The Sounding Arch Bridge in Maidenhead, England

Arches not only serve an important role above ground, as bridges, they also are an important feature of many underground structures, such as tunnels and drainage systems. The most well known network of voussoir tunnels is that used in the Paris, France sewers.

This grandfather of sewer systems was begun in 1370 by Hugues Aubriot and was expanded sporadically for the next five centuries by various others, including Napoleon Bonaparte. Some of the sandstone arches in the tunnels take on the form of greatest efficiency for a buried structure, known as an inverted pear arch (see Figure 2-6). The exterior forces are best balanced by allowing the structure to continue to curve inward at the base. This allows the load to be transferred more completely through axial forces, significantly reducing bending moments in the structure. The 1,300 mile long system of tunnels and culverts has a "clean" service history and is still used today as Paris's primary sewer.

Figure 2-6 – A sewer tunnel in Paris, France

Arches are used in some form in many aspects of early architecture. Massive roof structures are supported by Roman and Gothic arches in early Christian churches, such as Notre Dame de Paris, begun in 1163 by Bishop Maurice de Sully and finished in 1345. Various architects and engineers oversaw construction during its lengthy erection period. At times the roof structures are even a revolved form of an arch known as a dome. A dome roof is supported on four arches which are joined together and transition into the dome by pendentives, as shown in Figure 2-7b. Hagia Sophia, in Istanbul, Turkey is such a structure. The cathedral was dedicated in 537. The dome's span-to-height ratio, however, was too large for unreinforced masonry, and shortly after, in 558, the dome collapsed during an earthquake. The replacement collapsed five years later. Again, in 989 and 1364, the dome was damaged by earthquake. The dome, as it currently stands, was built by Mimar Sinan in the early 16th century.

a)

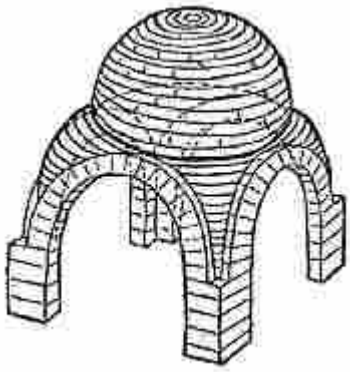

b)

Figure 2-7 – a) arches and pendentives in Notre Dame de Paris and b) a dome on arches with pendentives

The design of early arches was based upon a tried principle: experience and experimentation; there was no theoretical basis for design. These landmark structures are

testaments to their designers, and proof of the power of empiricism. In 1675 Sir Robert Hooke claimed to have come up with "a true mathematical and mechanical form of all manner of arches for building" (Miller, et. al., 2000). Other mathematicians, theorists, and scientists worked on tackling the problem of the arch for the next century, but no practical theoretical solution was achieved. Differences in opinion eventually caused practical and theoretical science to diverge. Engineering became a separate field of study from theoretical science. Schools were initiated specifically for the study of practical science and engineering. In time, each field discovered different principles to improve arch construction, yet animosity began to emerge between them.

2.2 Modern Arch History

Masonry voussoir arch construction diminished with the invention of reinforced concrete in the late 1800's. Arch structures lost their heavy Romanesque look and began to take on lighter, more graceful forms. With the ability to now resist tensile forces, and thus bending moments, through reinforcing steel, arches became flatter and more economical. Most of the early reinforced concrete bridges were very rudimentary in their use of steel. Some used I-beams and others used trusses as reinforcement. Many engineers began patenting their reinforced concrete bridge designs to try to get an edge on the market.

Daniel Luten was one of the most successful of these early engineers. His studies and experiments led to innovations that greatly reduced the amount of steel and concrete in arch bridge design (see Figure 2-8). He was so certain of the reliability of his bridges that they even came with a five year guarantee against failure. With greater economy,

guaranteed serviceability, and a patented design, Luten began to take over the small- to medium-span bridge market.

It was at this point that others began to have qualms with the patenting of design. One of the greatest opponents was Thomas MacDonald, who was, at the time, head of the Iowa State Highway Commission. MacDonald not only thought that Daniel Luten had an unfair edge on the market, but he also thought his design was unsafe, in spite of a good service record. After becoming director of the Bureau of Public Roads in 1919, and after an unsuccessful campaign against patenting, MacDonald began to require that all bridges within state or federal jurisdiction be based on theoretical design procedures (Miller, et. al., 2000).

Figure 2-8 – A 1926 Luten bridge in Washington County, Arkansas

Since the mathematics and mechanics of arches are complex, and hadn't been developed to a complete theoretical solution at that point, use of Luten and others' empirically designed arch bridges soon waned as these requirements were enforced. Soon steel girder and prestressed or precast concrete beam bridges took over the market.

By the 1930's arches were practically phased out of widespread use because of the lack of a theoretical design basis. The need for small economical bridges still existed, yet those being approved for use were not fulfilling this need as well as Luten and others' arch bridges had done.

About this same time there were imminent discoveries that would eventually reverse the devastating blow dealt to the arch industry. In 1941, two Iowa State professors, M. G. Spangler and Anson Marston, developed the Iowa, or Marston/Spangler, formula (Equation 2-1). This is a heavily theoretically based formula for the prediction of horizontal deflection in a flexible buried conduit or pipe.

$$\Delta x = \frac{KD_L W_c r^3}{EI + 0.061er^4} \qquad \textbf{(2-1)}$$

where
Δx is the horizontal diameter change in *in*,
K is a bedding constant,
D_L is a time lag factor to account for soil consolidation,
W_c is the vertical weight per unit length due to fill and factored surface loads in *lb/in*,
r is the undeformed radius of the pipe in *in,*
E is the modulus of elasticity of the pipe in *psi*,
I is the moment of inertia of the pipe wall per unit length in in^4/in, and
e is the modulus of passive soil resistance in *pci*.

The bedding constant and time lag factor are empirically determined. Note that the term EI is a measure of the pipe stiffness and er^4 is a measure of the soil resistance. In 1958 Reynold Watkins and Spangler revamped this formula and developed the equation:

$$\frac{\Delta x}{d} = \frac{KD_L P}{0.149s + 0.061E'} \qquad \textbf{(2-2)}$$

where
d is the undeformed diameter of the pipe (= $2r$) in *in*,
P is the vertical pressure on the pipe (= $0.5W_c/r$) in *psi*,

s is the pipe stiffness (= EI/r^3) in *psi*, and
E' is the modulus of soil reaction (= er) in *psi*.

which became known as the modified Iowa formula.

The use of these formulae allow designers to accurately compute the forces in a small diameter buried flexible pipe using ring compression and elastic buckling theories (introduced in the 1960's), which consider three failure modes, namely buckling, buckling and crushing, and crushing.

More recently a formula for the prediction of vertical deflection of a flexible pipe (Equation 2-3) has been developed using the same approach that Marston and Spangler used in deriving the original Iowa formula (Masada, 2000).

$$\frac{\Delta y}{d} = \frac{KP}{0.149s}\left(\frac{0.0595E'}{0.149s + 0.061E'} - 1\right) \qquad \textbf{(2-3)}$$

where
Δy is the horizontal diameter change in *in*.

The Iowa formulae provide good design tools for flexible pipes, like corrugated metal pipe (CMP), but because of the assumptions made in their development, they provide less accurate predictions for rigid structures such as reinforced concrete pipe (RCP). Most elliptical concrete buried arches fall between these two categories, as semi-flexible.

Because many arch and culvert structures are buried, the Iowa formulae became an important stepping stone in the return of arch use. Further, the development of these equations gave rise to a new engineering field known as soil-structure interaction. The complexities of soil-structure interaction systems exceed those of unburied structures many fold and do not lend themselves to a perfectly theoretical solution.

There are three main elements involved in soil-structure interaction. The first deals with the mobilization of soil due to structure deformations. As a structure deforms away from the soil some of the confinement provided by the structure is lost. As a result, the soil will have a tendency to shear along a plane inclined from horizontal at an angle of $45° + \frac{\varphi}{2}$, where φ is the friction angle of the soil in degrees. Small deformations of the structure away from the soil will result in a decrease in pressure on the structure, from the "at-rest pressure" to a level known as active pressure. However, when a structure deforms into the soil, additional resistance to movement due to the internal friction of the soil is provided, counteracting the forces causing deformation. This is known as passive pressure, and is generally an order of magnitude greater than its counterpart (see Figure 2-9). The development of these pressures is a function of deformation, and, therefore, varies along the structure. In dense sands and gravels, typical of compacted fill materials, passive pressure may require approximately ten times more movement to fully develop. Generally the active pressure has minimal consequences on the structure, but, the passive resistance provides a large amount of strength to the overall system.

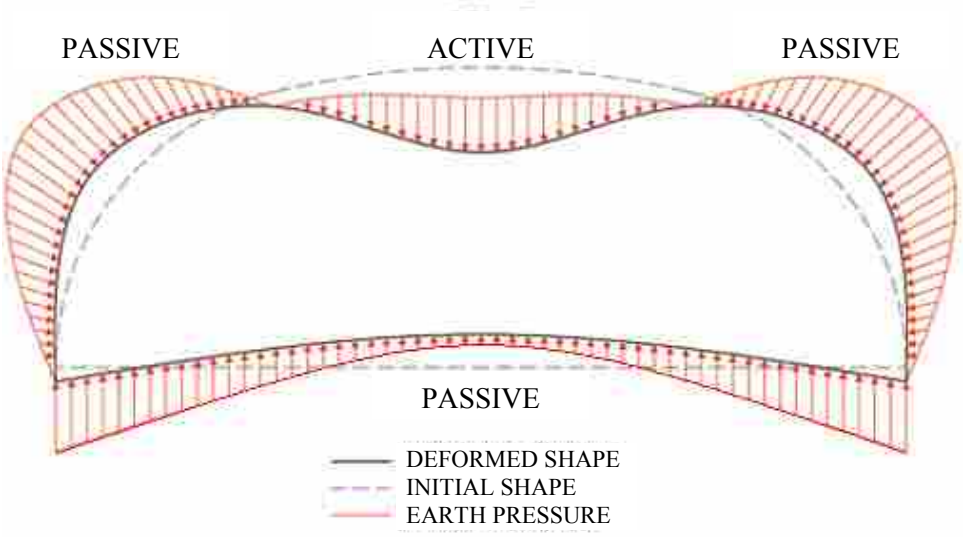

Figure 2-9 – Soil mobilization caused by structural deformations

The second element of soil-structure interaction is known as arching. Arching can be thought of as the reaction of active earth pressure. When the supporting structure under a soil layer begins to deform away from the soil, the soil begins to develop a failure wedge. This wedge is kept from slipping by support provided by the adjacent soil. The resistance provided by the adjoining soil redistributes some of the load, through shear forces, around the failure wedge. A more understandable analogy is a pin-pin beam continuously supported by an elastic base. When there is no external load applied to the beam, the dead load is equally distributed along the beam's length. Upon applying a discrete load, the beam and elastic support deflect and a portion of the force is transferred to the pins through transverse shear in the beam. At some deflection, a significant portion of the load will be redistributed to the pins. The exact amount depends on relative stiffnesses. When deformations are small, as they are in most soil-structure problems, the soil will not fail in shear; hence, a portion of the load is redistributed, or "arches" around the deformed soil through shear forces into the adjoining soil, as illustrated in Figure 2-10.

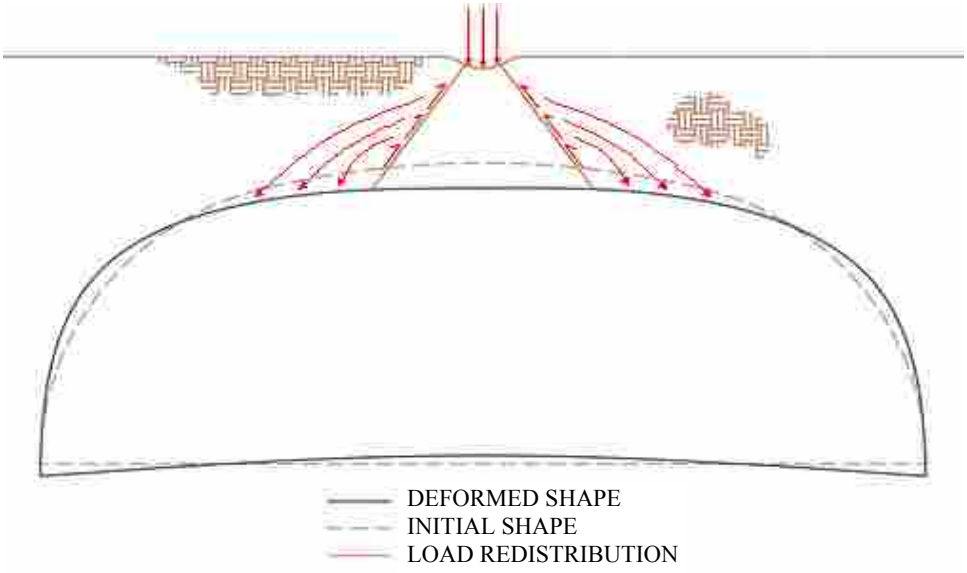

Figure 2-10 – Load redistribution through soil arching

Finally, load is transferred by interaction through interface friction. This friction is a product of normal force, surface roughness, and soil type. Slippage occurs as a result of deformation incompatibilities. In a bonded system, deformation compatibility at the interface is provided through shear forces. "Unlimited" load transfer is available between elements. In a frictionless system, deformation compatibility is not possible at the interface. No load is transferred between components through shear. Forces in bonded systems differ significantly from frictionless systems. In frictional bonds, the amount of shear transfer between elements is limited by the friction at the interface. This means that up to a stress equal to the friction capacity, the system will act like a bonded system. Once the frictional resistance has been overcome, the system will exhibit behavior of both a frictionless and bonded system. Since interface forces vary along the perimeter, the behavior of the structure varies also. Figure 2-11 illustrates the frictional shear forces acting on the structure due to soil deformation and structure settlement and deformation.

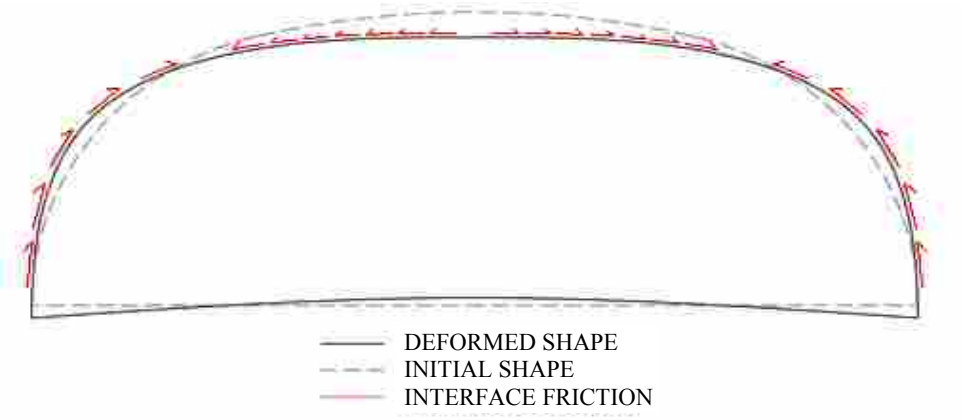

Figure 2-11 – Force transfer through interface friction

In the 70's, Mike Katona, of Notre Dame University, pioneered the first finite element program to tackle the complex problem of soil-structure interaction. The final

product was released in 1976 as CAnDe 2-D (Culvert Analysis and Design), and proved to be a godsend to designers of buried structures, despite its cryptic functionality. Since the release of CAnDe 2-D, other two-dimensional FE programs have been released, such as NLSSIP and Plaxis, that deal with the same sort of problems.

Today, Plaxis 3-D Tunnel provides one the most robust and accurate three-dimensional finite element programs for analysis of tunnel structures. Development of Plaxis began in 1987 at the Delft University of Technology in the Netherlands, as an initiative of the Dutch Ministry of Public Works and Water Management, to analyze river embankments in Holland. It was later expanded to include most geotechnical applications. In 2001, Plaxis 3-D Tunnel was released and has since provided analyses for various tunnel projects around the world.

Many researchers and practitioners are currently involved in the continual development and betterment of the art and science of soil-structure interaction and arch technology. Transportation organizations and design firms now invest millions each year in this field of research, with the end goal of finally capturing the understanding that eluded scientists, mathematicians, and designers for so long. In ancient times arches were erected as monuments of triumph. Again we find ourselves standing at this threshold.

2.3 Arches Today

The main uses of buried arches today are as drainage systems, small bridges, storage facilities, and tunnels. Arch shapes, in general, take an elliptical form because height restrictions limit the use of semicircles and segmental shapes are inefficient.

With the advent of CAnDe, and the engineering help of Mike Katona, in 1983, Bill Lockwood began CON/SPAN, Inc. Over the next few years, CON/SPAN developed a precast arch system that began the buried arch revolution. Since its inception, CON/SPAN has provided arches for more than 4,000 projects, in North, Central, and South America, the Caribbean Islands, and Asia. CON/SPAN holds patents on many of its design technologies and anxiously participates in the expansion of the industry.

In 1988, just five years after CON/SPAN educed the arch market, Wolf Michelson began Hydro-Arch, in Henderson, NV. Hydro-Arch specializes in cast-in-place concrete arches (see Figure 2-12), primarily for use in drainage systems, tunnels, small bridges, and storage facilities. The majority of their business is in the Nevada/Southern California region. They have created an efficient construction process that rivals CON/SPAN in economy and reliability. In spite of a proven service record, substantial resistance has still arisen in approval of buried arches for use in many projects. Hydro-Arch has played an important role in gaining greater acceptance of its own and similar products, as well as in producing a more efficient design methodology.

Figure 2-12 – A Hydro-Arch bridge in Las Vegas, Nevada

In 1994 another competitor entered the market when C.L. Ridgeway Construction Co. introduced their Con-Arch system. Several years prior, significant time was spent working with the Highway Innovative Technology Evaluation Center (HITEC) to develop safe and high-performance structures, for which they later received a patent, trademarked Con-Arch. In 2001 C.L. Ridgeway was obtained by Hunter Contracting Co., and currently operates in the Nevada/Arizona area.

Unique differences and competitive designs fuel continual growth for this industry as its products become more widely used, proven, and researched. The combined yearly revenue in concrete arch construction of these three companies alone is nearly $300 million, and all show increasing profitability.

3 Design Theory and Tools

Research and experience have provided today's designer with better tools and aids for designing buried structures. There are currently several methods available for design, each of which has its own inherent strengths and weaknesses. These include simplified empirical and analytical equations as well as two- and three-dimensional finite element analysis.

3.1 Simplified Equations

As previously outlined, all early arch structures were designed solely on past experience. The Romans had nearly perfected the arch of their day, yet they had no theoretical tools to aid them in creating an economically efficient structure. The development of theoretically based design equations for buried arches proved to be just beyond the grasp of scientists and mathematicians' until the latter half of the twentieth century. The lack of a viable analytical design procedure was enough to nearly stifle out this once dominant form. However, such an occurrence wasn't without justification. With the inability to determine the structural forces created by loading, it is impossible to determine accurate limit states for a structure. Load and resistance factor and ultimate-state design methods allow for a degree of statistical uncertainty due to variations in

loading and material properties, but uncertainty regarding the mechanics of the entire system is unacceptable by today's standard.

The use of the modified Iowa formula in conjunction with elastic buckling and ring compression theories are tools widely used today for design of small diameter CMP and RCP. It is understood that these methods result in generally conservative analyses, yet use of more sophisticated tools aren't often times justifiable. In such structures conservatism doesn't result in a large economical impact on a project, and in cases of non-conservative design, the consequences of failure are not disastrous. However, these methods are unsuitable for large diameter pipes. Conservatism results in large material waste and failure could be catastrophic. Further, non-circular structures, such as elliptical arches and boxes are outside the scope of these methods. Designers will sometimes turn to empirical methods such as the funicular polygon, middle-third rule, and/or plastic hinge method to analyze and design arches, yet it is generally wise, and often necessary in such cases, to use more exact modern analysis techniques.

Most designers today turn to closed-form solutions specified by code, such as those published by the American Association of State Highway and Transportation Officials (AASHTO), for analysis and design procedures of arches, pipes, and boxes. For example, the 1998 AASHTO-LRFD Sections 12.7, 12.10, and 12.11 outline analysis procedures for metal pipes and arches, reinforced concrete pipes, and precast and cast-in-place concrete boxes and arches, respectively. Software is commercially available that uses these procedures to aid in the analysis and design processes. BoxCAR (Box Culvert Analysis and Reinforcing design), developed by the American Concrete Pipe Association, is such an example. It is widely used to analyze and design concrete boxes.

AASHTO recognizes and addresses such influences as soil-structure interaction and load distribution (see 1998 AASHTO Sections 3.6.1.2.6, 4.6.2.1.3, and 12.11.2.2). However, in generalizing such phenomena, there is consequently a compromise of exactitude. In such cases where economy and/or safety necessitate more accurate solutions, designers will often resort to numerical procedures of analysis.

3.2 Finite Element (FE) Analysis

The behavior of materials and structures can be simulated by systems of differential equations. Each system has unique boundary conditions, and interactions between systems make their exact solution difficult in rare cases, and impossible in most. Solutions to some simple problems are available. For example, Boussinesq's solution of a point load on an elastic half-space is well known by geotechnical engineers. Timoshenko and others have published solutions to many elastic theory problems. However, these analytical solutions are normally based on idealization or simplifying assumptions, and their employment on real systems results in unrealistic solutions. When an exact solution is not possible or feasible, as is the case most of the time in buried structure analysis, it becomes convenient to use numerical methods to approximate their solution. One common way of doing this is called the finite element method.

FE analysis provides a means by which a continuum is broken into finite pieces called elements. The governing differential equations are then approximated, using numerical approaches, as a set of linear equations for each sub-domain created in this discretization process. Once the entire system has been approximated it then becomes a large set (on the order of 10^3) of independent linear equations. This method was not

feasible in practice until recently, when sufficient computing power became available to the masses for solving such large systems of equations. FE analysis can accurately capture the effects of soil-structure interaction and load spreading within its domain. From FE analysis, structural forces, such as shear and axial forces and bending moment can be obtained (see Figure 3-1), as well as soil stresses.

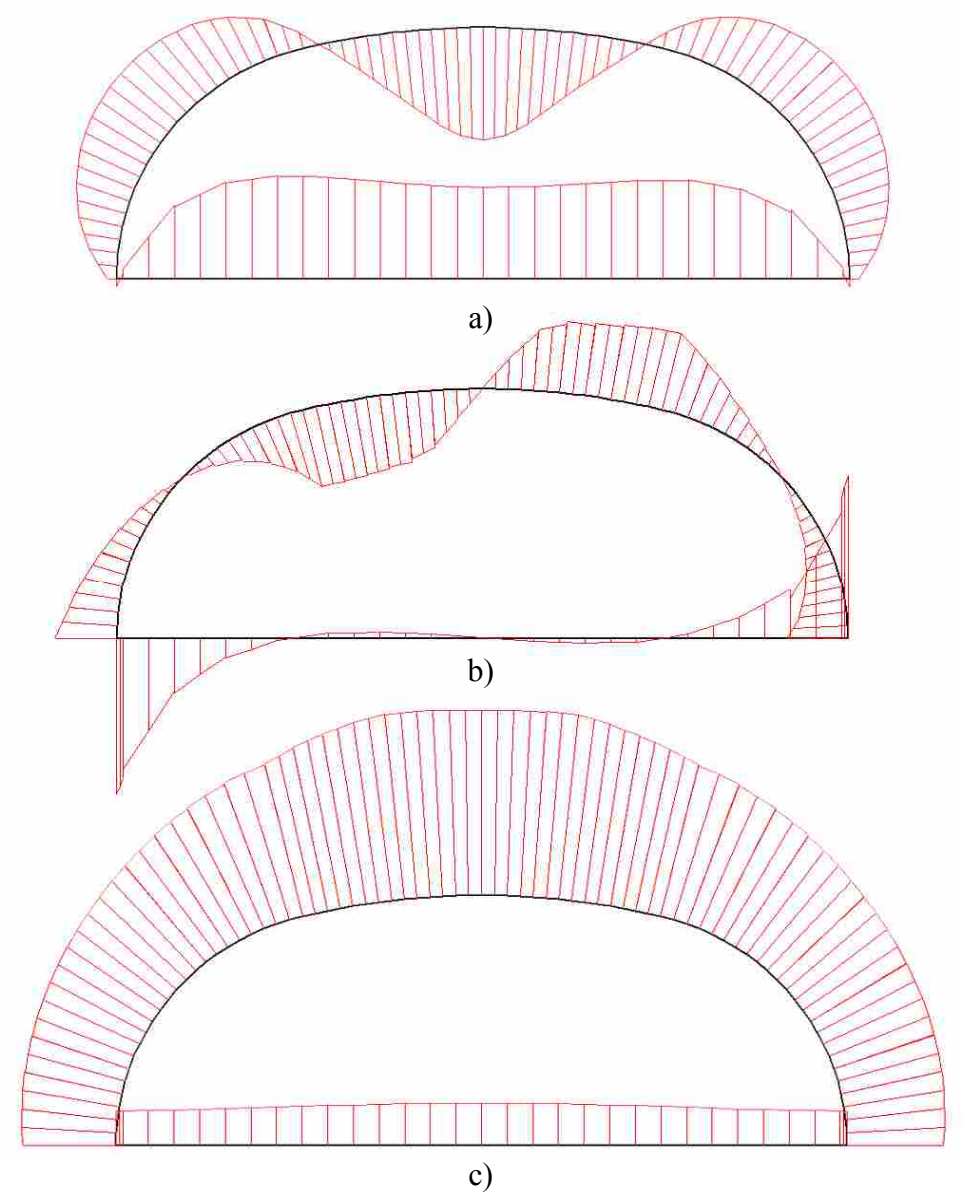

Figure 3-1 – Typical arch a) bending moment and b) shear and c) axial force diagrams obtained from FE analysis in the loading plane

Two general model spaces, or domains, are used in FE analysis: two- or three-dimensional. The 2-D method models soil using "plane-strain" elements and the structure is modeled using "beam" elements. The development of the mathematics behind these elements assumes that all strain occurs in a two-dimensional plane. Such models are convenient to use because they require less setup time, cost less, compute much faster (up to 30,000 times faster than 3-D), and are somewhat more foolproof. For cases where a structure is to be analyzed as having the same boundary conditions and geometry in the third dimension, a 2-D analysis provides accurate results. In the case of longitudinal geometric variation or discrete loading, two-dimensions fail to capture the correct behavior of the system. Again, AASHTO addresses this limitation and makes allowances for both distribution of the load through the soil and within the structure itself in the third dimension. However, as will be shown in Section 4.2, these allowances do not fully capture the benefits of such distributions, even when used in conjunction with this more exact method of analysis.

Three-dimensional FE analysis allows a user to vary geometry, loading, or both as a function of the third dimension. In this way, a model can correctly account for out-of-plane effects, as well as in-plane effects. In 3-D analysis, the soil is modeled using "volume" elements and the structure using "plate" or "shell" elements. Because of the increased complexity of the system and the reduction of simplifying assumptions within its mathematical base, three-dimensional analysis naturally requires much more computation time, but results in more accurate analysis where loading and/or geometry vary in the third dimension.

The designer must be familiar with the assumptions and limitations of whichever model space is being used, as well as have the ability to correctly model boundary conditions and material properties. The inability to do such can lead to false results.

There are many finite element programs commercially available today. Included in these are I-DEAS, Plaxis, CAnDe, ABAQUS, and Nastran. Each of these programs has a specific target user and varying degrees of user-friendliness, robustness, and capability. In order to model soil-structure problems, advanced material models and analysis methods are necessary. The conclusions of this study will be based primarily on results obtained from Plaxis 3-D Tunnel and verification and comparison provided by Plaxis V8 and I-DEAS. These programs are capable of modeling soil-structure systems. Plaxis uses nonlinear analysis for both soil and plates and I-DEAS uses linear analysis to solve the finite element systems. Studies have been done concluding that linear analysis of both soil and structure is sufficiently accurate in cases such as this, where deflections under service loading are relatively small (see Katona, 1979 and Emdal, 2000).

4 Current Analysis Methods and Limitations

Even with today's modern technology and a myriad of research supporting analysis techniques, arches with low soil cover and increasing spans are still conservatively designed. Certainly, a degree of conservatism serves as a precautionary measure, and is preferable to most designers, but when it begins to result in excessive costs, it requires further consideration. Methods specified by code can result in varying degrees of conservatism and "diseconomy". This is not the designer's fault, but rather arises because of a deficiency of research in the area of buried concrete arches. Much of the research governing the design of arches is based on concrete bridge decks and fails to produce an accurate arch analysis for three principle reasons. First, it does not account well for the load dissipation through cover soil or within the structure. Second, it does not account for varying geometries. Third, it does not account for support on an elastic medium (beam-on-elastic-foundation behavior).

The sum total of these oversights provides the potential for an over-designed structure for low fill heights and larger spans. A 3-D finite element analysis of an 18' span flat plate with no fill cover and an 18' span arch with one foot of fill cover having equal section properties were analyzed with an applied discrete load in the center. The plate model was constrained against x- and y-translation along the edges. Model properties for the arch (equal for the plate) are outlined in Section 5.1.

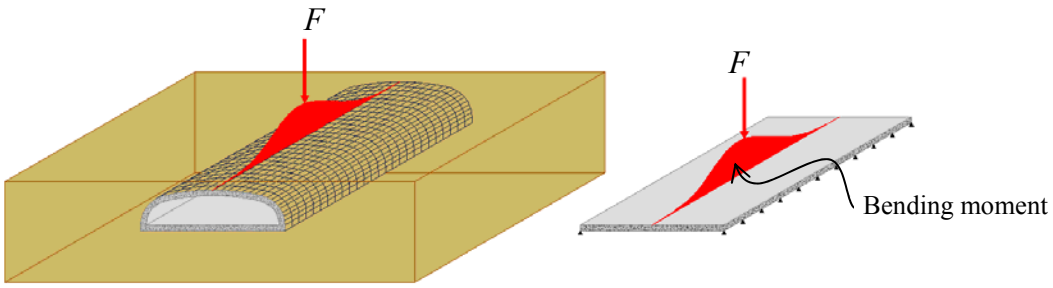

Figure 4-1 – 18' span arch and plate models used for comparison of moment dissipation and magnitude at mid-span as a function of longitude

Figure 4-2 compares the percentage of maximum moment as a function of longitudinal distance from mid-length of the model for both the plate and arch ring at mid-span (see also Figure 4-1). It can be seen that the load dissipation in both is very similar, suggesting that the angle of load spread within the structure is very similar as well (see Appendix A for additional spans). This is to be expected since an arch is effectively a curved plate. The difference arises in the magnitude of these forces.

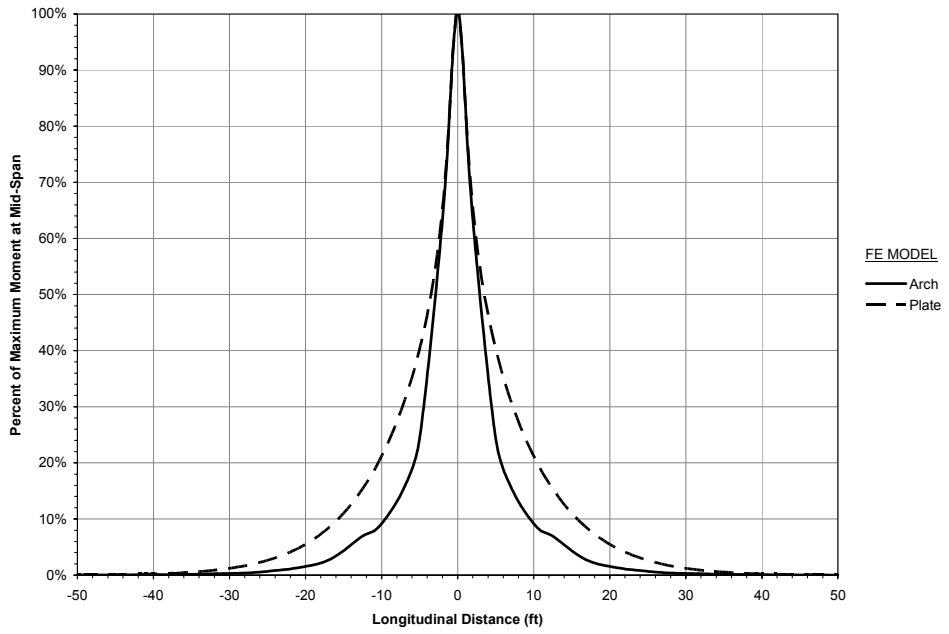

Figure 4-2 – Percent of maximum moment at the crown/mid-span as a function of longitude for an 18' span arch ring with one foot of fill and a similar plate with no fill

Figure 4-3 shows the difference in moment magnitude for this same arch/plate set. It is clearly seen from this chart that the behavior of the two structures is very different. Large amounts of energy are dissipated into the soil through soil deformation and soil-structure interaction and much of the force is carried through axial forces, rather than bending moments. Results from a two-dimensional analysis of an equivalent 18' span arch model done in Plaxis V8 using 1996 AASHTO specified reductions are also shown as a reference for current allowances. Because the model is 2-D, the computed moment remains constant with longitudinal distance (see Appendix A for additional spans).

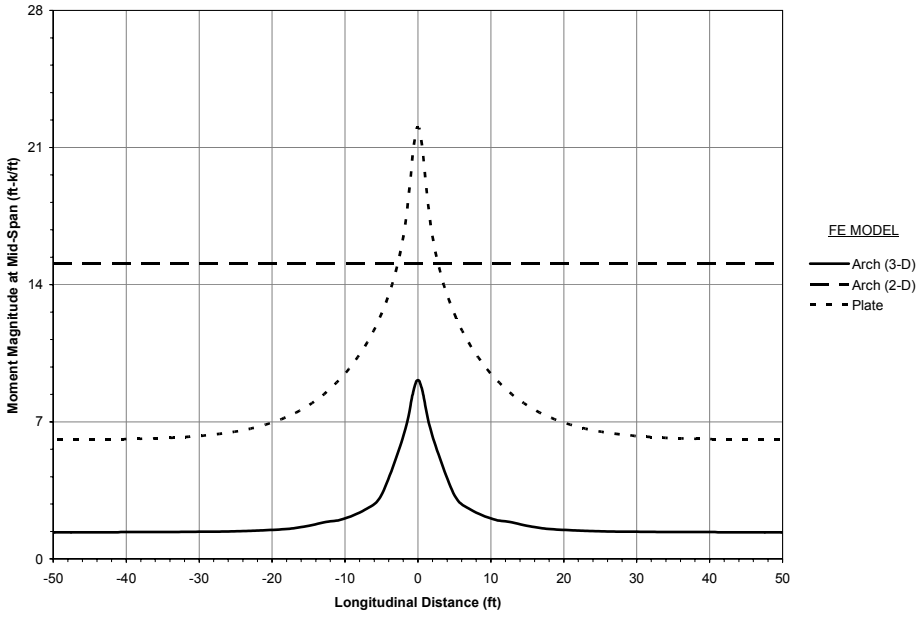

Figure 4-3 – Moment magnitude at the crown/mid-span as a function of longitude for an 18' span arch ring with one foot of fill and a similar plate with no fill

The significant discrepancy between the plate and buried arch analyses suggests, first, that the arch carries a load more efficiently than a plate, and second, that something must be done to account for the soil-structure interaction and elastic support problems

encountered with all buried arches. Further, the 2-D analysis shows that current AASHTO allowances to account for these factors can be highly conservative (this will be discussed more fully in Section 4.2).

4.1 A Brief Explanation of Design Procedure Using FE Analysis

There are several extant arch design types today, including precast, pre- and post-tensioned precast, cast-in-place, and post-tensioned cast-in-place systems. Each of these designs differs to some extent and some are proprietary. In spite of the difference in details, the general design process is similar for all. Initially, a client will specify some basic constraints for design. These constraints will include items such as hydraulic capacity, clearance, shape, and/or span. The engineer will then design an arch shape to most efficiently meet these specifications. However, there are different approaches to this step. After an arch shape is determined, the designer will create a FE model – almost always 2-D. Soil parameters are based upon the soil that will be used in the project, whether it be engineered fill, native material, or both. Section properties for the arch are assumed based on past experience and judgment. There are several options for modeling the concrete section. An uncracked section is typically unrealistic, since there is always cracking, so most designers typically use a partially cracked section, where the concrete is cracked up to the bottom of the reinforcing. The reinforcing can then be ignored completely, or a transformed section can be used. Both result in similar values. Loads are determined and applied based upon current code specifications (see '98 AASHTO Section 3). The structure is then analyzed to determine shear and axial forces as well as bending moment. Finally, deflections are checked to make sure they are tolerable.

AASHTO specifies *S/800* as a maximum deflection, where *S* is the span of the arch. Deflection rarely governs.

Once the structural forces have been determined, the section is designed using interaction diagrams for conventionally reinforced columns. These diagrams allow the designer to select the appropriate thickness and steel percentage for a one-foot strip of arch. Several computer programs are commercially available to aid in this process. Once an efficient section has been chosen, the model is checked for shear, which is rarely a concern in arch design except under high loads with low fill covers.

When an arch will be pre- or post-tensioned, other methods are employed to determine the thickness of the section and the required tendon tension and size.

4.2 AASHTO Code Allowances

Figure 4-4 illustrates two types of load spread allowed by AASHTO to account for 3-D load spread effects in a 2-D FE model. The 1996 AASHTO-LRFD specifications stipulate that, for fill heights, *H* in *ft*, greater than three feet, the load dissipates longitudinally only through the soil, according to the equation:

$$l_s = 1.75H \qquad \textbf{(4-1)}$$

where
l_s is the soil distribution length in *ft*.

When fill height is less than or equal to three feet, it states that the load dissipates longitudinally only through the structure, according to the equation:

$$l_c = 4\,ft + 0.06S \le 7.0ft \qquad \textbf{(4-2)}$$

where
l_c is the structure distribution length in *ft* and
S is the span of the structure in *ft*.

The 1998 AASHTO-LRFD code allows the combination of soil and structural distribution for all fill heights. However, the load spread within the soil, l_s, is reduced by nearly 35 percent, to

$$l_s = 1.15H \tag{4-3}$$

The load spread within the structure is also specified differently for positive and negative moments regions respectively as,

$$l_c^+ = 2.17\,ft + 0.55S \le 12\,ft \tag{4-4}$$

$$l_c^- = 4\,ft + 0.25S \le 12\,ft \tag{4-5}$$

where

l_c^+ is the structure distribution length for positive moment in *ft* and

l_c^- is the structure distribution length for negative moment in *ft*.

The total distribution length, l in *ft*, is then determined for the 1998 code as:

$$l = l_s + l_c \tag{4-6}$$

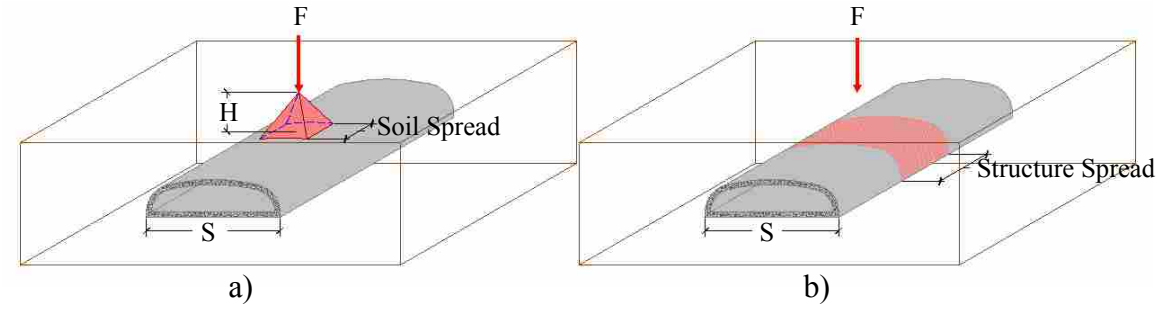

Figure 4-4 – Load distribution by a) soil spread and b) structure spread

For both codes, the specified load is then divided by the applicable distribution length to account for the effects of the third dimension (see 1998 AASHTO C4.6.2.1.3).

The 1998 code is more accurate, yet it still results in a conservative design in most cases. Figure 4-5 and Figure 4-6 compare the moments obtained from a 2-D FE analysis using the '96 AASHTO provisions and the moments directly below the load point of a 3-D FE analysis for an 18' span arch with one foot of fill cover in the ring and invert, respectively.

The conservatism of the code is readily seen in these two charts (see also Appendix B), as in Figure 4-2. Even with the load reduction, the maximum positive moment from the 2D analysis is still much higher (67% in this case) than predicted by a more realistic 3-D model. Also, the negative and invert moments for the 2-D analysis are much higher than predicted by the 3-D analysis (both 230% in this case). It appears, from these and other results, that the conservatism of the current AASHTO provisions are both a function of fill cover and span.

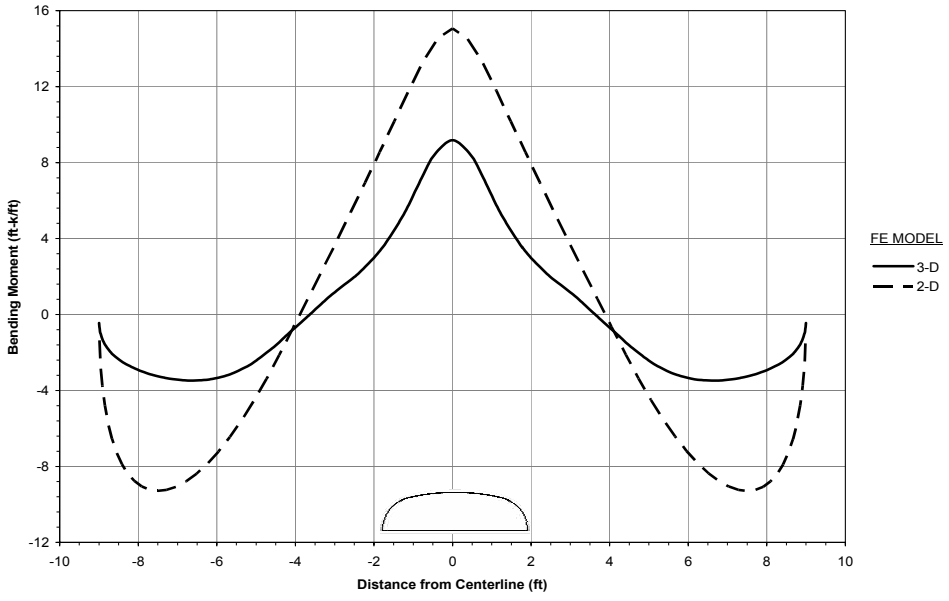

Figure 4-5 – Comparison of 2-D and 3-D moment results in the plane of loading for an 18' span arch ring with one foot of fill

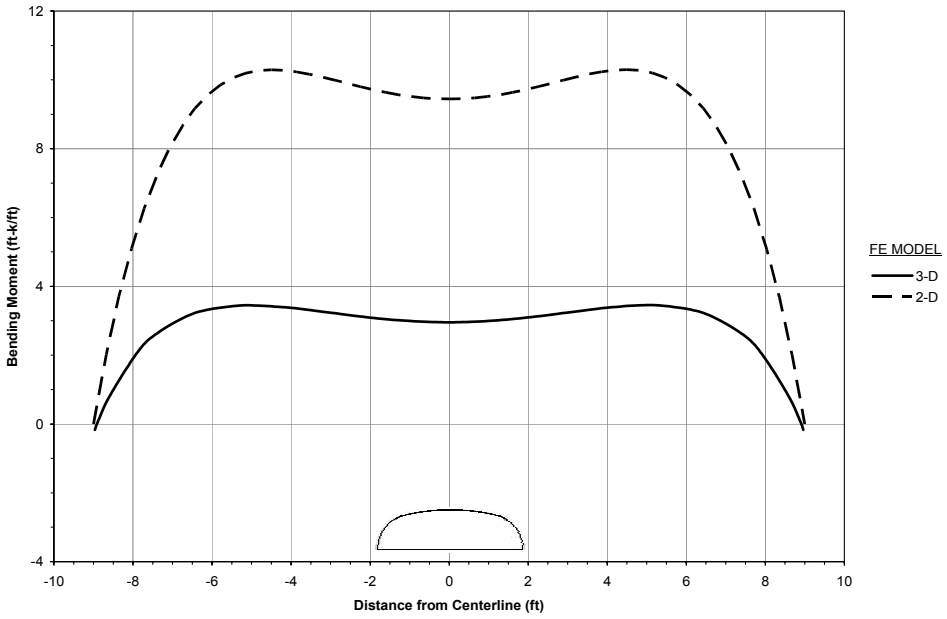

Figure 4-6 – Comparison of 2-D and 3-D moment results in the plane of loading for an 18' span arch invert with one foot of fill

Current research has investigated much of the behavior of box culverts, which are slightly more similar to bridge decks than are arches. Several studies have also been directed toward various aspects of buried arches (see Bacher & Klein, 1980; McGrath & Mastroianni, 2002; and McGrath, *et al*., 2002, for example). Currently, however, there is very little research specifically aimed at providing an accurate prediction of distribution length for buried concrete arches. In fact, recent studies recognize this short-coming and recommend further research be done to provide this additional tool to designers (see McGrath and Mastroianni, 2002).

5 Research Methods and Results

The inaccuracies of current load distribution equations necessitate the development of a more reliable method of accounting for three-dimensional behavior in a two-dimensional FE model. Because there are infinite geometries possible for buried arch structures, a study resulting in a statistically representative design equation for all possibilities would be a tremendous undertaking. Instead, it would be useful to derive a correlation with a simple, cheap, and widely available method using a limited number of 3-D finite element analyses from which an appropriate distribution length for any geometry can be obtained. This correlation is made with a beam-on-elastic-foundation analysis. Since the BOEF analysis considers such things as structure width and moment of inertia and soil stiffness, the need for analysis of a large quantity of varying geometries and soil parameters becomes less necessary.

The desired end product of this research is to provide the designer with the ability to use a universally available BOEF program to determine the distribution length for any buried concrete arch with specific geometric, loading, and soil characteristics. This length is used in reducing 2-D loads to a point where the magnitudes of the structural forces are equivalent to those obtained from a three-dimensional analysis in the plane of discrete loading.

5.1 3-D Finite Element Analysis

To begin, data must be obtained from 3-D finite element analyses of several buried concrete arch models with varying fill heights and spans. Three spans with increasing fill heights were initially selected to show span/fill height relationships, then, using SAS OPTEX (a statistical optimization program), six other span/fill height combinations were chosen to best represent the rest of the domain of $1ft \leq H \leq 10ft$ and $6ft \leq S \leq 40ft$, where H is the fill height and S is the span. Figure 5-1 shows all twenty-one span/fill height combinations used for this research.

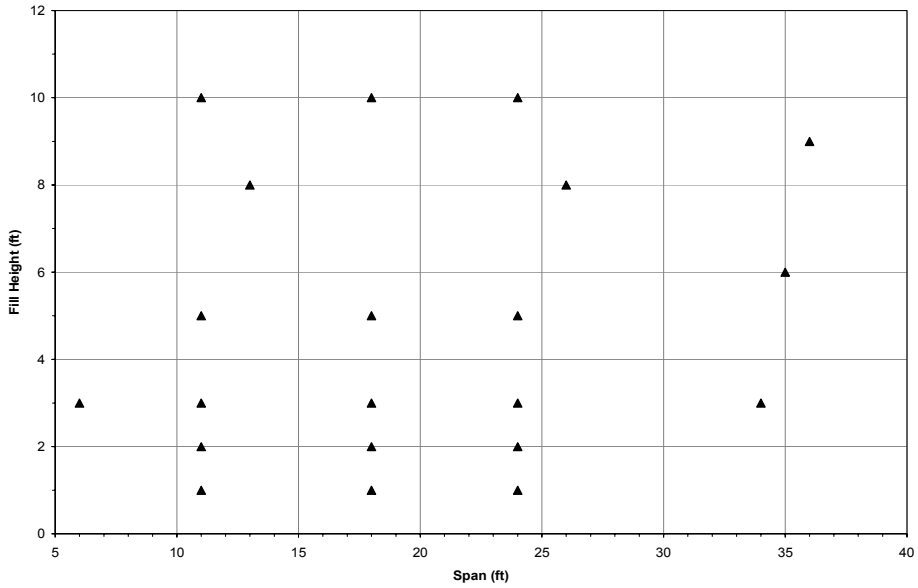

Figure 5-1 – Spatial representation of arch models used in this research

The geometry of each model created in Plaxis 3-D Tunnel (version 2.0, Build 1188. Plaxis B.V.) is shown in the following three figures. A "hinge" was created between the arch and invert; this is because the arch is cast after the invert, and is connected by rebar only. This connection makes transfer of moment between the arch and invert minimal.

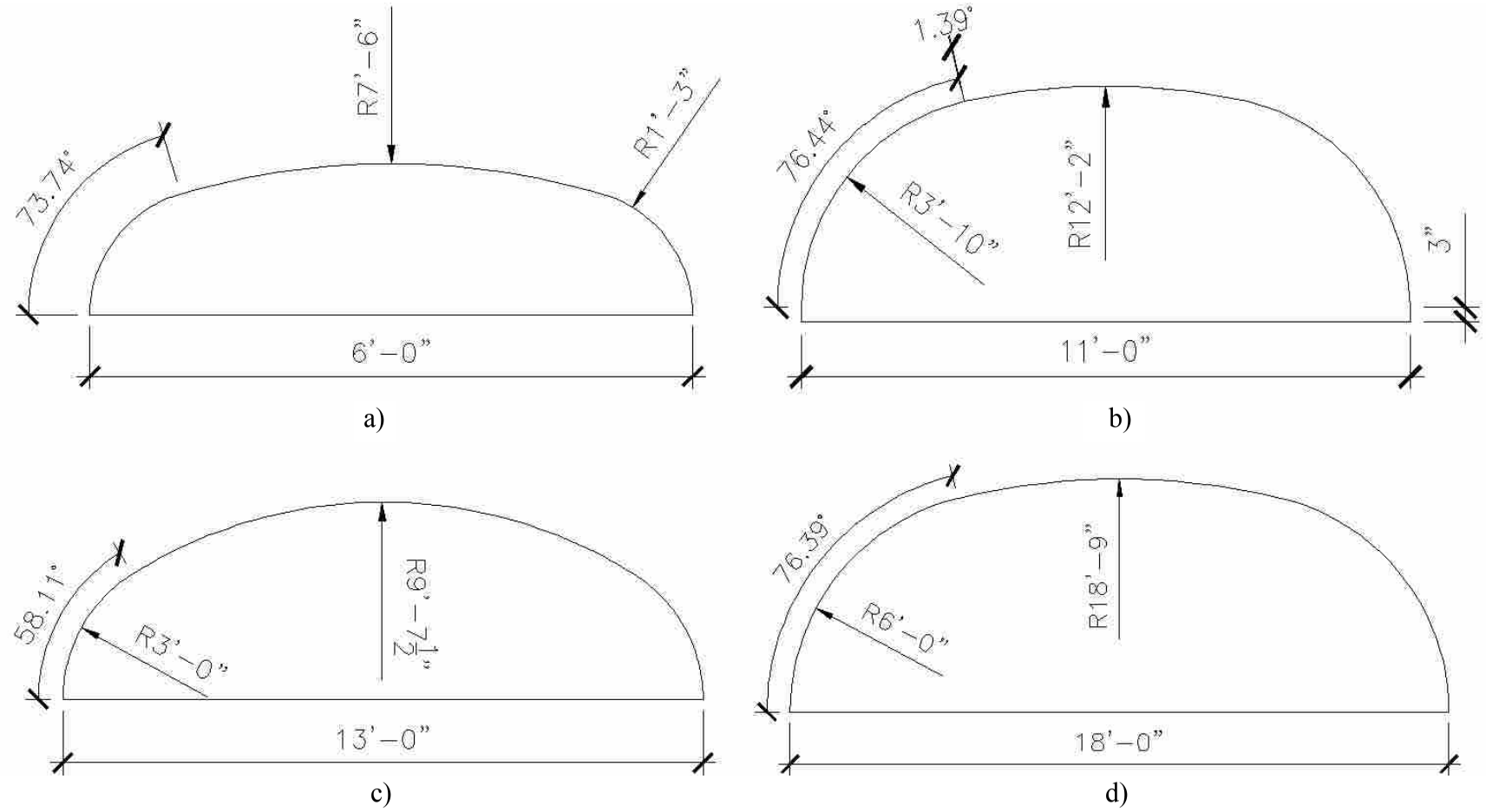

Figure 5-2 – Arch models used in Plaxis: a) 6' Model, b) 11' Model, c) 13' Model, and d) 18' Model

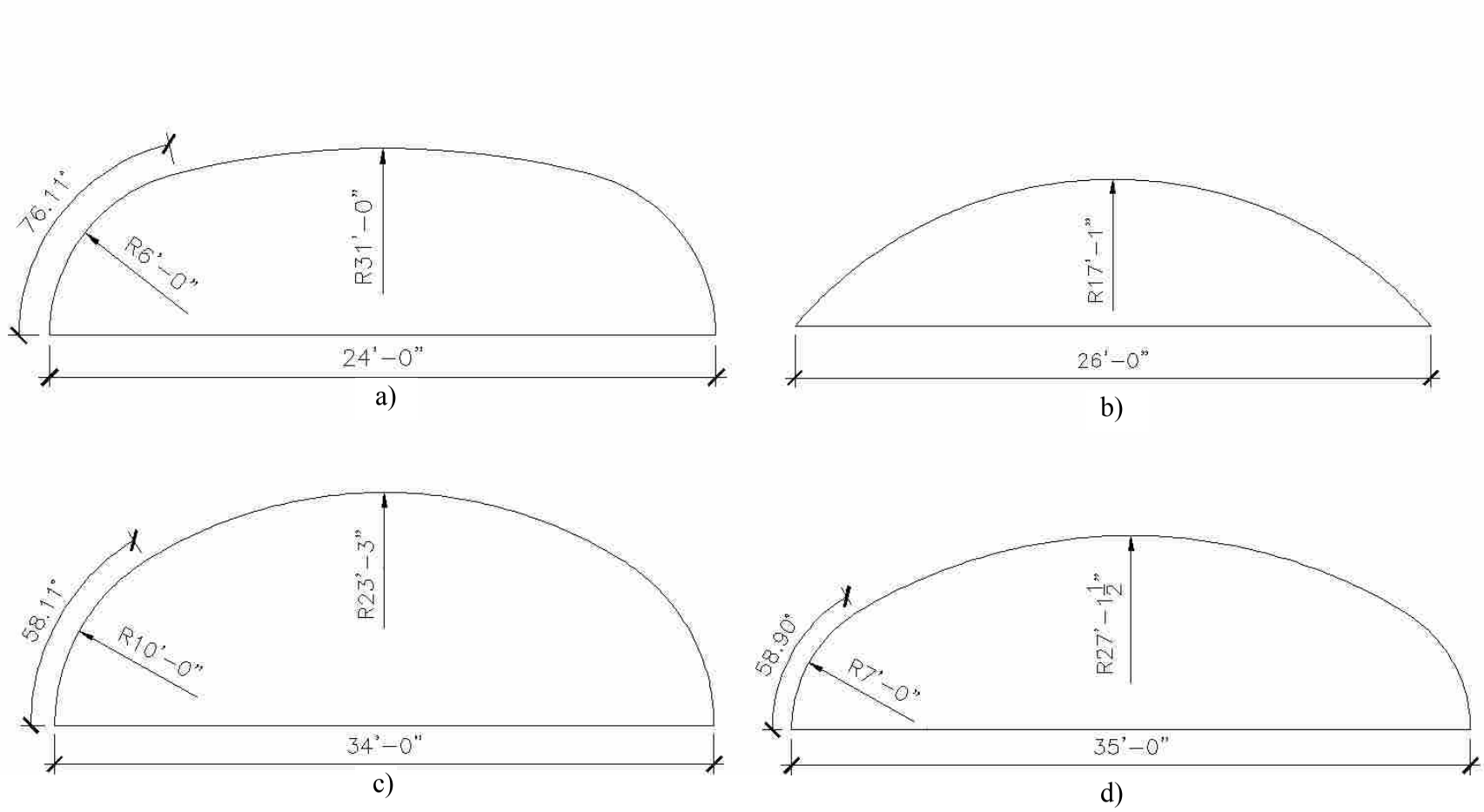

Figure 5-3 – Arch models used in Plaxis: a) 24' Model, b) 26' Model, c) 34' Model, and d) 35' Model

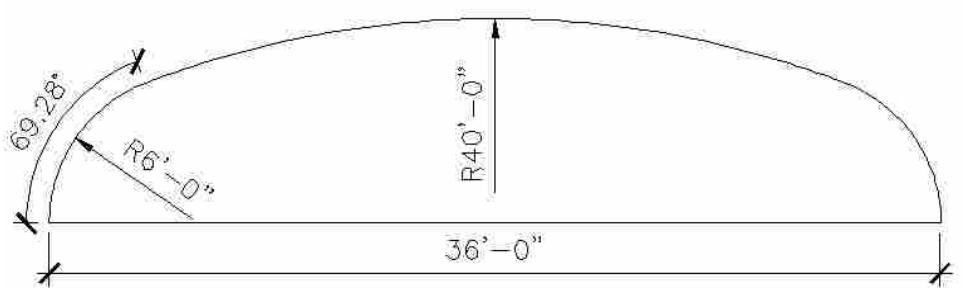

Figure 5-4 – 36' span arch model used in Plaxis

Table 5-1 – Outline of arch model section properties used in FE analyses

Property	SECTION PROPERTIES							
	ARCH					INVERT		
	6"	8"	10"	12"	14"	10"	12"	14"
A (ft^2/ft)	0.50	0.67	0.83	1.00	1.17	0.83	1.00	1.17
Reinforcing	#4@10	#5@10	#5@10	#5@10	#6@10	#5@10	#5@10	#6@10
I_{cr} (in^4/ft)	65	220	530	1030	1800	905	1035	1825
EA (k/ft)	259560	346080	432600	519120	605640	432600	519120	605640
EI_{cr} (k-ft^2/ft)	1610	5550	13215	25825	45100	22645	25920	45660
~ Model(s) using this section ~	6'	11' 13'	18'	24' 26'	34' 35' 36'	6'	11' 13' 18' 24' 26'	34' 35' 36'

The structural properties for the arch and invert models are summarized in Table 5-1, where A is the cross-sectional area of a one foot strip and E is the elastic modulus of the concrete. The partially cracked moment of inertia, I_{cr}, for all sections is based upon a one foot strip of transformed section two inches less than its actual thickness. The arch sections use one mat of reinforcing bar with 1.5" of concrete cover and the invert uses two mats of reinforcing with 2" of top cover and 3" of bottom cover. The reinforcing in the arch is positioned so as to resist tensile forces (at the intrados at the crown and at the extrados at the haunches). All reinforcement has a yield strength, f_y, of 60 ksi and all concrete is normal weight (150 pcf) with a compressive strength, f'_c, of 4000 psi and

Poisson's ratio, v, of 0.17. Plaxis 3-D uses Reissner-Mindlin shell elements to model the arch and invert.

The soil properties used in the finite element models are shown in Figure 5-5. The top six inches of backfill were modeled using a linear elastic soil model to prevent failure directly below the point of load application due to high loading pressure. The backfill extends 24" below the base of the arch to account for soil disturbances caused in the excavation process. The fill height above the crown of the arch is varied as one of the parameters of interest.

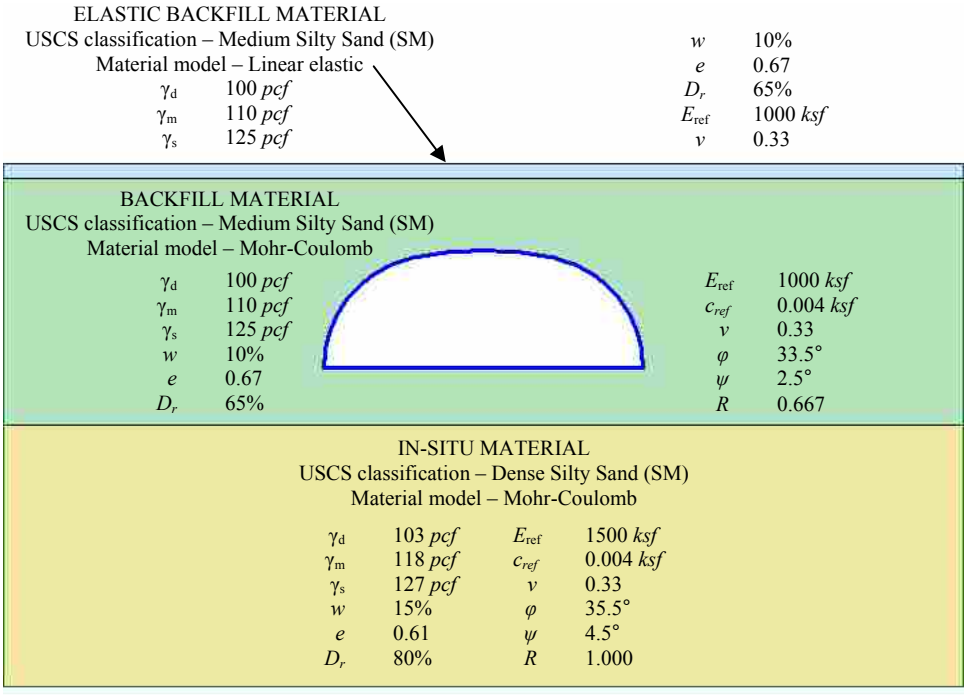

Figure 5-5 – Properties used for soil models in FE analyses

In Figure 5-5,
γ_d is the dry unit weight,
γ_m is the moist unit weight,
γ_s is the saturated unit weight,
w is the moisture content,
e is the initial void ratio,

D_r is the density relative to the maximum possible density,
E_{ref} is the reference modulus of elasticity,
c_{ref} is reference cohesion, and is present only to prevent numerical errors,
v is Poisson's ratio,
φ is the friction angle,
ψ is the angle of dilation, and
R is the interface friction ratio; 1.0 means no slippage and 0.0 is frictionless.

The finite element models of an 11' span arch with three feet of fill generated in Plaxis are shown in Figure 5-6. The global mesh coarseness for all models was set to *coarse*, resulting in about 100 elements per plane. A local refinement factor of 0.25 was applied at the load and around the structure. This means that the mesh was reduced to 25 percent of the global coarseness to better capture the model behavior in the vicinity of interest or highest loading. A dead load analysis considering only the weight of the soil and structure was initially performed, then the load was applied and the model re-analyzed. Analyses were performed assuming small displacements.

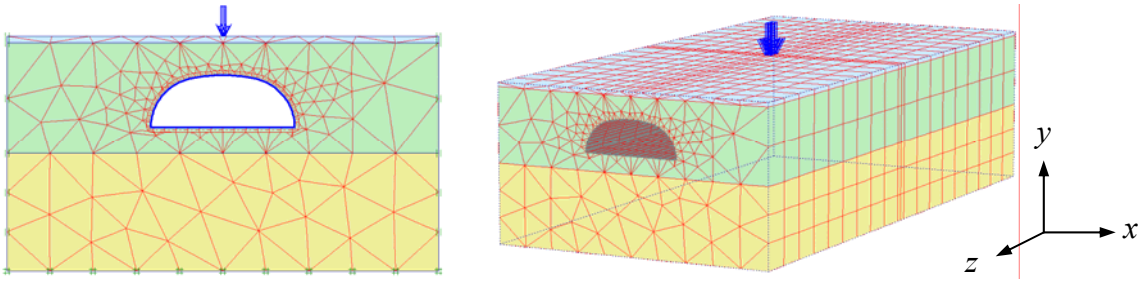

Figure 5-6 – 2-D and 3-D finite element models for an 11' span arch with three feet of fill

The 3-D model uses tetrahedral volume elements for the soil and Reissner-Mindlin shell elements for the structure. The parallel planes are automatically generated by Plaxis to keep the element aspect ratio approximately equal to unity. Such an aspect ratio results in more accurate results. The boundary conditions used are translation fixities. The front and back are restrained in the z-direction, the sides are restrained in the

x-direction, and the bottom is restrained in the *y*-direction. The top is a free surface. HL-93 loading is applied as a pressure to an AASHTO specified tire contact area of 7"x 20" directly above the crown of the arch at mid-length using the appropriate impact and load factors. Table 5-2 outlines the loading used on the FE models. The water table was assumed to be below the bounds of the model. In most cases this should be a valid assumption. However, inadequate drainage or the presence of a water table will produce very different results. The scope of this research does not include such instances, but the designer should be aware of its influence on soil strength and structure loading.

Table 5-2 – Summary of HL-93 loading applied above the arch crown at mid-length

Fill Height, *H* (ft)	Impact Factor, I_f	Loading Area, *A* $A = 0.58ft \times 1.67ft$ (ft^2)	Pressure, *P* $P = (16k \times 2.17 \times I_f)/A$ (ksf)
1	1.3	0.97	46.45
2	1.2	0.97	42.87
3	1.1	0.97	39.30
>3	1.0	0.97	35.73

The models are three times wider than the span and the soil extends one span width below the invert. To minimize end effects and provide reasonable accuracy, it was determined that a length equal to six times the span would be sufficient (see Figure 5-11). Because of use of the Mohr-Coulomb criterion, which is essentially elastic-perfectly plastic (see Figure 5-7), for the bulk of the soil models, Plaxis uses an iterative process that applies the load in increments to account for the effects of the plastic points in the soil.

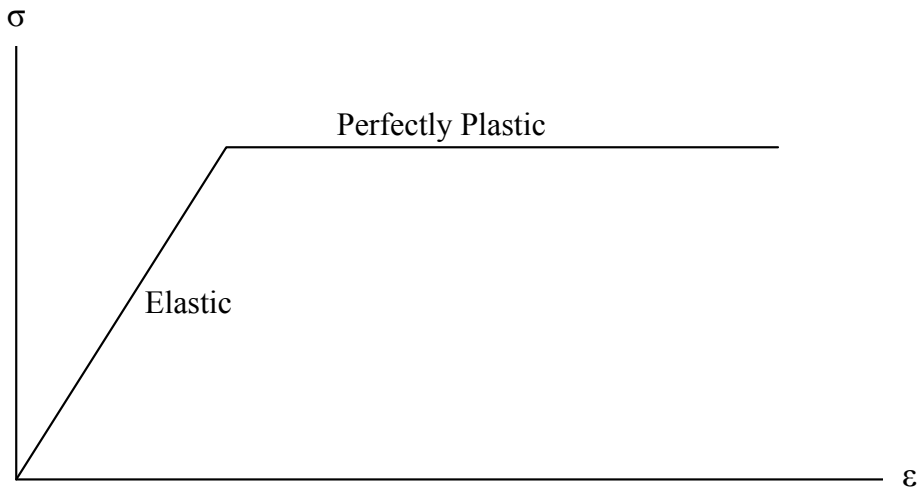

Figure 5-7 – Elastic-perfectly plastic behavior of a Mohr-Coulomb soil model

A small number of plastic points were created at the ends of the invert, in the vicinity of the haunches, and directly below the load where the stress reached the strength of the soil. This is expected since these are the areas in which the soil strength is most highly mobilized.

5.2 Determination of Distribution Length

When an exterior force deforms a material, energy is stored internally throughout its volume. Because deformations are directly related to material strains, this internal energy is called strain energy. The amount of strain energy per unit volume is known as strain energy density. There are four contributors to the total strain energy in a material: axial force, bending moment, shear force, and torsion. Shear and axial forces and torsion cause about half of the total strain energy in a buried arch (except at very low fill heights, where shear comprises nearly all strain energy). The remainder of the strain energy is a result of bending moment (see Figure 5-8).

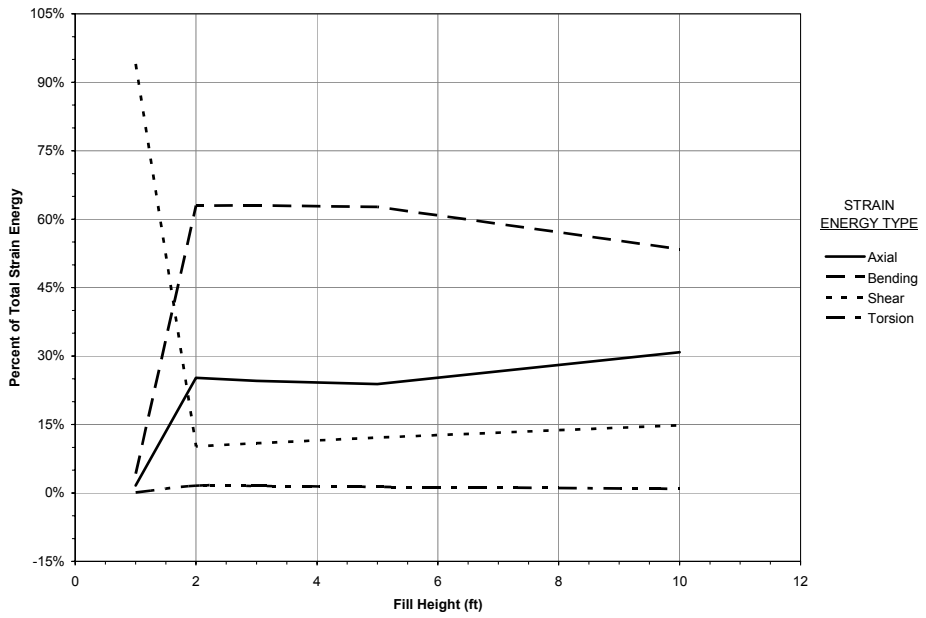

Figure 5-8 – Effect of fill height on percent of total strain energy by type for an 18' span arch ring

In order to have equal forces in similar structures, both must have equal strain energy densities. Strain energy can be generated in a system by a discrete load or a continuous load (or thermal load, or support movement, etc.). In the case of discrete loading, strain energy will be densest directly below the load and will diminish as distance from the load increases. For constant continuous loading, strain energy density will remain constant parallel to the load. In order for the quantity of strain energy in a plane under a continuous load to be equal to the quantity of strain energy in a plane at the discrete load point, the magnitude of the continuous load will always be some fraction of the discrete load (see Figure 5-9, where F is the magnitude of the discrete load and l is the distribution length).

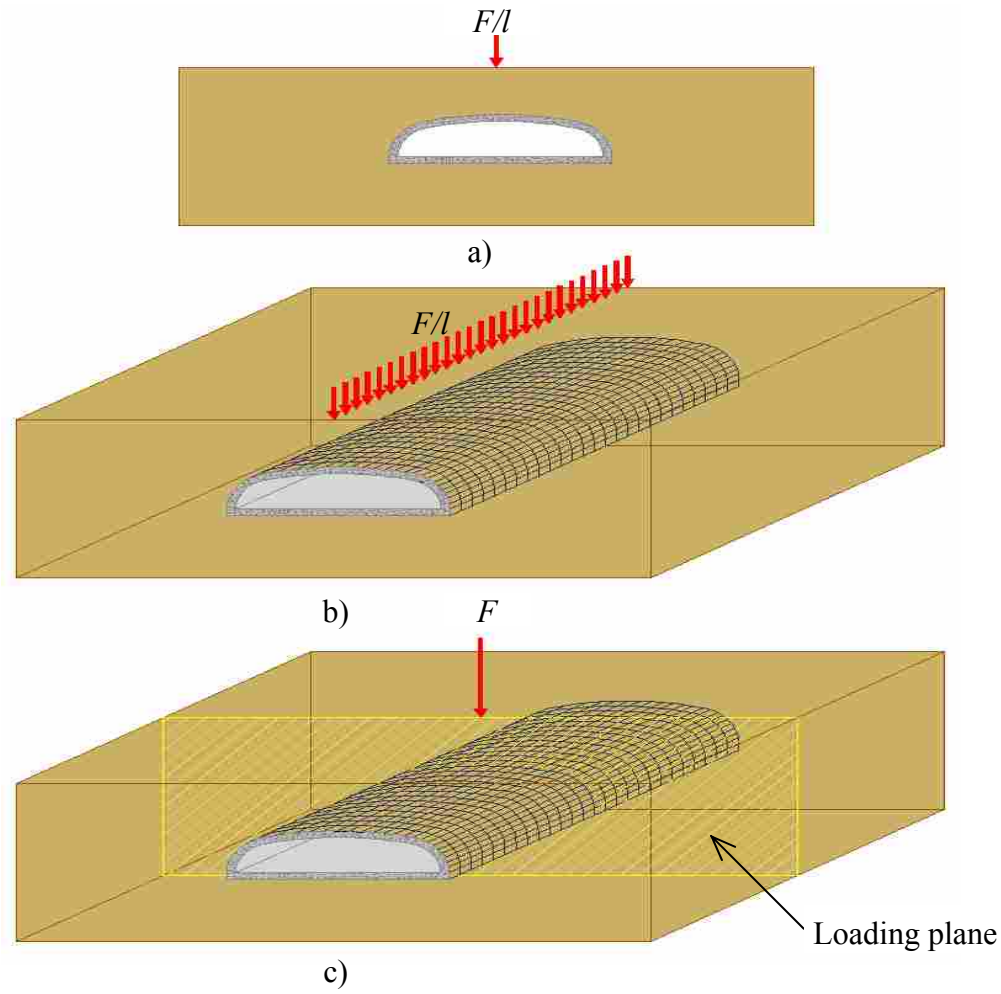

Figure 5-9 – Load magnitudes resulting in equivalent structural forces for a) 2-D, b) continuous, and c) discrete loads in the plane of loading

A 2-D FE model essentially assumes that an applied load is a line or strip of constant magnitude. This 2-D load must be factored down in order to produce the same structural forces as those produced in a 3-D system in the plane of loading. This factor will vary depending on the form of strain energy (*i.e.* bending energy, shear energy, etc.), geometry, fill cover, and material properties. To determine the reduction factor corresponding to a particular strain energy type, the total strain energy in a 3-D system must be divided by the total strain energy in the loading plane; both of the same type. This will, in essence, produce a required length of structure in which the same volume of

strain energy with a constant density profile will be produced (see Figure 5-10). This density profile is equal to that in the loading plane of the 3-D structure under discrete loading, and is the result of a constant continuous load. In simple terms, the magnitude of the discrete load is distributed over a specific length (*i.e.* turned into a line load), called the distribution length, *l*, to produce structural forces under a continuous load that are equivalent to those produced in the plane of discrete loading.

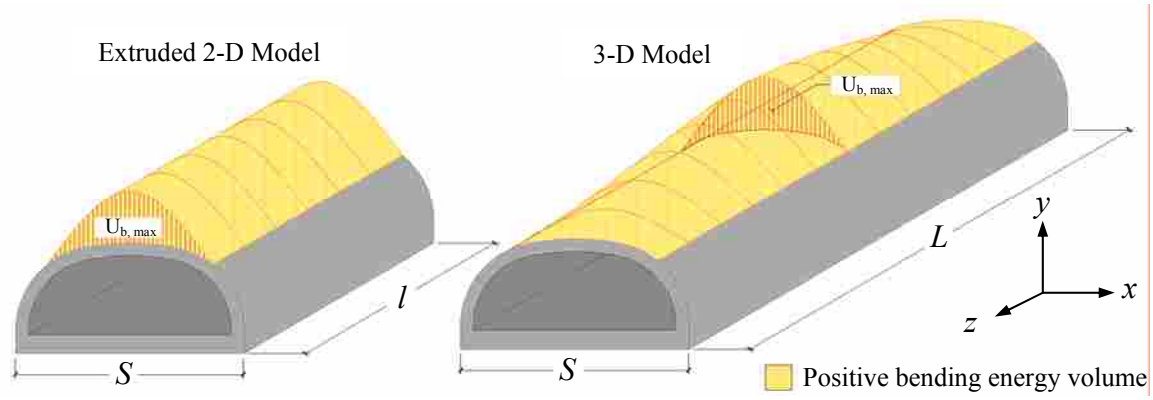

Figure 5-10 – Illustration of equivalent positive bending energy volumes

Since bending energy contributes most significantly to the total in most cases, it will be used to determine the distribution lengths for all forms of strain energy. A similar method was mentioned by McGrath (2005) to model behavior of box culverts under discrete loads. Planar bending energy is calculated using the equation

$$U_b = \int_S \frac{M(x)}{2EI}\,dx \qquad \textbf{(5-1)}$$

where

U_b is the bending energy in a plane,
$M(x)$ is the magnitude of the bending moment as a function of x in *ft-k/ft*,
E is the elastic modulus of the material in *ksf*,
I is the moment of inertia of the structure in ft^4/ft, and
S is the span of the structure in *ft*.

The distribution length, l, is a ratio of bending energies. Assuming E and I are constant, which is reasonable when cracking is within tolerable limits, it is convenient to disregard them initially, since they will cancel out in the end result. This results in the planar bending energy equation being reduced to the planar moment equation

$$M_P = \int_S M(x)dx \qquad \textbf{(5-2)}$$

where
M_P is the planar moment in *ft-k*.

The following outlines a mathematical procedure for the previously stated method – the bending energy method – of determining distribution length for a discrete live load.

1. Volumetric moment represents the total moment in the structure. Determine the total positive or negative volumetric moment created in the structure by overburden weight using the equation

$$M^{\pm}_{V,overburden} = \int_L \int_S M^{\pm}_{overburden}(x,z)dxdz \qquad \textbf{(5-3)}$$

where
$M^{\pm}_{V,overburden}$ is the total positive or negative overburden volumetric moment in ft^2-*k*,
$M^{\pm}_{overburden}(x,z)$ is the positive or negative magnitude of the overburden moment as a function of position in *ft-k/ft*, and
L is the length of the structure in *ft*.

2. Determine the total positive or negative volumetric moment created in the structure due to live load. Overburden loads are assumed to be constant and continuous within the length of influence, therefore, they need to be disregarded for determining distribution length of a discrete load. This is accomplished by subtracting the overburden volumetric moment from the total volumetric moment using the formula

$$M^{\pm}_{V,LL} = \int_L \int_S M^{\pm}_{total}(x,z)dxdz - M^{\pm}_{V,overburden} \quad \textbf{(5-4)}$$

where

$M^{\pm}_{V,LL}$ is the total positive or negative live load volumetric moment in ft^2-k and

$M^{\pm}_{total}(x,z)$ is the positive or negative magnitude of the total moment caused by overburden and live loads as a function of position in *ft-k/ft*.

3. Planar moment represents the total moment in a plane of the structure. Determine the maximum planar moment due to live load, which occurs in the same plane as the discrete load (at mid-length). This is done by subtracting the planar moment due to overburden from the total planar moment and is given by the expression

$$M^{\pm}_{P,LL\max} = \int_S M^{\pm}_{total}(x,\frac{L}{2})dx - \frac{M^{\pm}_{V,overburden}}{L} \quad \textbf{(5-5)}$$

where

$M^{\pm}_{P,LL\max}$ is the positive or negative live load planar moment at mid-length in *ft-k*.

4. Determine the positive or negative moment distribution length as the ratio of total positive or negative live load volumetric moment to maximum planar moment.

$$l^{\pm} = \frac{M^{\pm}_{V,LL}}{M^{\pm}_{P,LL\max}} \quad \textbf{(5-6)}$$

where

$l^{\pm}$ is the positive or negative moment distribution length in *ft*.

To determine the structure length required to minimize end effects, a series of FE analyses were performed for an 11’ span arch model with three feet of fill at differing

length-to-span ratios. The distribution length was determined for each using the outlined procedure. The results are shown in Figure 5-11 as a function of length-to-span ratio.

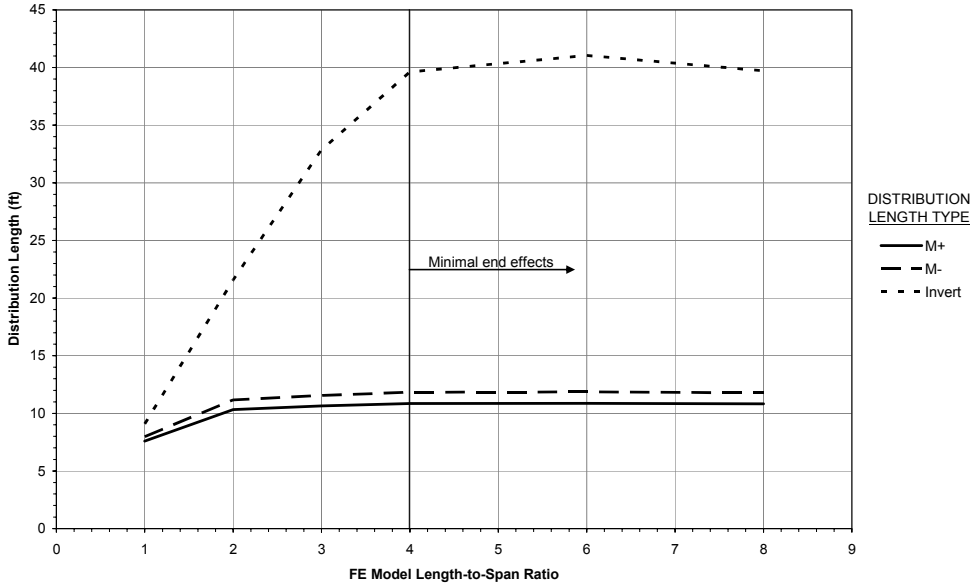

Figure 5-11 – Length-to-span ratio effects on distribution length for an 11' span arch with three feet of fill

From these results, it was determined that to account for the entirety of the live load effects, the 3-D FE model would have to be a minimum of four times the span in length. Shorter models do not allow sufficient length for the load to be naturally dissipated into the structure. This is similar to the problem that arises with 2-D finite element models. It can be seen that the third-dimension is an important factor in the behavior of the structure in response to the discrete loading, especially for the invert.

The program Mathematica was used to determine the distribution lengths for all span/fill height combinations using the bending energy method. Figure 5-12 shows a sample Mathematica calculation for determining the distribution length for positive moment for an 11’ span arch ring with one foot of fill.

■ 11' Arch with 1' Fill

■ Distribution Length for Positive Moment

Compute $M^{+}_{V,\text{overburden}}$ (ft^2-k).

$$M^{+}_{V,\text{overburden}} = \sum_{i=1}^{\text{Length}[M^{+}_{\text{overburden}}]} \text{ListIntegrate}[M^{+}_{\text{overburden}}[[i]], 4]\ t[[i]]$$

139.292

Compute $M^{+}_{V,\text{LL}}$ (ft^2-k).

$$M^{+}_{V,\text{LL}} = \sum_{i=1}^{\text{Length}[M^{+}_{\text{total}}]} \text{ListIntegrate}[M^{+}_{\text{total}}[[i]], 4]\ t[[i]] - M^{+}_{V,\text{overburden}}$$

107.828

Compute $M^{+}_{P,\text{LL max}}$ (ft-k).

$$M^{+}_{P,\text{LL max}} = \text{ListIntegrate}[M^{+}_{\text{total}}[[\text{Length}[Z] / 2]], 4] - M^{+}_{V,\text{overburden}} / L$$

13.3267

Compute the distribution length (ft).

$$l^{+}_{11\text{-}1} = \frac{M^{+}_{V,\text{LL}}}{M^{+}_{P,\text{LL max}}}$$

8.09113

Figure 5-12 – Sample bending energy method calculations for an 11' span arch with one foot of fill

Computed distribution lengths using the bending energy method and AASHTO recommended methods are compared in Table 5-3, where S is the model span, H is the fill height, l^{+} is the distribution length for positive moment, l^{-} is the distribution length for negative moment, and l^{I} is the distribution length for invert moment.

Table 5-3 – Distribution lengths from the bending energy method and AASHTO provisions

Model (S – H)	BENDING ENERGY METHOD			'96 AASHTO l^+, l^-, l^1 (ft)	'98 AASHTO	
	l^+ (ft)	l^- (ft)	l^1 (ft)		l^+ (ft)	l^-, l^1 (ft)
6' – 3'	6.99	7.75	16.04	4.36	8.92	8.95
11' – 1'	8.09	9.40	41.18	4.66	9.37	7.90
11' – 2'	9.13	10.23	41.23	4.66	10.52	9.05
11' – 3'	10.88	11.87	41.05	4.66	11.67	10.20
11' – 5'	12.75	13.31	40.22	8.75	13.97	12.50
11' – 10'	19.30	20.00	40.65	17.50	19.72	18.25
13' – 8'	19.42	19.79	41.54	14.00	18.52	16.45
18' – 1'	12.81	15.23	66.47	5.08	13.15	9.65
18' – 2'	13.57	15.81	66.39	5.08	14.30	10.80
18' – 3'	15.73	17.65	65.85	5.08	15.45	11.95
18' – 5'	19.55	20.64	63.45	8.75	17.75	14.25
18' – 10'	23.59	24.99	60.14	17.50	23.50	20.00
24' – 1'	16.86	21.31	75.50	5.44	13.15	11.15
24' – 2'	18.08	21.80	74.70	5.44	14.30	12.30
24' – 3'	19.10	22.48	73.39	5.44	15.45	13.45
24' – 5'	21.95	26.05	72.24	8.75	17.75	15.75
24' – 10'	27.08	29.37	70.16	17.50	23.50	21.50
26' – 8'	27.60	30.32	57.59	14.00	21.20	19.70
34' – 3'	33.22	39.51	118.28	6.04	15.45	15.45
35' – 6'	39.91	42.48	103.37	10.50	18.90	18.90
36' – 9'	38.20	43.02	97.54	15.75	22.35	22.35

*Underlined values represent liberality in AASHTO recommendations

The conservatism of the code is readily seen from these values. Plots defining the degree of conservatism of the AASHTO distribution lengths for positive moment in comparison with those obtained from this research (all outlined in Table 5-3) with respect to span and fill height, are shown in Figure 5-13 and Figure 5-14, respectively.

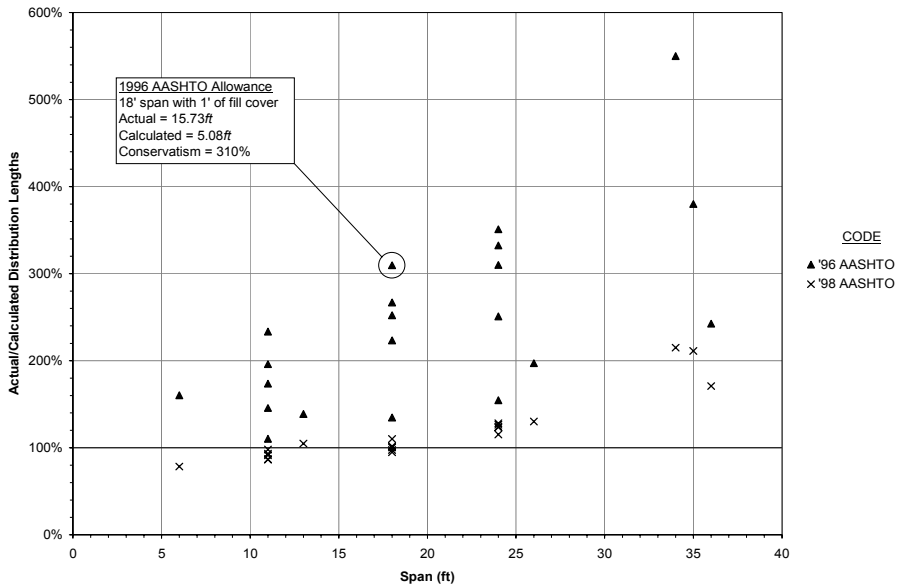

Figure 5-13 – Conservatism of AASHTO computed distribution lengths for positive moment for varying fill covers as a function of span

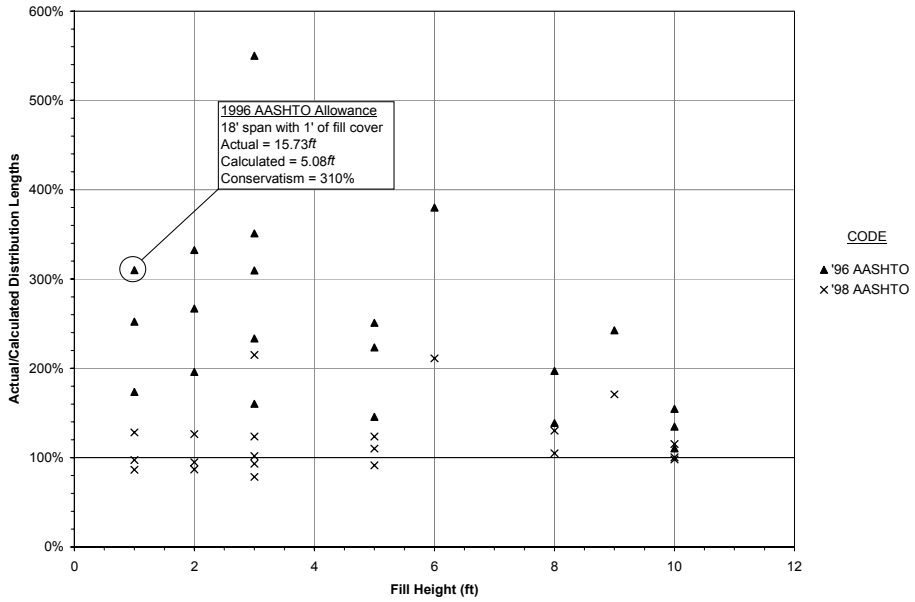

Figure 5-14 – Conservatism of AASHTO computed distribution lengths for positive moment for varying spans as a function of fill cover

AASHTO provisions are also very conservative for distribution lengths for invert moment for both span and fill heights, as shown in Figure 5-15 and Figure 5-16, respectively.

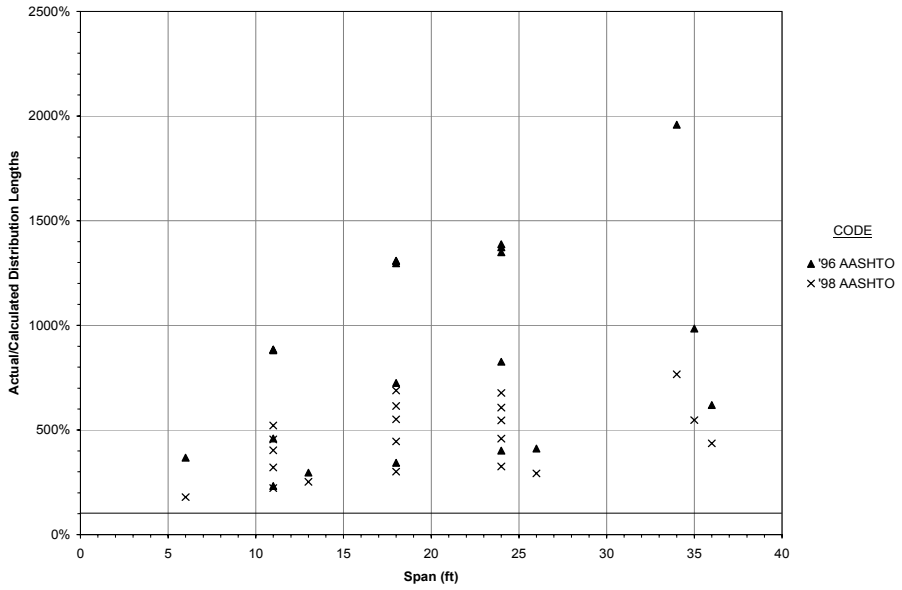

Figure 5-15 – Conservatism of AASHTO computed distribution lengths for invert moment for varying fill covers as a function of span

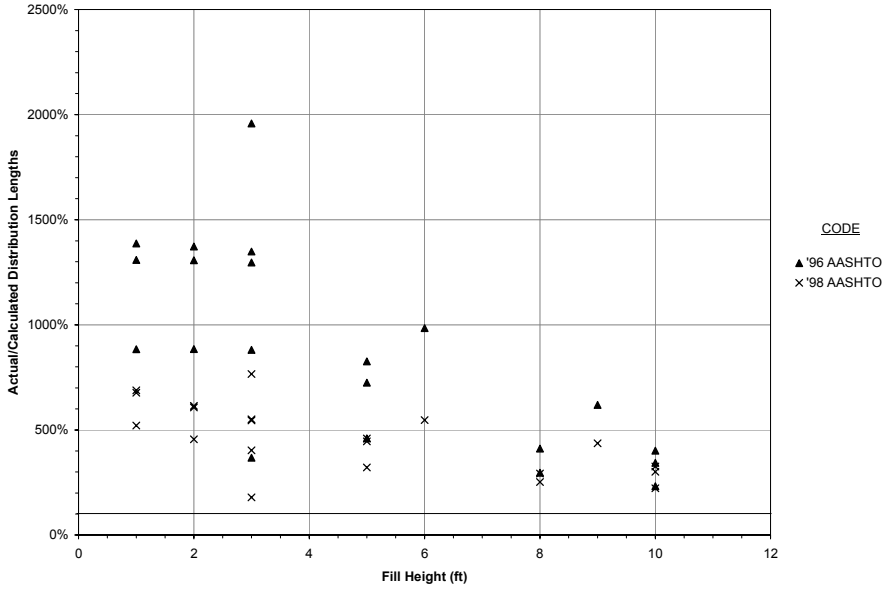

Figure 5-16 – Conservatism of AASHTO computed distribution lengths for invert moment for varying spans as a function of fill cover

The code provisions are more accurate at short spans and higher fill heights, as seen in these figures. At low fill heights, the effects of the live load overpower the effects of the overburden, so the load spread is a more important factor. Distribution lengths for negative moment are also very conservative, and show a similar pattern for both fill height and span (see Appendix C).

5.3 Beam-on-Elastic-Foundation (BOEF) Analysis

In confronting the problem of a flexible structure supported continuously on an elastic medium, a beam-on-elastic-, or Winkler foundation analysis is a good method of determining forces and deflections. This method is derived by assuming a rectangular elastic beam (structure) is supported on an infinite number of springs (soil). The springs are said to have a stiffness, *k'*, known as the subgrade modulus, or coefficient of subgrade reaction. Vesic (1961) proposed that Equation 5-7, which considers parameters of the entire system, be used to determine the subgrade modulus for long beams:

$$k' = 0.65\, S^{-12}\sqrt{\frac{E_s S^4}{E_b I_b}}\,\frac{E_s}{S(1-\nu^2)} \qquad \textbf{(5-7)}$$

where
k' is the subgrade modulus in *kcf*,
E_s is the elastic modulus of the soil in *ksf*,
E_b is the elastic modulus of the beam material in *ksf,*
S is the width of the beam in *ft*,
I_b is the moment of inertia of the beam in ft^4, and
ν is Poisson's ratio of the soil.

Since BOEF programs are universally available, a detailed explanation of the derivation, assumptions, and limitations will not be given here. Correlations to distribution length will be based on BOEF deflection. Such was attempted using bending moment, but there was no readily apparent correlation. Because buried arches exhibit

behavior similar to a beam-on-elastic-foundation, it was hypothesized that there would be an accurate correlation between BOEF and FE analyses (Figure 5-17).

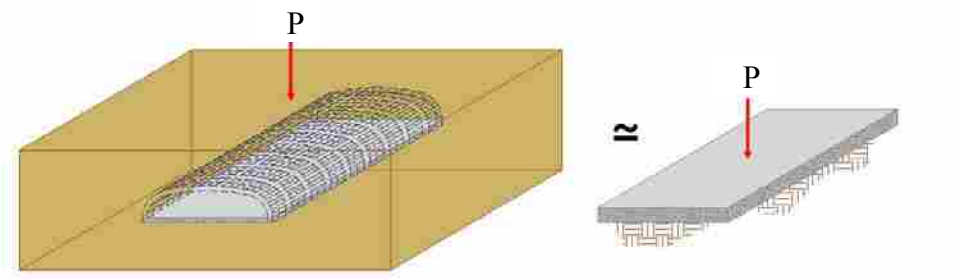

Figure 5-17 – Similarities between buried arch and beam-on-elastic-foundation models

Width and moment of inertia are required for the BOEF analysis, which provide a good representation of geometric variations, minimizing such problems as having the same moment of inertia but a different geometry (*i.e.* narrow and deep vs. wide and shallow). The location on an arch that is most likely to exhibit the same type of behavior as a flat plate is at the connection of the barrel to the invert. This point is especially resistant to the effects of deflections in the barrel or invert of the arch.

Table 5-4 – Representative arch model values used in BOEF analyses

Parameter	ARCH MODEL								
	6'	11'	13'	18'	24'	26'	34'	35'	36'
I_b (ft^4)	12	212	197	935	1511	1020	9278	5812	3723
L (ft)	36	66	96	108	144	156	204	210	216
k' (kcf)	710	684	727	710	753	799	727	763	799

Table 5-4 outlines the parameters used in carrying out the BOEF analysis to develop possible correlations with distribution length from the 3-D FE analysis, where I_b is the moment of inertia of the beam (or arch), L is the length of the model, and k' is the

subgrade modulus of the soil. Arch moment of inertia values were obtained from AutoCAD using the arch models shown in Section 5.1 with ring and invert thicknesses summarized in Table 5-1. Vesic's formula was used for determining the subgrade moduli. Elastic modulus and Poisson's ratio were representative of those used in the FE soil models ($\nu = 0.33$ and $E_s = 1100ksf$). The HL-93 loads outlined in Table 5-2 were applied as point loads (equal to the pressure multiplied by the contact area from the AASHTO procedure) at mid-length.

A comparison of vertical deflection of a BOEF model and an 18' span arch with three feet of fill at the ring/invert connection point is shown in Figure 5-18. It is apparent that BOEF analysis does not accurately predict the deflections in a buried arch. However, there is a close linear relationship between the deflections obtained by BOEF and FE analyses. This suggests that both exhibit similar force dissipation behavior under a discrete load, thus enabling an accurate correlation between distribution lengths obtained from FE analyses and deflections obtained from BOEF analyses.

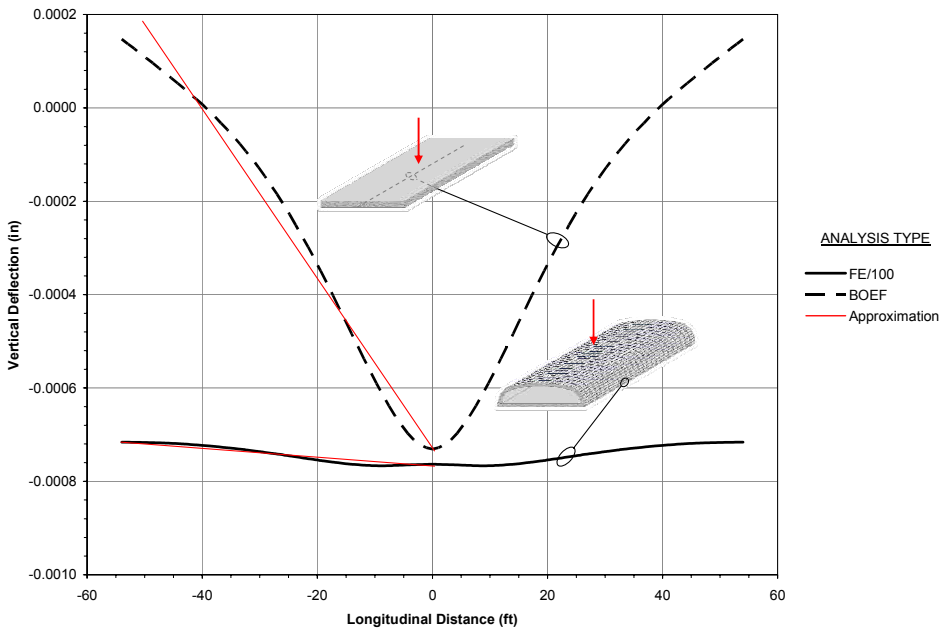

Figure 5-18 – Comparison of BOEF and FE analysis deflections at the ring/invert connection point for an 18' span model with three feet of fill

5.4 BOEF and FE Analysis Correlations

To eliminate the problem of varying deflection magnitudes, correlations will be based on a modified deflection ratio, defined as:

$$\Delta_{R,i} = 1 - \frac{\Delta_{\max} - \Delta_i}{\Delta_{\max} - \Delta_{end}} \qquad \textbf{(5-8)}$$

where

$\Delta_{R,i}$ is the deflection ratio at a point i, some longitudinal distance from the load point,

Δ_i is the deflection at point i,

$\Delta_{\max}$ is the deflection of largest magnitude for the entire beam, and

Δ_{end} is the deflection at the beam end.

Because BOEF analysis assumes the beam ends are unrestrained, there may be some amount of uplift at the ends. However, this modified deflection ratio will result in values of zero at the ends and unity at the load point. Deflection ratio values as a function of distance along the length of the arch from the BOEF and FE analyses for the

24’ span arch with five feet of fill are presented in Figure 5-19 (see Appendix D for similar figures).

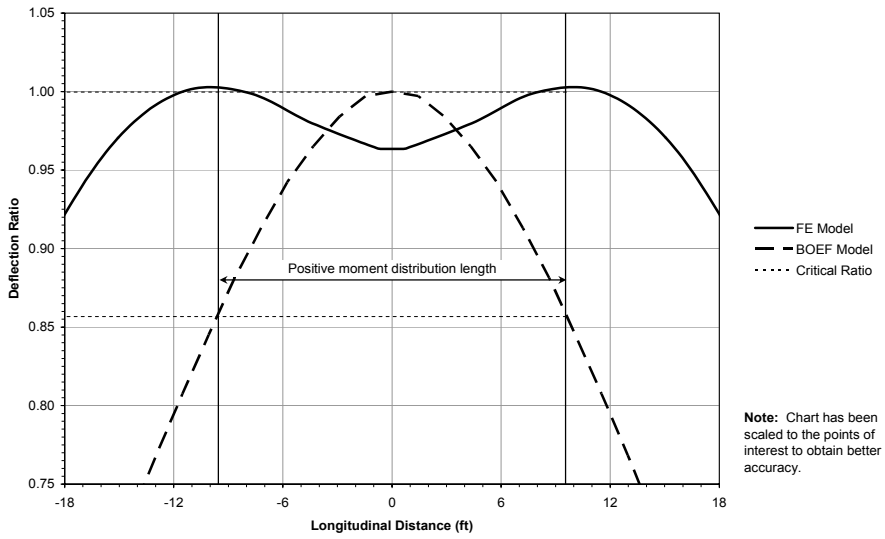

Figure 5-19 – Deflection ratios for 24’ span BOEF and FE models with three feet of fill

The value of the deflection ratio at a distance of one half the distribution length, as determined in Section 5.2, from mid-length of the arch/beam model is defined as the critical deflection ratio. Critical deflection ratios for all span/fill height combinations were ascertained from charts such as Figure 5-19 to use for correlation purposes. The deflection ratios for FE analysis are shown only for comparison purposes; they are not used for correlation.

Again, it can be seen that BOEF analysis is a poor predictor of buried arch deflection. However, positive moment critical deflection ratio values for both FE and BOEF models, shown in Figure 5-20 for the 24’ span model, show there is a good linear correlation between these values. Negative and invert moment critical deflection values

show a similar linear correlation (see Appendix D). This correlation suggests that critical deflection ratios are good indicators of distribution length.

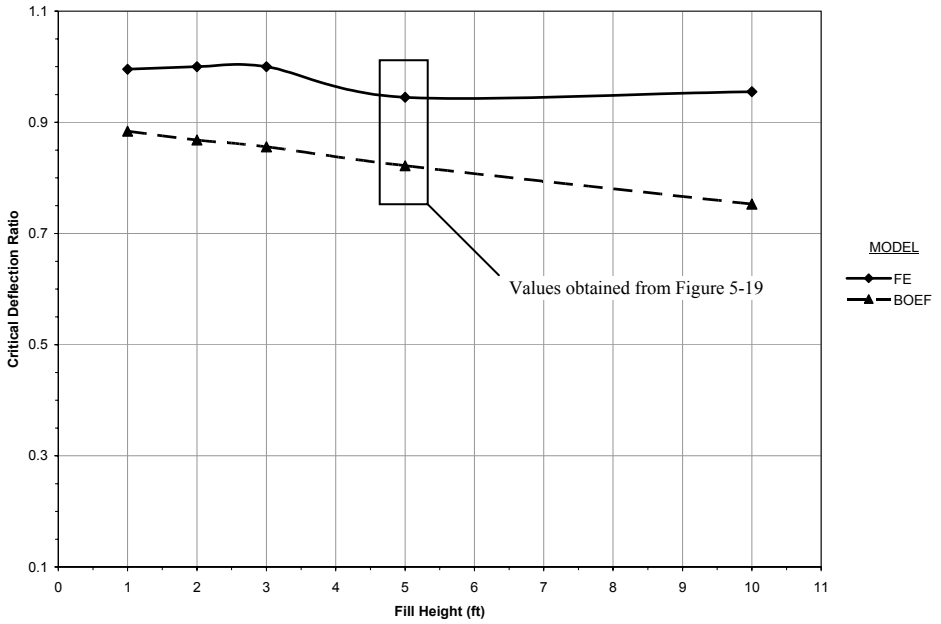

Figure 5-20 – Critical deflection ratios for positive moment distribution length for 24' span BOEF and FE models as a function of fill height

Figure 5-21 shows the critical deflection ratios for positive moment distribution lengths for the 11', 18', and 24' span BOEF models. Values for the distribution lengths for negative moment produce similar results. Invert moment distribution length values also produce similar results, with positive, rather than negative slopes (see Appendix D). The critical deflection ratios for the BOEF models are summarized in Table 5-5.

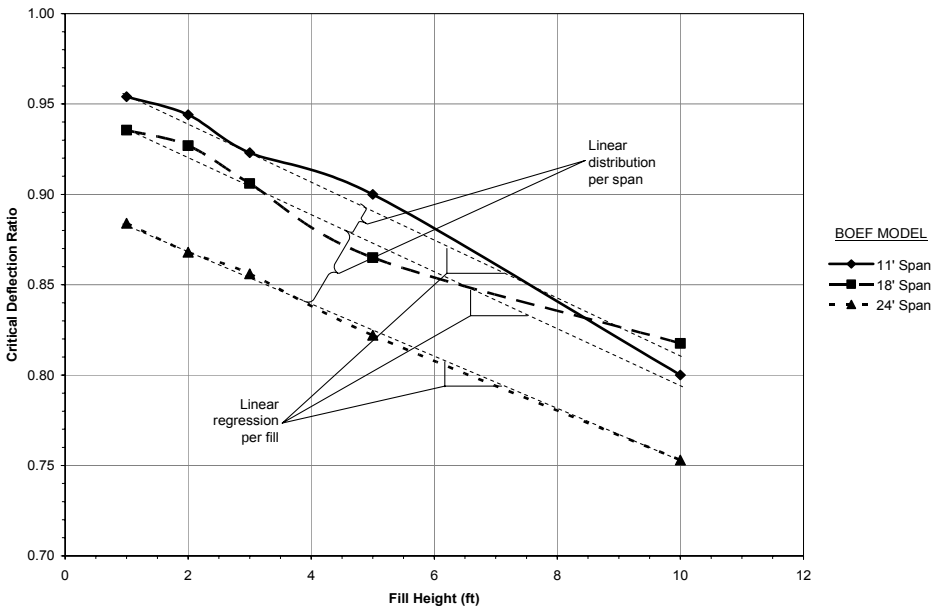

Figure 5-21 – Critical deflection ratios for positive moment distribution lengths for BOEF models as a function of fill height

Table 5-5 – Critical deflection ratios for BOEF models

Model ($S-H$)	$\Delta^{+}_{R,cr}$	$\Delta^{-}_{R,cr}$	$\Delta^{I}_{R,cr}$	Model ($S-H$)	$\Delta^{+}_{R,cr}$	$\Delta^{-}_{R,cr}$	$\Delta^{I}_{R,cr}$
6' – 3'	0.902	0.882	0.637	18' – 10'	0.818	0.800	0.378
11' – 1'	0.954	0.940	0.406	24' – 1'	0.884	0.828	0.200
11' – 2'	0.944	0.931	0.407	24' – 2'	0.868	0.823	0.202
11' – 3'	0.923	0.910	0.409	24' – 3'	**0.856**	0.813	0.214
11' – 5'	0.900	0.892	0.416	24' – 5'	0.822	0.766	0.223
11' – 10'	0.800	0.788	0.412	24' – 10'	0.753	0.720	0.237
13' – 8'	0.776	0.769	0.405	26' – 8'	0.659	0.611	0.206
18' – 1'	0.936	0.912	0.316	34' – 3'	0.810	0.755	0.173
18' – 2'	0.927	0.906	0.316	35' – 6'	0.666	0.640	0.107
18' – 3'	0.906	0.888	0.322	36' – 9'	0.610	0.541	0.035
18' – 5'	0.865	0.853	0.348				

*Bold value represents positive moment critical deflection ratio obtained from Figure 5-19

Since the critical deflection ratios, $\Delta_{R,cr}$, appear to be a linear combination of span and fill height, a model equation of the form

$$\Delta_{R,cr} = (a + bH)(c + dS) + e \qquad \textbf{(5-9)}$$

will be used to predict them. Three equations will be developed for predicting critical deflection ratios for positive, negative, and invert moment distribution lengths. The coefficients *a*, *b*, *c*, *d*, and *e* were obtained using the FindFit function in Mathematica for all data points. The following equations were determined to best represent the critical deflection ratios within the domains of $1ft \le H \le 10ft$ and $6ft \le S \le 40ft$:

$$\Delta^{+}_{R,cr} = 1.049 - (2.319 + 0.396H)(0.020 + 0.002S) \quad \textbf{(5-10)}$$

$$\Delta^{-}_{R,cr} = 1.053 - (4.694 + 0584H)(0.011 + 0.001S) \quad \textbf{(5-11)}$$

$$\Delta^{I}_{R,cr} = 1.856 + (-0.014 + 0.0001H)(89.250 + 1.074S) \quad \textbf{(5-12)}$$

where

S is the model span,

H is the fill height,

$\Delta^{+}_{R,cr}$ is the critical deflection ratio for positive moment distribution length,

$\Delta^{-}_{R,cr}$ is the critical deflection ratio for negative moment distribution length, and

$\Delta^{I}_{R,cr}$ is the critical deflection ratio for invert moment distribution length.

Predictions for fill heights greater than ten feet will be limited to those obtained at $H = 10ft$, since the live load plays a less important role with large fill heights. This will also help eliminate inaccuracies that could arise from being outside the domain upon which the equations are based. Table 5-6 summarizes the critical deflection ratio values predicted by these equations.

Table 5-6 – Critical deflection ratios obtained from prediction equations

Model ($S-H$)	$\Delta^{+}_{R,cr}$	$\Delta^{-}_{R,cr}$	$\Delta^{I}_{R,cr}$	Model ($S-H$)	$\Delta^{+}_{R,cr}$	$\Delta^{-}_{R,cr}$	$\Delta^{I}_{R,cr}$
6' – 3'	0.947	0.941	0.509	18' – 10'	0.753	0.732	0.338
11' – 1'	0.950	0.932	0.430	24' – 1'	0.897	0.858	0.233
11' – 2'	0.935	0.919	0.432	24' – 2'	0.875	0.836	0.235
11' – 3'	0.921	0.906	0.433	24' – 3'	0.852	0.815	0.236
11' – 5'	0.892	0.879	0.436	24' – 5'	0.808	0.771	0.240
11' – 10'	0.819	0.812	0.443	24' – 10'	0.697	0.664	0.247
13' – 8'	0.832	0.819	0.410	26' – 8'	0.725	0.686	0.214
18' – 1'	0.921	0.892	0.324	34' – 3'	0.800	0.745	0.085
18' – 2'	0.903	0.874	0.326	35' – 6'	0.708	0.652	0.075
18' – 3'	0.884	0.857	0.327	36' – 9'	0.613	0.555	0.065
18' – 5'	0.847	0.821	0.330				

*Underlined values represent non-conservative predictions

To determine the validity of these equations, a square-root-of-average-square-of-differences procedure is used, which is a method for determining the variation of data from a model equation. This procedure is as follows:

1. Determine the coefficients *a*, *b*, *c*, *d*, and *e* for the model equation using all data points except one.
2. Predict the value of the excluded data point using the model equation with coefficients determined in Step 1.
3. Square the difference between the actual and predicted values.
4. Repeat Steps 1-3 for all data points in the set.
5. Find the average of all the squared differences found in Step 3 and take the square root of it.

This procedure will give a range of average variation of the data from the model equation. Determination of the coefficients *a*, *b*, *c*, *d*, and *e* was accomplished using the FindFit function in Mathematica. The values obtained from this procedure are given in

Table 5-7 and show that the actual values vary from the prediction model, on average, by ±5% or less. This indicates that the base equation is, indeed, a good representation of the actual data points.

Table 5-7 – Average variation of data from prediction model

Variation in $\Delta^{+}_{R,cr}$	Variation in $\Delta^{-}_{R,cr}$	Variation in $\Delta^{I}_{R,cr}$
±0.039	±0.044	±0.054

In summary, the distribution length for any structure is predicted as follows:

1. Determine the critical deflection ratio as a function of fill height and span for positive and invert moment distribution lengths. (Load reduction by the distribution length for negative moment produces nearly the same results as the distribution length for positive moment. The slight decrease in required area of steel would not be feasible because reinforcing is continuous around the barrel. The prediction equation for determining critical deflection ratios for negative moment distribution length was determined for completeness, but is not expected to be used in practice).
2. Generate a BOEF model that is six times the span in length, using appropriate soil (E_s and v) and structure parameters (E_b, S, and I_b).
3. Apply a factored point load of appropriate magnitude at mid-length of the BOEF model. Do not include self-weight in the analysis.
4. Determine the deflections along the length of the beam.
5. Calculate the deflection ratios along the length of the beam.

6. Determine the distance from mid-span of the beam at which the deflection ratio is equal to the appropriate critical deflection ratio. Use linear interpolation as necessary.
7. Compute the distribution length as twice the value obtained in Step 6.

The ratio (times 100%) of actual to predicted distribution lengths determined using this method is shown in Figure 5-22 and Figure 5-23 as a function of fill height and span, respectively (see also Appendix E). The random pattern of the data points about 100% as a function of fill height in Figure 5-22 is an indication that the equations used for predicting these values are unbiased with respect to fill height. This means that they are not more or less accurate at either end of the fill height domain. However, the pattern of the data points about 100% in Figure 5-23 indicates that these equations provide somewhat better prediction for longer spans. This is because the error increases slightly at shorter spans, and suggests that accurate predictions for spans greater than 40' can be obtained by extrapolation. Nevertheless, the average degree of conservatism or liberality of these predictions is within ± 10% or less. As shown in Figure 5-13, Figure 5-14, and Appendix C, the AASHTO methods for predicting distribution length are nearly always conservative, sometimes up to 300%, or more.

Table 5-8 summarizes the distribution length values predicted by this method using a BOEF spreadsheet and the model parameters indicated in Table 5-4.

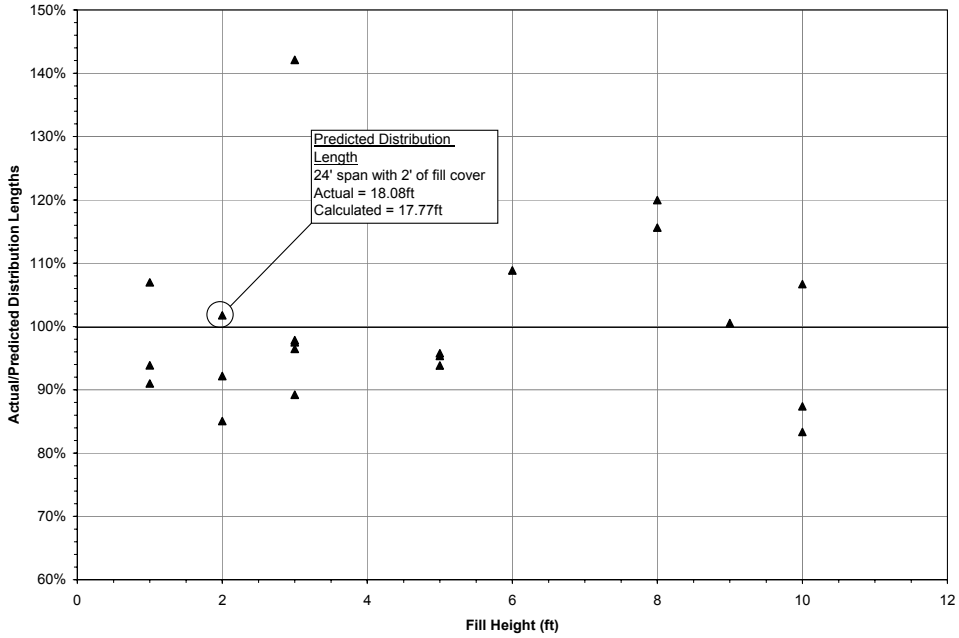

Figure 5-22 – Conservatism of predicted to actual distribution lengths for positive moment as a function of fill height

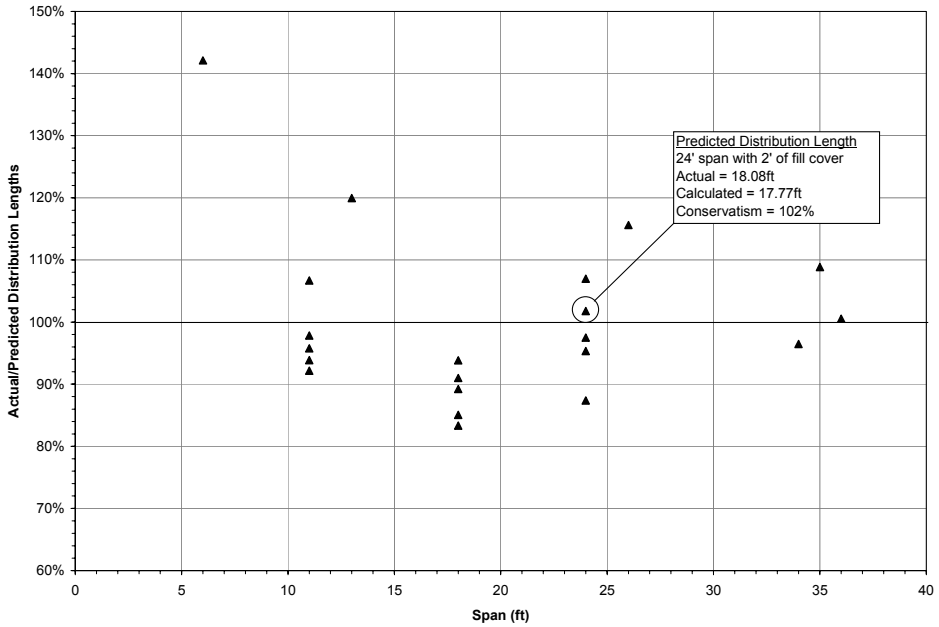

Figure 5-23 – Conservatism of predicted to actual distribution lengths for positive moment as a function of span

Table 5-8 – Distribution lengths predicted by recommended method

Model ($S - H$)	l^+ (ft)	l^- (ft)	l^I (ft)	Model ($S - H$)	l^+ (ft)	l^- (ft)	l^I (ft)
6' – 3'	4.92	5.24	19.73	18' – 10'	28.30	29.94	63.56
11' – 1'	8.62	10.18	40.26	24' – 1'	15.76	19.09	70.79
11' – 2'	9.91	11.26	40.17	24' – 2'	17.77	20.83	70.64
11' – 3'	11.12	12.30	40.10	24' – 3'	19.59	22.50	70.50
11' – 5'	13.31	14.21	39.94	24' – 5'	23.02	25.66	70.01
11' – 10'	18.09	18.52	39.55	24' – 10'	30.99	33.36	69.01
13' – 8'	16.19	16.99	41.27	26' – 8'	23.87	26.08	56.77
18' – 1'	14.08	16.91	64.97	34' – 3'	34.44	40.54	148.15
18' – 2'	15.95	18.51	64.83	35' – 6'	36.67	41.30	111.19
18' – 3'	17.63	20.02	64.66	36' – 9'	38.00	42.15	91.45
18' – 5'	20.83	22.97	64.36				

*Underlined values represent liberality in predictions

where,

S is the model span,
H is the fill height,
l^+ is the distribution length for positive moment,
l^- is the distribution length for negative moment, and
l^I is the distribution length for invert moment.

The plots in Figure 5-24 provide a comparison of computed bending moments in a 2-D FE model arch ring for an 18' span arch with three feet of fill using a) no load reduction, b) 1996 AASHTO prescribed positive moment distribution length, and c) proposed distribution length for positive moment, to 3-D FE analysis results.

Figure 5-24 shows that the proposed reduction method provides the best reconciliation between 2-D and discrete 3-D loading. The plots in Figure 5-24 also clearly show the need for reducing the load from a 2-D analysis to avoid large errors in predicting moment. Results for lower fill heights show a greater difference between reduction methods and higher fill cover brings the reduction methods into closer agreement (see Figure 4-5 and Appendix B for variation in bending moment using AASHTO methods as a function of fill height). Using the proposed method, structural forces can be reduced anywhere from 0% to 200$^+$% from those obtained using AASHTO

methods, depending on span and fill height. Figure 5-25 shows a similar comparison for shear forces. The proposed method again provides the most accurate results.

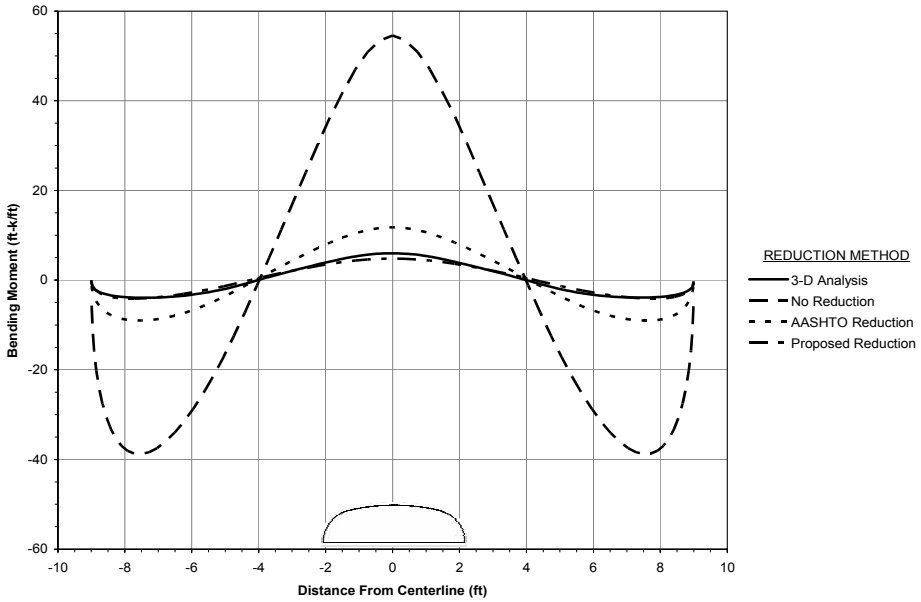

Figure 5-24 – Bending moment comparison for an 18' span arch ring with three feet of fill using various reduction methods

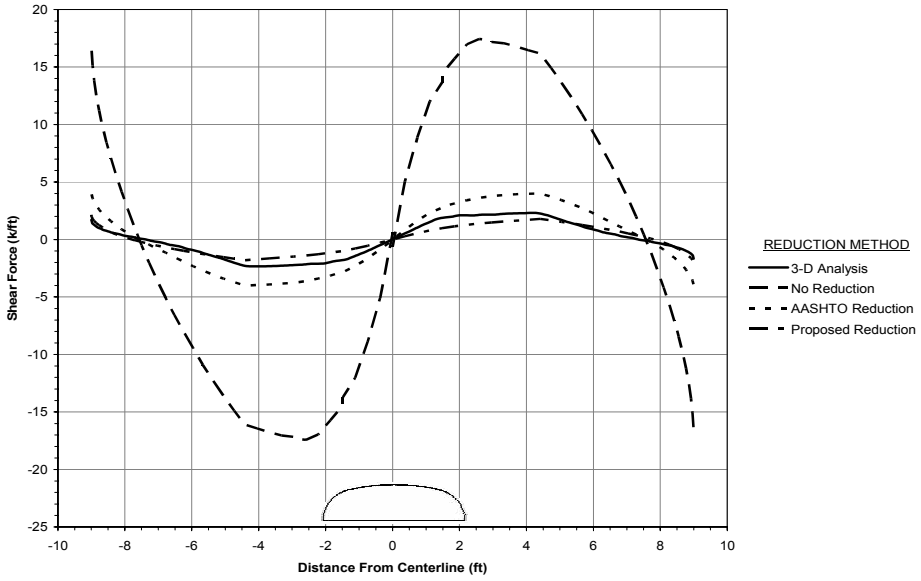

Figure 5-25 – Shear force comparison for an 18' span arch ring with three feet of fill using various reduction methods

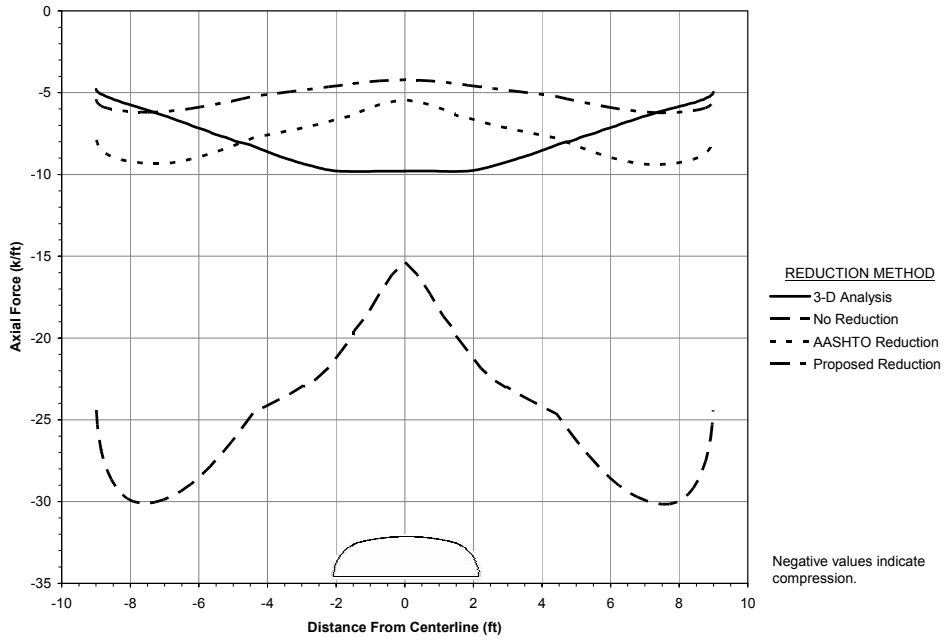

Figure 5-26 – Axial force comparison for an 18' span arch ring with three feet of fill using various reduction methods

Figure 5-26 provides similar plots of computed axial force. There is, however, a significant discrepancy between the location of maximum axial force caused by continuous and discrete loading within the arch ring. The effects of discrete loading at low fill heights cause the axial force to be greater at the crown than at the haunches. This difference in location of maximum axial force – at the crown for discrete loading and at the haunches for continuous loading – is evidence of longitudinal load dissipation. Strain energy density is greatest directly below a discrete load and dissipates as distance from the point of application increases. In the case of continuous loading, energy cannot dissipate in the longitudinal direction, and therefore, axial forces will increase as the arch becomes more vertical and more energy is transferred through axial strains, rather than bending. For this case then, reduction per the proposed distribution length

underestimates the axial force in the crown in comparison to the AASHTO distribution length, but provides better estimates at the haunch.

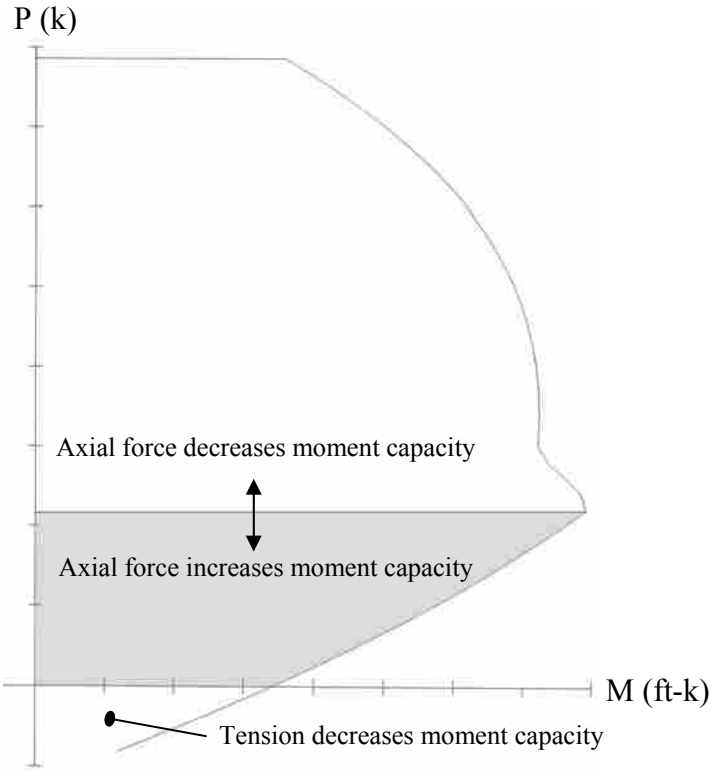

Figure 5-27 – Effects of axial force on moment capacity

The axial forces in the ring are typically similar or smaller in the 2-D model than in the 3-D discrete load model (see Appendix F and Figure 5-28). In design of the arch ring, interaction typically falls within the region where axial forces mitigate tension caused by bending moments (see Figure 5-27 – shaded area). In this case, under-prediction results in slight design conservatism. Further, even under large fill heights (**>**40*ft*), crushing is not a concern, so this under-prediction will not lead to unexpected crushing failure. For these reasons, further inquiry will not be made in this research to attempt to rectify the axial forces in the arch ring. As has been shown, sufficient

rectification has been provided for shear forces and bending moment to result in a more economically designed structure overall. It should be noted, however, that a high concentration of force directly below the load may result in local buckling, similar to non-compact steel sections under high force concentrations. The designer should be aware of this issue, as well as punching shear (see Figure 5-8, where most of the load is resisted through shear forces), when low fill cover is provided. Determination of compactness criteria would help provide assurance against local buckling failure, but is outside the scope of this research.

The overburden is effectively a continuous load, thus at higher fill covers, where live load no longer governs, this axial force discrepancy no longer exists, as shown in Figure 5-28. This suggests that the magnitude of axial forces around the barrel of the arch is not merely a function of the load magnitude, but also the load type. Figure 5-29 compares axial forces in a 2-D FE model of an 18' span arch ring with three feet of fill for varying load magnitudes. Under 2-D/continuous loading, the axial forces are always greater at the haunches, no matter the magnitude of the load.

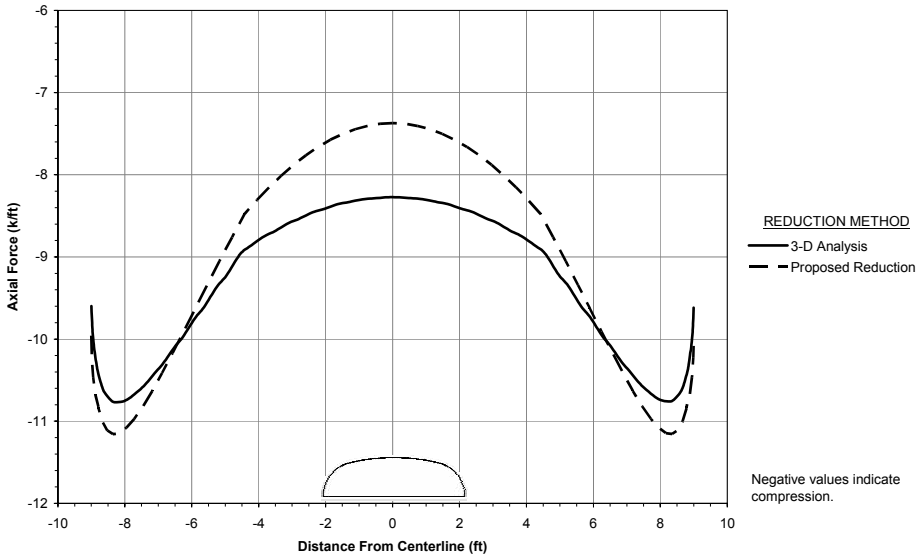

Figure 5-28 – Axial force comparison for an 18' span arch ring with ten feet of fill using proposed distribution length for positive moment and 3-D FE analysis

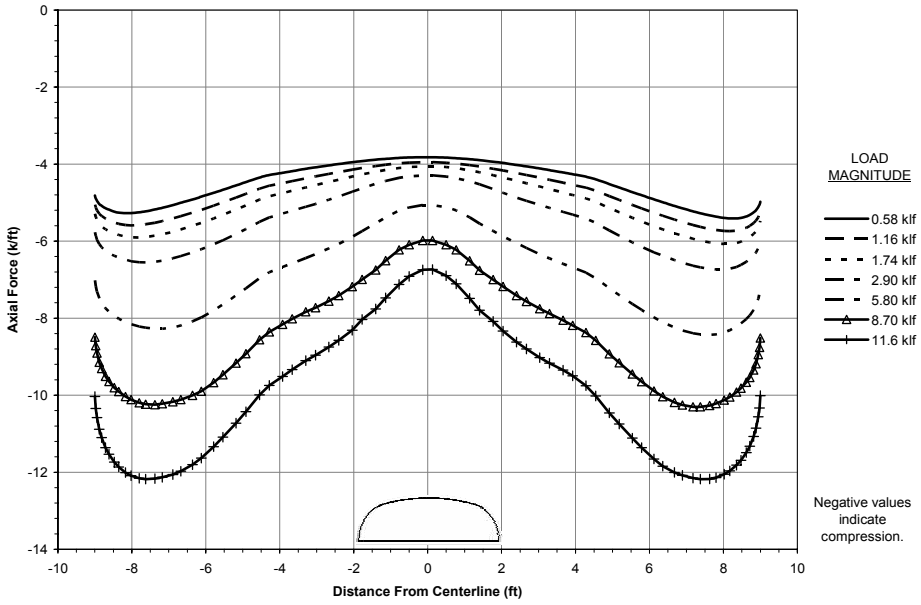

Figure 5-29 – Axial force as a function of 2-D/continuous load magnitude for an 18' span arch ring with three feet of fill

The plots in Figure 5-30 to Figure 5-32 provide a comparison of computed structural forces in a 2-D FE model invert for an 18' span arch with three feet of fill using a) no load reduction, b) 1996 AASHTO prescribed distribution length for negative moment, and c) proposed distribution length for invert moment, to 3-D FE analysis results. The results of c) are not easily visible because they lie nearly directly below the 3-D analysis results for the bending moment and shear force cases.

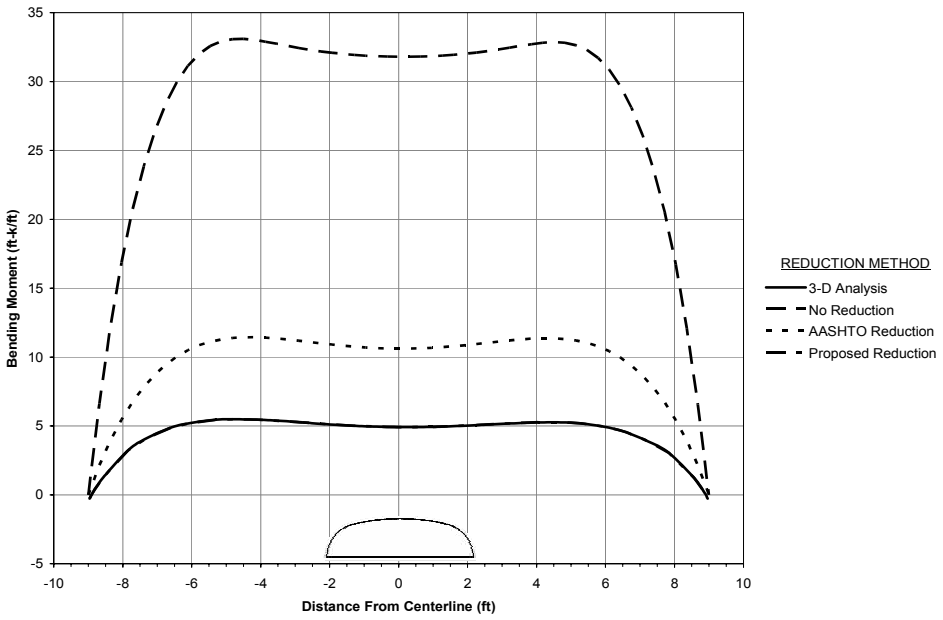

Figure 5-30 - Bending moment comparison for an 18' span invert with three feet of fill using various reduction methods

These plots show that the proposed reduction method provides the best reconciliation between 2-D and discrete 3-D loading. Results for lower fill heights show a greater difference between reduction methods and higher fill cover brings the reduction methods into closer agreement (see Figure 4-6 and Appendix B for variation in invert bending moment using AASHTO methods as a function of fill height). Using the

proposed method, shear forces and bending moment can be reduced in the invert anywhere from 0% to 275^{+}% from those obtained using AASHTO methods, depending on span and fill height.

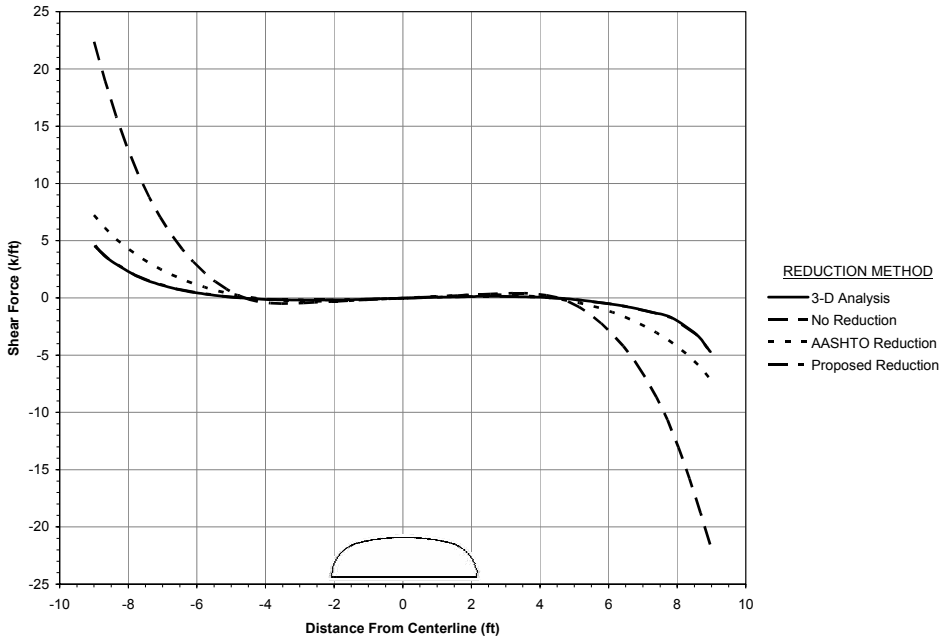

Figure 5-31 – Shear force comparison for an 18' span invert with three feet of fill using various reduction methods

The determination of axial forces in the invert, using the distribution length for invert moment to reduce the load, results in lower forces than those obtained using 3-D analysis (see Figure 5-32). However, where axial forces are tensile, as is the case for the invert, under-prediction leads to a non-conservative design. For this reason, the Author recommends that the axial forces obtained from 2-D analysis using distribution length for positive moment be multiplied by a factor of 1.3 until further procedures for reconciling axial forces are developed. This factor will result in axial forces that are slightly conservative.

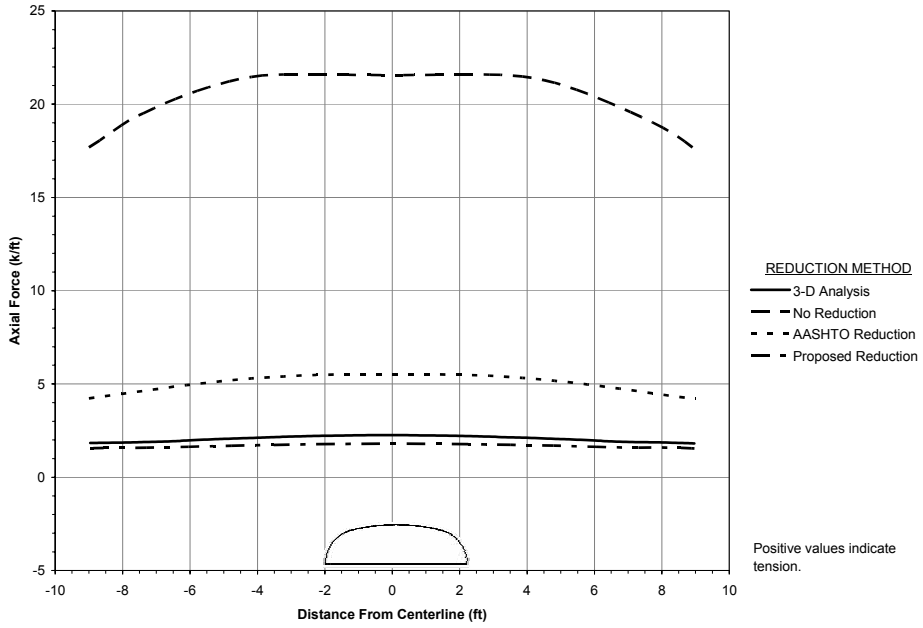

Figure 5-32 – Axial force comparison for an 18' span invert with three feet of fill using various reduction methods

5.5 Example of Obtaining Distribution Length Using BOEF Analysis

The following example illustrates how to obtain distribution lengths for an 18' span arch model with 3' of fill using the proposed method.

1. Determine the critical deflection ratios for $S = 18ft$ and $H = 3ft$. Distribution length for negative moment will be computed for completeness.

$$\Delta^{+}_{R,cr} = 1.049 - (2.319 + 0.396 \times 3\,ft)(0.020 + 0.002 \times 18\,ft) = 0.884$$

$$\Delta^{-}_{R,cr} = 1.053 - (4.694 + 0584 \times 3\,ft)(0.011 + 0.001 \times 18\,ft) = 0.857$$

$$\Delta^{I}_{R,cr} = 1.856 + (-0.014 + 0.0001 \times 3\,ft)(89.250 + 1.074 \times 18\,ft) = 0.327$$

2. Create a BOEF model that is six times the span long, using the appropriate soil and structure parameters.

$$L = 108ft \qquad I_b = 935ft^4 \qquad k' = 710kcf$$

3. Apply an HL-93 point load with appropriate impact and load factors at mid-length of the beam. Do not include self-weight in the analysis.

$$F = 16k \times 2.17 \times 1.1 = 38.192k$$

(1.1 is the impact factor and $2.17 = 1.3 \times 1.67$ are load factors)

4. Determine the deflections along the length of the beam.

See Table 5-9

5. Calculate the deflection ratios along the length of the beam.

Table 5-9 shows the values obtained from a BOEF spreadsheet program as well as the deflection ratios at each point for half of the model length. The other half of the model is symmetrical.

Table 5-9 – Example BOEF deflection values and deflection ratios

x (ft)	δ x 100	$\Delta_{R,i}$	x (ft)	δ x 100	$\Delta_{R,i}$	x (ft)	δ x 100	$\Delta_{R,i}$
0.00	-0.0009	100.0%	18.36	-0.0005	64.6%	36.72	-0.0001	25.2%
1.08	-0.0009	99.7%	19.44	-0.0005	61.9%	37.80	-0.0001	23.4%
2.16	-0.0009	99.1%	20.52	-0.0005	59.2%	38.88	0.0000	21.7%
3.24	-0.0009	98.1%	21.60	-0.0004	56.4%	39.96	0.0000	20.0%
4.32	-0.0009	96.8%	22.68	-0.0004	53.8%	41.04	0.0000	18.4%
5.40	-0.0009	95.1%	23.76	-0.0004	51.2%	42.12	0.0000	16.7%
6.48	-0.0009	93.3%	24.84	-0.0003	48.8%	43.20	0.0000	15.1%
7.56	-0.0008	91.2%	25.92	-0.0003	46.3%	44.28	0.0001	13.6%
8.64	**-0.0008**	**88.9%**	27.00	-0.0003	43.9%	45.36	0.0001	12.0%
9.72	**-0.0008**	**86.5%**	28.08	-0.0003	41.5%	46.44	0.0001	10.5%
10.80	**-0.0008**	**83.9%**	29.16	-0.0002	39.3%	47.52	0.0001	9.0%
11.88	-0.0007	81.4%	30.24	-0.0002	37.1%	48.60	0.0001	7.4%
12.96	-0.0007	78.7%	31.32	-0.0002	34.9%	49.68	0.0002	6.0%
14.04	-0.0007	75.9%	**32.40**	**-0.0002**	**32.9%**	50.76	0.0002	4.4%
15.12	-0.0006	73.1%	**33.48**	**-0.0001**	**30.9%**	51.84	0.0002	3.0%
16.20	-0.0006	70.3%	34.56	-0.0001	28.9%	52.92	0.0002	1.5%
17.28	-0.0006	67.5%	35.64	-0.0001	27.1%	54.00	0.0002	0.0%

*Bold values represent those between which critical deflection ratios fall

where

x is the distance from mid-length of the BOEF model,
δ is the deflection of the BOEF model in *in*, and
$\Delta_{R,i}$ is the deflection ratio at point i.

6. Determine the distance from mid-span of the beam at which the deflection ratio is equal to the appropriate critical deflection ratio. Use linear interpolation as necessary.

   From Table 5-9, the distribution lengths have been determined to be between the values listed in Table 5-10.

Table 5-10 – Example interpolation values for determining distribution lengths

½ l^+ interpolation values (ft)		½ l^- interpolation values (ft)		½ l^I interpolation values (ft)	
Above actual	Below actual	Above actual	Below actual	Above actual	Below actual
8.64	9.72	9.72	10.80	33.48	32.40

where
l^+ is the positive moment distribution length,
l^- is the negative moment distribution length, and
l^I is the invert moment distribution length.

Linearly interpolating between these computed values will give the prediction for half of the distribution length.

$$\frac{l^+}{2} = \left(\frac{0.884 - 0.865}{0.889 - 0.865}\right)(8.64\,ft - 9.72\,ft) + 9.72\,ft = 8.87\,ft$$

$$\frac{l^-}{2} = \left(\frac{0.857 - 0.840}{0.865 - 0.840}\right)(9.72\,ft - 10.80\,ft) + 10.80\,ft = 10.08\,ft$$

$$\frac{l^I}{2} = \left(\frac{0.327 - 0.309}{0.329 - 0.309}\right)(32.40\,ft - 33.48\,ft) + 33.48\,ft = 32.49\,ft$$

7. Compute the distribution length as twice the value obtained in Step 6.

$$l^+ = 2 \times 8.87\,ft = 17.73\,ft$$

$$l^- = 2 \times 10.08\,ft = 20.15\,ft$$

$$l^I = 2 \times 32.49\,ft = 64.98\,ft$$

will be used to predict them. Three equations will be developed for predicting critical deflection ratios for positive, negative, and invert moment distribution lengths. The coefficients *a*, *b*, *c*, *d*, and *e* were obtained using the FindFit function in Mathematica for all data points. The following equations were determined to best represent the critical deflection ratios within the domains of $1ft \le H \le 10ft$ and $6ft \le S \le 40ft$:

$$\Delta^{+}_{R,cr} = 1.049 - (2.319 + 0.396H)(0.020 + 0.002S) \quad \textbf{(5-10)}$$

$$\Delta^{-}_{R,cr} = 1.053 - (4.694 + 0584H)(0.011 + 0.001S) \quad \textbf{(5-11)}$$

$$\Delta^{I}_{R,cr} = 1.856 + (-0.014 + 0.0001H)(89.250 + 1.074S) \quad \textbf{(5-12)}$$

where

S is the model span,

H is the fill height,

$\Delta^{+}_{R,cr}$ is the critical deflection ratio for positive moment distribution length,

$\Delta^{-}_{R,cr}$ is the critical deflection ratio for negative moment distribution length, and

$\Delta^{I}_{R,cr}$ is the critical deflection ratio for invert moment distribution length.

Predictions for fill heights greater than ten feet will be limited to those obtained at $H = 10ft$, since the live load plays a less important role with large fill heights. This will also help eliminate inaccuracies that could arise from being outside the domain upon which the equations are based. Table 5-6 summarizes the critical deflection ratio values predicted by these equations.

6 Conclusions and Recommendations

Twenty-one finite element models of buried concrete arches with varying spans and fill covers were created and analyzed in Plaxis 3-D Tunnel to best represent spans between six to 40 feet and fill heights from one to ten feet. Distribution lengths were determined from these FE analyses using the bending energy method. Corresponding beam-on-elastic-foundation analyses were carried out using soil and structure properties representative of these buried arch models. A correlation was determined between critical percentages of BOEF deflection and distribution lengths for positive, negative, and invert moments. Where the AASHTO prescribed distribution lengths are up to 300^{+}% greater than calculated values, these predictions are, on average, within ±10% (well within the degree of accuracy of the soil and structure parameters and load magnitude). The results provide an accurate method of rectification of 2-D to discrete 3-D loading, such that the resulting bending moments and shear forces are nearly equivalent between 2-D and 3-D FE analyses. In summary:

- Using the methods developed herein, shear forces and bending moments within the arch ring and invert obtained from a 2-D FE analysis can be rectified in such a manner that they are nearly equal to those obtained in more accurate 3-D analysis under discrete loading. This is accomplished

by dividing the 2-D load by a load distribution length. Distribution lengths are different for positive, negative, and invert bending moments.

- Axial forces obtained from 2-D FE analysis using the methods proposed by this research are generally similar to or less than axial forces obtained from 3-D FE analysis under discrete loading. This results in an accurate to conservative design for the arch ring and an accurate to non-conservative design for the invert. It is recommended that the distribution length for positive moment be used to predict invert axial forces to eliminate this non-conservatism.
- Two-dimensional analysis fails to correctly predict axial forces in a buried concrete arch under discrete loading, no matter the magnitude of the load.

6.1 Implementation of Results

The proposed methods were developed specifically for structures spanning 40*ft* or less; however, accuracy of the model appears to increase with increasing span, therefore, using this method for greater spans (within reason) will still likely produce accurate results. It is recommended that these procedures be employed in all 2-D FE analyses of buried arch structures exhibiting characteristics similar to those for which this research was designed (*i.e.* small- to medium-span buried concrete arches longer than four times the span).

The correlations made have been shown to accurately rectify the design shear forces and bending moments obtained from 2-D FE analysis to those obtained using 3-D

analysis. There arises, however, a discrepancy in the prediction of axial forces in both the arch ring and invert. The recommended application of this research in practice is shown in Table 6-1.

Table 6-1 – Recommended use of distribution lengths for load reduction

Reduction Method	ARCH RING FORCES			INVERT FORCES		
	Moment	Shear	Axial	Moment	Shear	Axial
l^+	X	X	X			
l^- [(a)]						
l^I				X	X	X[(b)]

a. The derivation and determination of the negative moment distribution length was done for completeness; it is not expected to be used in practice.

b. Axial forces obtained from 2-D analysis using l^I are to be multiplied by a factor of 1.3.

where

l^+ is the distribution length for positive moment,
l^- is the distribution length for negative moment, and
l^I is the distribution length for invert moment.

A design example of an 18' span arch with one foot of fill using 1996 AASHTO methods and the method proposed in this research is provided in Appendix G for comparison.

6.2 Recommendations for Future Studies

In doing this research, additional research opportunities have been identified by the Author. The following outlines recommendations for future studies in these areas:

- Many buried structures exhibit behavior similar to that shown by semi-flexible concrete arches in this research. It is recommended that experiments be performed following the same general approach for box culverts, reinforced concrete pipe, corrugated metal pipe, plastic pipe, and

like structures to develop similar design methods as those developed herein for buried arches.

- A discrepancy arises in axial forces in the arch ring caused by point and continuous loads which is not solely a result of force magnitude. Development of procedures for eliminating these axial force discrepancies and development of compactness criteria to avoid local buckling under low fill covers would benefit designers.
- This research provides methods which are highly automatable and would require relatively little computational effort. Therefore, implementation of these and future results for similar structures into 2-D finite element code developed specifically for analysis of buried arches, RCP, CMP, boxes, etc., could provide another breakthrough in ease of application and accuracy of FE analysis.

References

AASHTO LRFD bridge design specifications. (1996). Washington, D.C.: American Association of State Highway and Transportation Officials - AASHTO, 2nd Ed.

AASHTO LRFD bridge design specifications. (1998). Washington, D.C.: American Association of State Highway and Transportation Officials - AASHTO, 2nd Ed.

Bacher, A.E. & Klein, E.G. Jr. (1980). "Reinforced-concrete arch culvert research by the California department of transportation." *Transportation Research Record*, 33-36.

Boothby, T.E., Domalik, D.E., & Dalal, V.A. (1998). "Service load response of masonry arch bridges." *Journal of Structural Engineering*, 124(1), 17-23.

Clemente, P., Occhiuzzi, A., & Raithel, A. (1995). "Limit behavior of stone arch bridges." *Journal of Structural Engineering*, 121(7), 1045-1050.

Heyman, J. (1982). The masonry arch. Chichester: E. Horwood and New York: Halsted Press.

Katona, M.G., Meinhert, D.F., Orillac, R., & Lee, C.H. (1979). "Structural Evaluation of New Concepts for Long-Span Culverts and Culvert Installations." Report No. FHWA-RD-79-115. Washington, D.C: Federal Highway Administration.

Luscher, U. & Höeg, K. (1964). "The beneficial action of the surrounding soil on the load-carrying capacity of buried tubes." *Proceedings, Symposium of Soil-Structure Interaction*, Univ. of Arizona, Tucson, AZ, 393-402.

Loo, Y. & Yang, Y. (1991). "Cracking and failure analysis of masonry arch bridges." *Journal of Structural Engineering*., 117(6) 1641-1659.

Masada, T. (2000). "Modified Iowa formula for vertical deflection of buried flexible pipe." *Journal of Transportation Engineering*, 126(5), 440-446.

McGrath, T.J., Liepins, A.A., & Beaver, J.L. (2005). "Live load distribution widths for reinforced concrete box sections." *Transportation Research Board - 6th*

International Bridge Engineering Conference: Reliability, Security, and Sustainability in Bridge Engineering, 99-108.

McGrath, T.J. & Mastroianni, E.P. (2002). "Finite-element modeling of reinforced concrete arch under live load." *Transportation Research Record*, 1814, 203-210.

McGrath, T.J., Moore, I.D., Selig, E.T., Webb, M.C., & Taleb, B. (2002). "Recommended Specifications for Large-Span Culverts." *NCHRP Report 473, Transportation Research Board, National Research Council*. Washington, DC: National Academy Press.

Miller, A.B., Clark, K.M., & Grimes, M.C. (2000). "A survey of masonry and concrete arch bridges in Virginia." Virginia transportation research council, report VTRC 00-R11.

Montgomery, C.J., Morison, R.M., Channon, J.R., & Tutty, D.O. (1993). "Design and construction of a buried precast prestressed concrete arch." *PCI Journal*, 38(1), 40-57.

Shen, H.S. (2000). "Nonlinear bending of simply supported rectangular Reissner-Mindlin plates under transverse and in-plane loads and resting on elastic foundations." *Engineering Structures*, 22(7), 847-856.

Simpson Grumpertz & Heger, Inc. (2001). Evaluation of the con-arch reinforced concrete buried arch system. ASCE.

Smeltzer, P.D. & Daigle, L. (2005). "Field performance of a concrete pipe culvert installed using standard installations." *Proceedings: First Canadian Conference on Effective Design of Structures, Hamilton, Ont.*, 591-601.

Tufekci, E. & Dogruer, O.Y. (2006). "Exact solution of out-of-plane problems of an arch with varying curvature and cross section." *Journal of Engineering Mechanics*, 132(6), 600-609.

Vesic, A.S. (1961). "Bending of beams resting on isotropic solid." *Journal of the Engineering Mechanics Division*, ASCE, 87(EM2), 35-53.

Yang, M.Z., Drumm, E.C., Bennett, R.M., & Mauldon, M. (1999). "Measurement of earth pressures on concrete box culverts under highway embankments." *ASTM Special Technical Publication*, 1358, 97-100.

Appendix A. Moment Dissipation and Magnitude Differences

This appendix supplements Figure 4-2 and Figure 4-3.

Figure A-1 and Figure A-2 show that the moment dissipates nearly the same in an 11' and 24' span arch ring with one foot of fill cover as it does in a plate with an equal span and section properties and no fill cover. See also Figure 4-2.

Figure A-3 and Figure A-4 show that the magnitude of the moments is much less in an 11' and 24' span arch ring with one foot of fill cover than in a plate with an equal span and section properties and no fill cover. See also Figure 4-3.

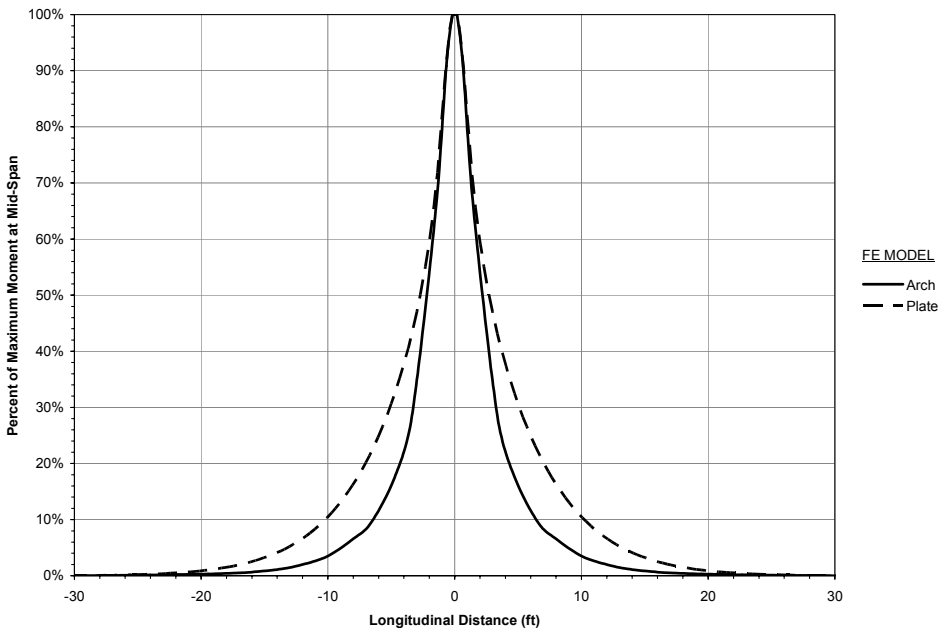

Figure A-1 – Percent of maximum moment at the crown/mid-span as a function of longitude for an 11' span arch ring with one foot of fill and a similar plate with no fill

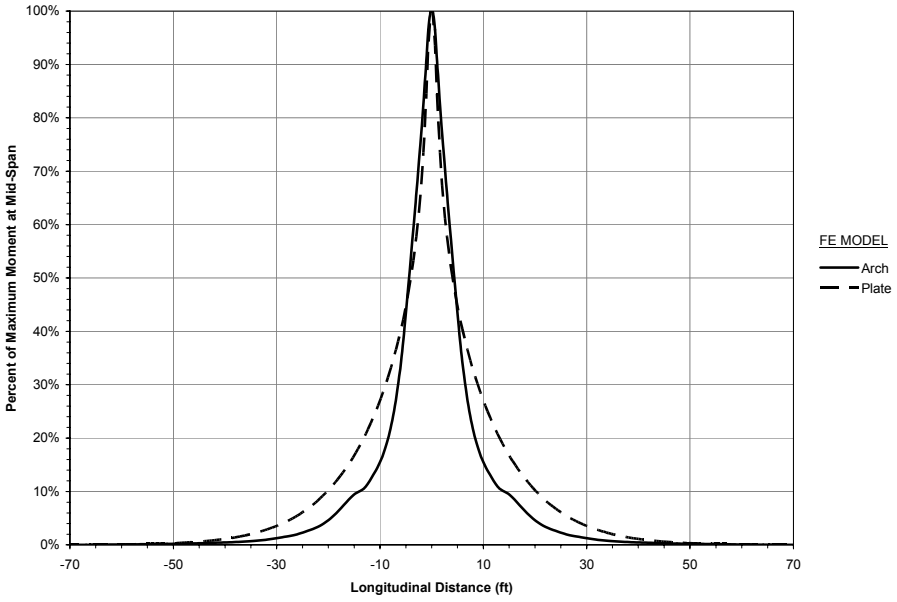

Figure A-2 – Percent of maximum moment at the crown/mid-span as a function of longitude for a 24' span arch ring with one foot of fill and a similar plate with no fill

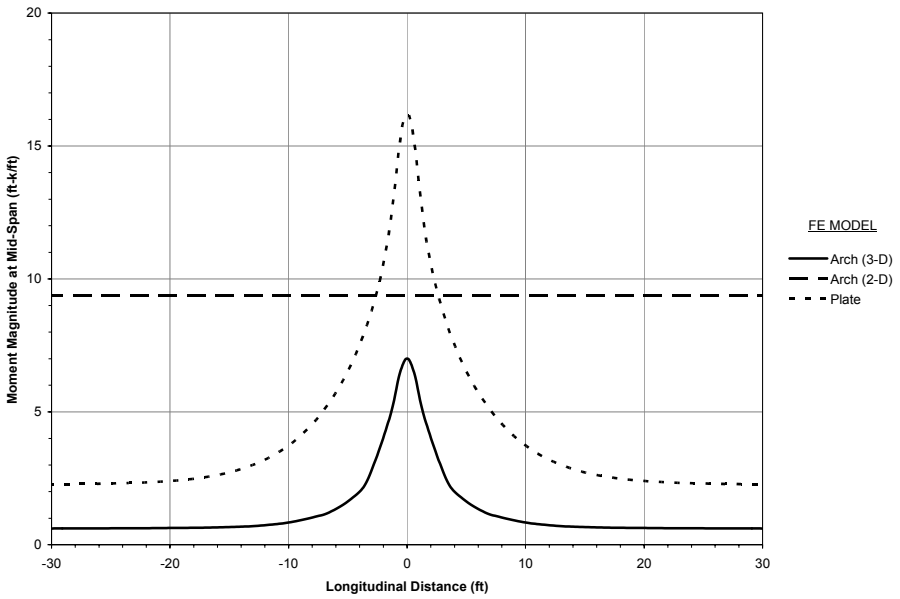

Figure A-3 – Moment magnitude at the crown/mid-span as a function of longitude for an 11' span arch ring with one foot of fill and a similar plate with no fill

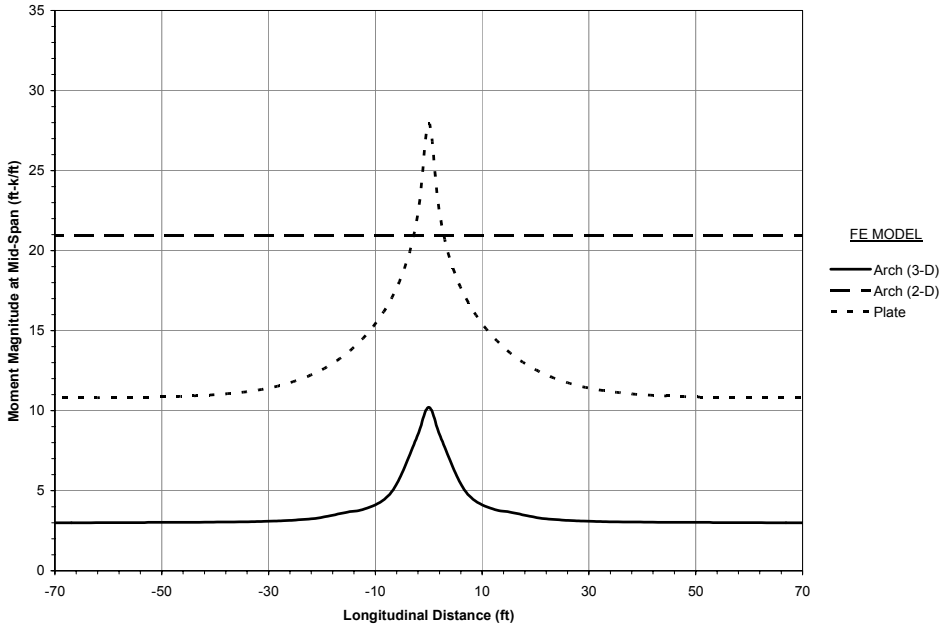

Figure A-4 – Moment magnitude at the crown/mid-span as a function of longitude for a 24' span arch ring with one foot of fill and a similar plate with no fill

Appendix B. Effects of Fill Height on AASHTO Conservatism

This appendix supplements Figure 4-5 and Figure 4-6.

Figure B-1 to Figure B-4 show that with increasing fill heights the current AASHTO provisions become increasingly more accurate for the arch ring. See also Figure 4-5.

Figure B-5 to Figure B-8 show that with increasing fill heights, the current AASHTO provisions also become increasingly more accurate for the invert. See also Figure 4-6.

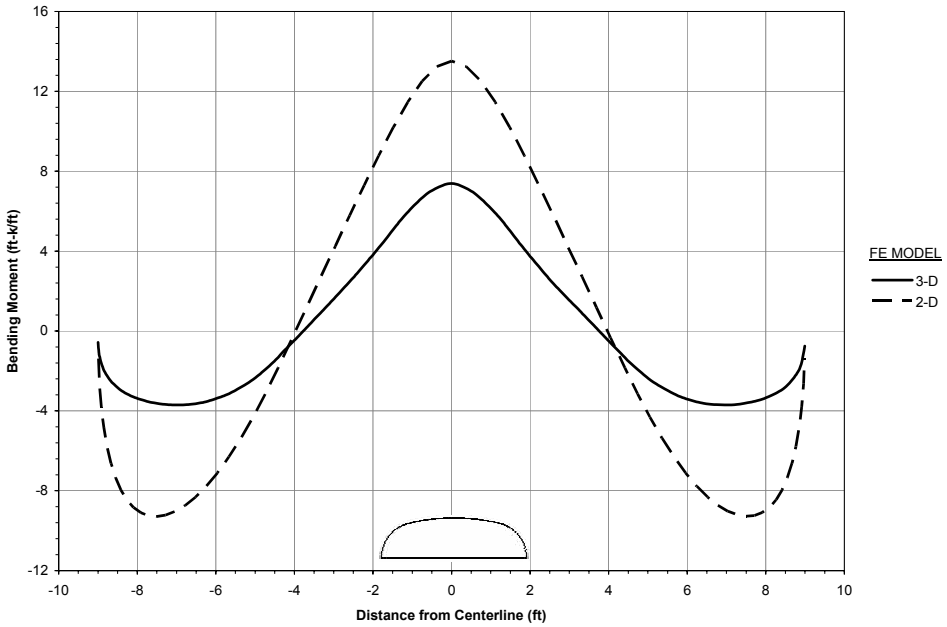

Figure B-1 – Comparison of 2-D and 3-D moment results in the plane of loading for an 18' span arch ring with two feet of fill

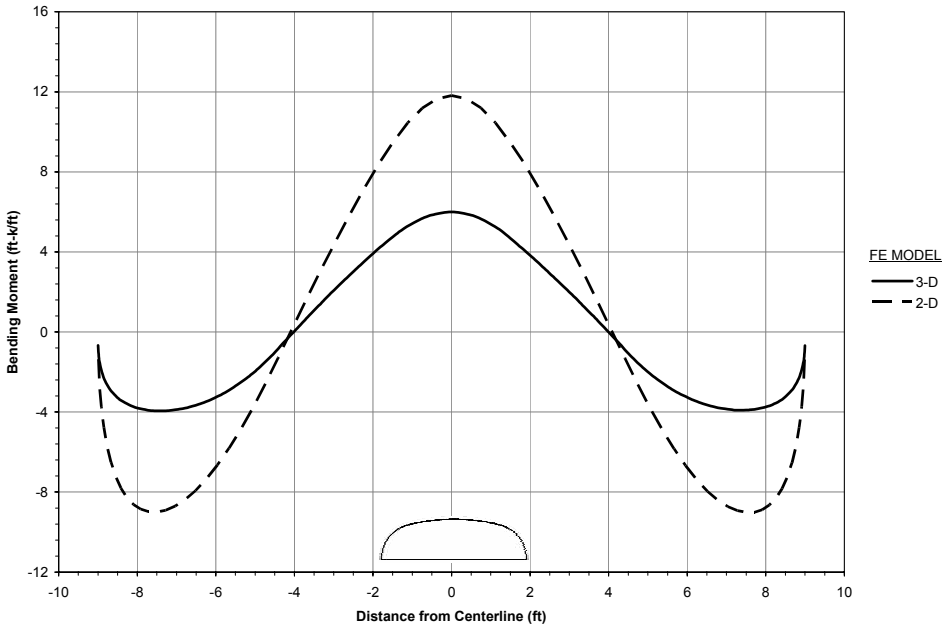

Figure B-2 – Comparison of 2-D and 3-D moment results in the plane of loading for an 18' span arch ring with three feet of fill

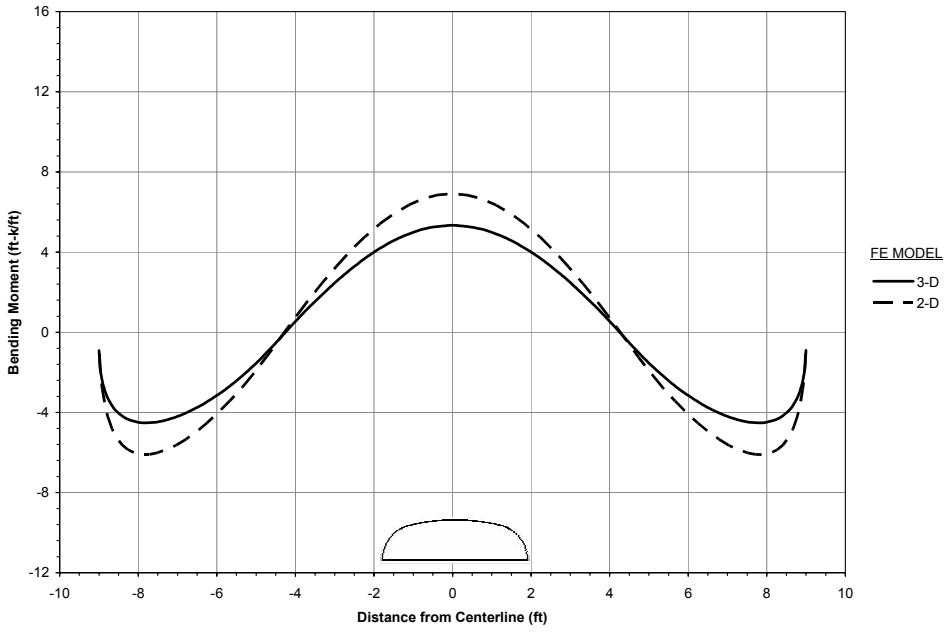

Figure B-3 – Comparison of 2-D and 3-D moment results in the plane of loading for an 18' span arch ring with five feet of fill

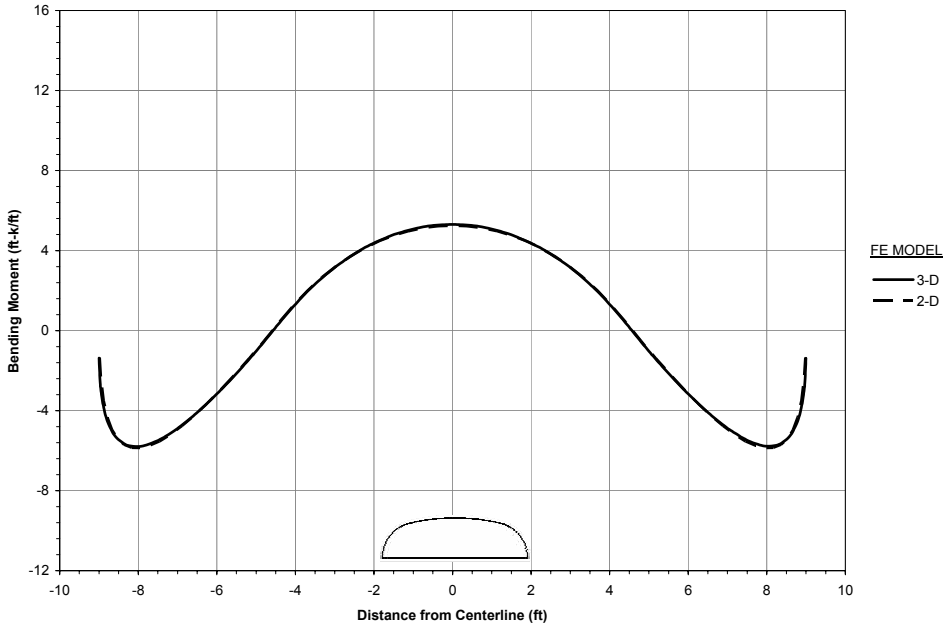

Figure B-4 – Comparison of 2-D and 3-D moment results in the plane of loading an 18' span arch ring with ten feet of fill

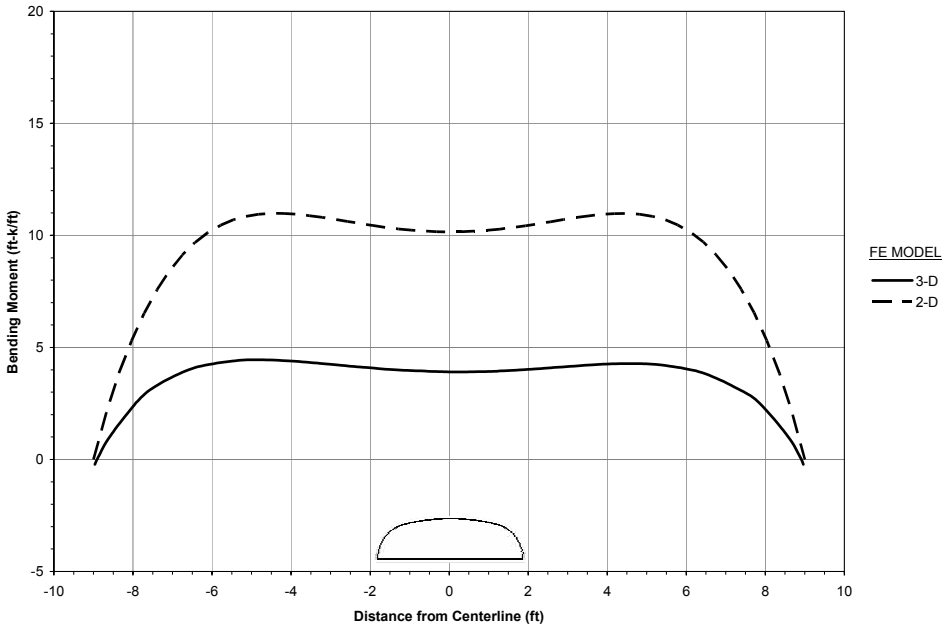

Figure B-5 – Comparison of 2-D and 3-D moment results in the plane of loading for an 18' span arch invert with two feet of fill

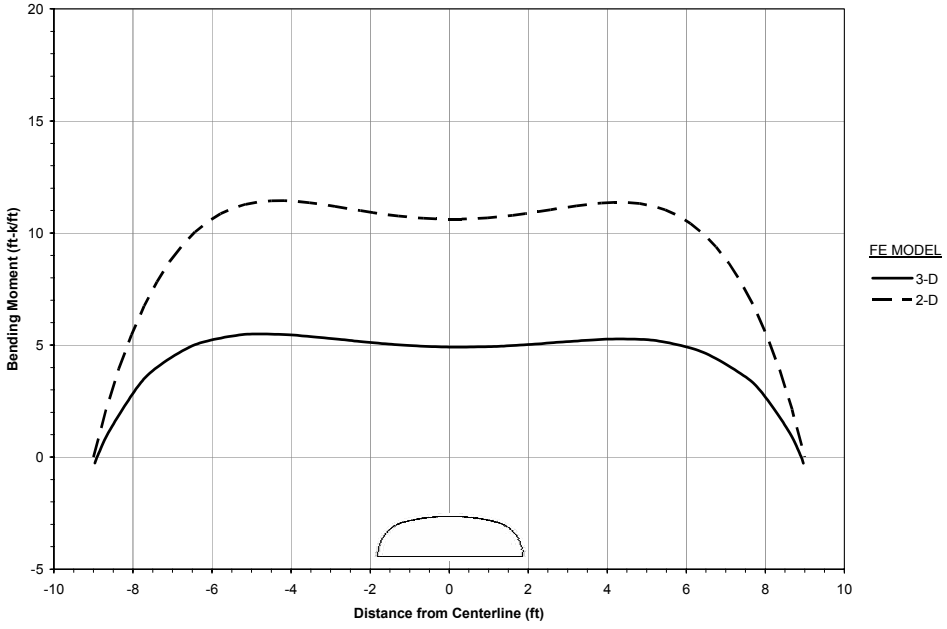

Figure B-6 – Comparison of 2-D and 3-D moment results in the plane of loading for an 18' span arch invert with three feet of fill

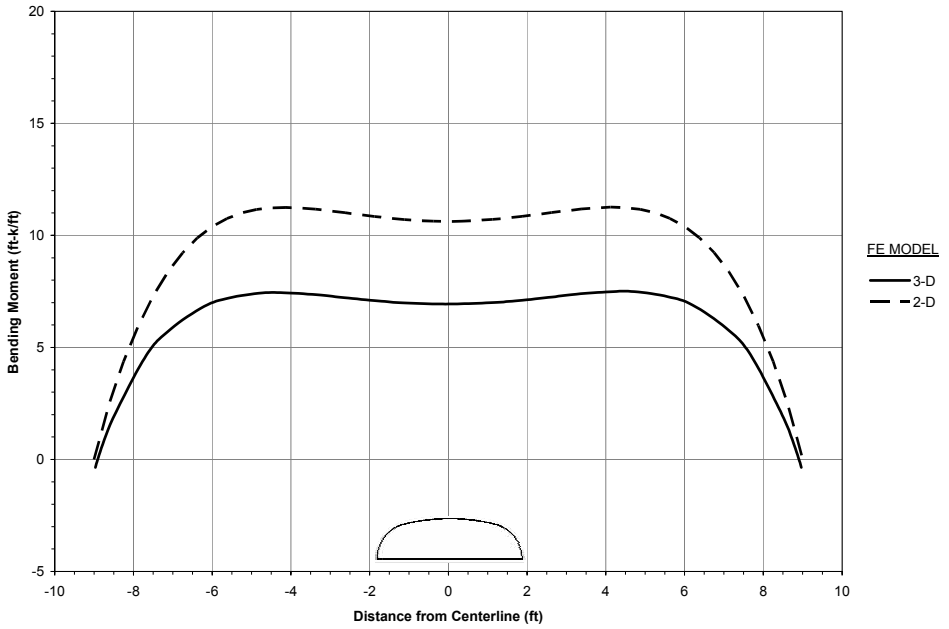

Figure B-7 – Comparison of 2-D and 3-D moment results in the plane of loading for an 18' span arch invert with five feet of fill

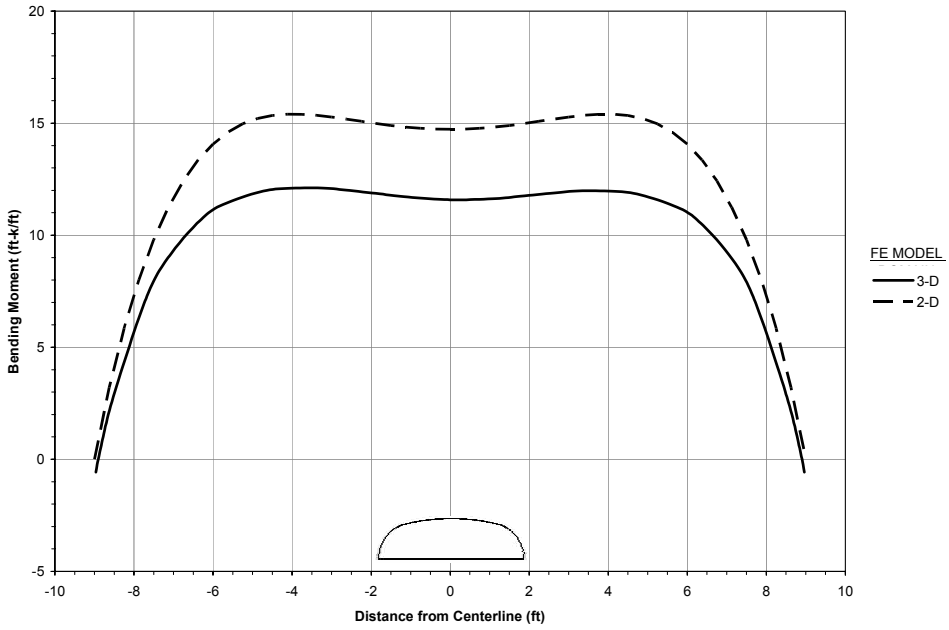

Figure B-8 – Comparison of 2-D and 3-D moment results in the plane of loading for an 18' span arch invert with ten feet of fill

Appendix C. Conservatism of AASHTO Provisions

This appendix supplements Figure 5-13 through Figure 5-16.

Figure C-1 shows the relationship between span and conservatism of current AASHTO distribution length provisions for negative moment. It is clear that the code is much more conservative for larger spans. See also Figure 5-13 and Figure 5-15.

Figure C-2 shows the relationship between fill height and conservatism of current AASHTO distribution length provisions for negative moment. The code is much more conservative for low fill heights. See also Figure 5-14 and Figure 5-16.

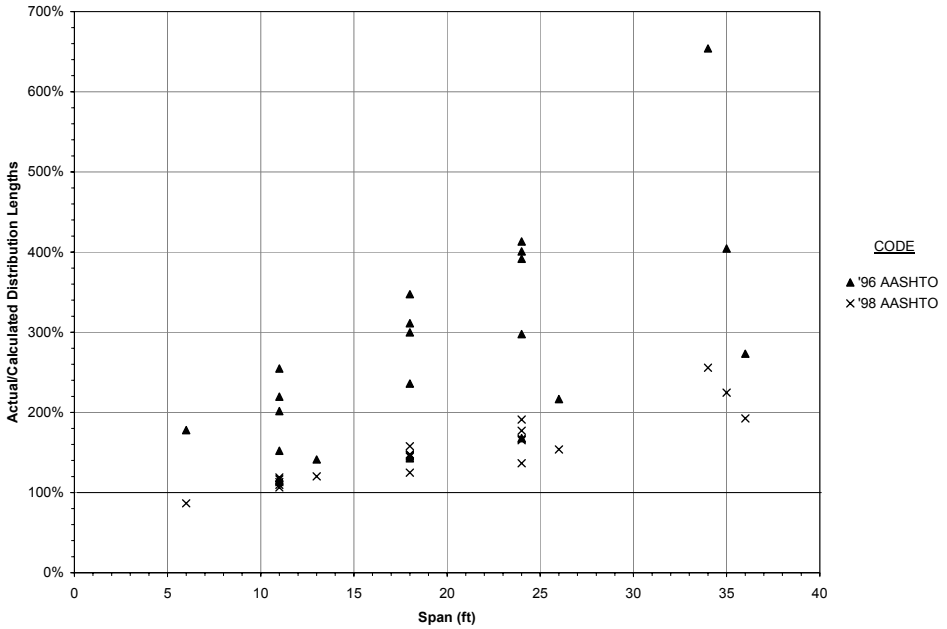

Figure C-1 – Conservatism of AASHTO computed distribution lengths for negative moment for varying fill covers as a function of span

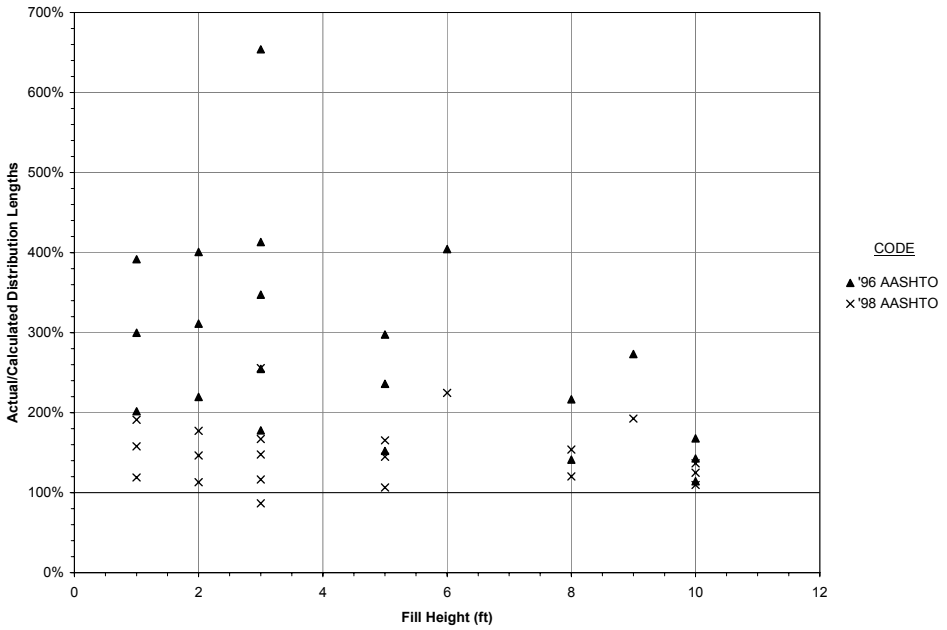

Figure C-2 – Conservatism of AASHTO computed distribution lengths for negative moment for varying spans as a function of fill cover

Appendix D. Critical Deflection Ratios

The following appendix supplements Figure 5-19 to Figure 5-21.

Figure D-1 to Figure D-4 show relationships between deflection ratio and distribution length for a 24’ model with varying fill heights. See also Figure 5-19.

Figure D-5 and Figure D-6 show the relationship between critical deflection ratios for 11’ and 18’ span FE and BOEF models. See also Figure 5-20.

Figure D-7 and Figure D-8 show that this relationship is similar for negative and invert critical deflection ratios for an 18’ span arch.

Figure D-9 and Figure D-10 show the correlation between the span, fill height, and critical deflection ratios for negative and invert moment distribution lengths for BOEF models. See also Figure 5-21.

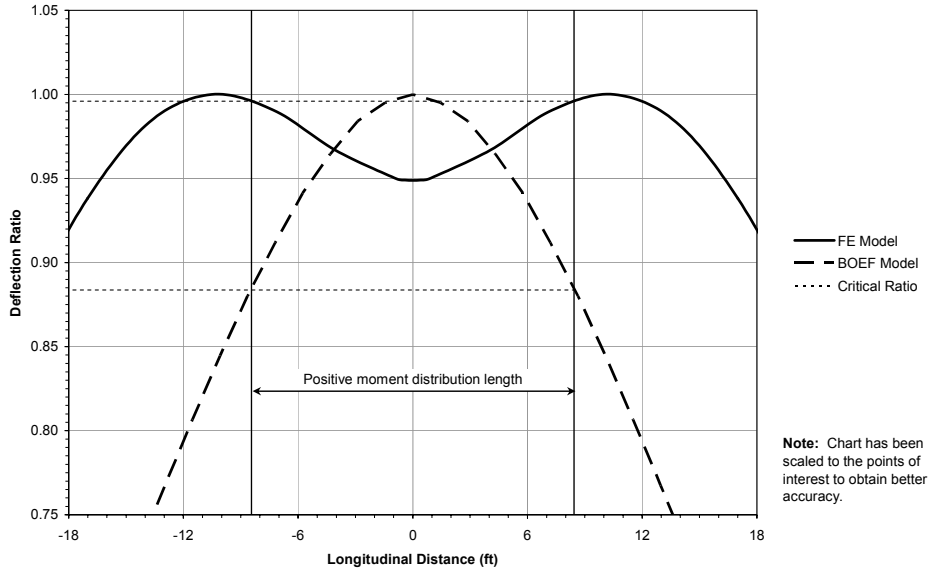

Figure D-1 – Deflection ratios for 24' span BOEF and FE models with one foot of fill

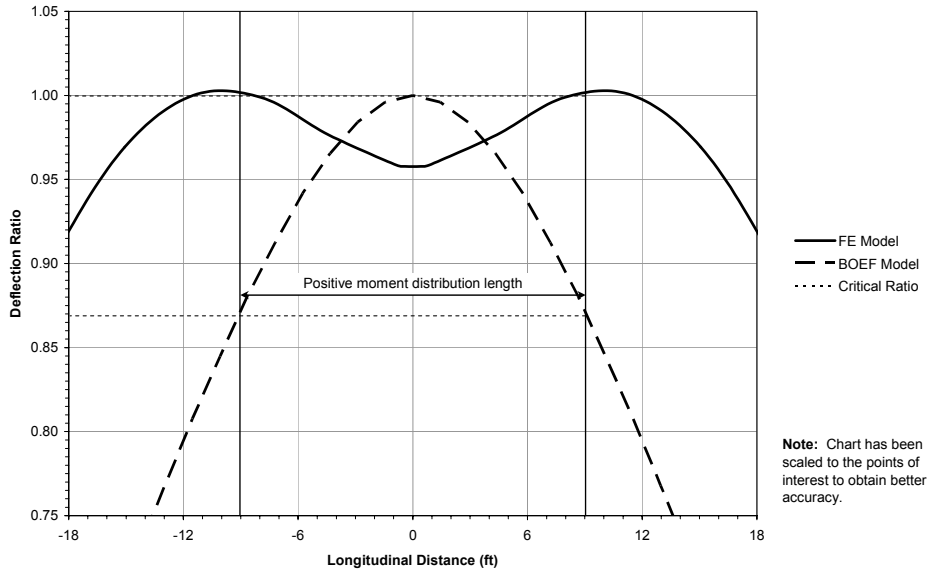

Figure D-2 – Deflection ratios for 24' span BOEF and FE models with two feet of fill

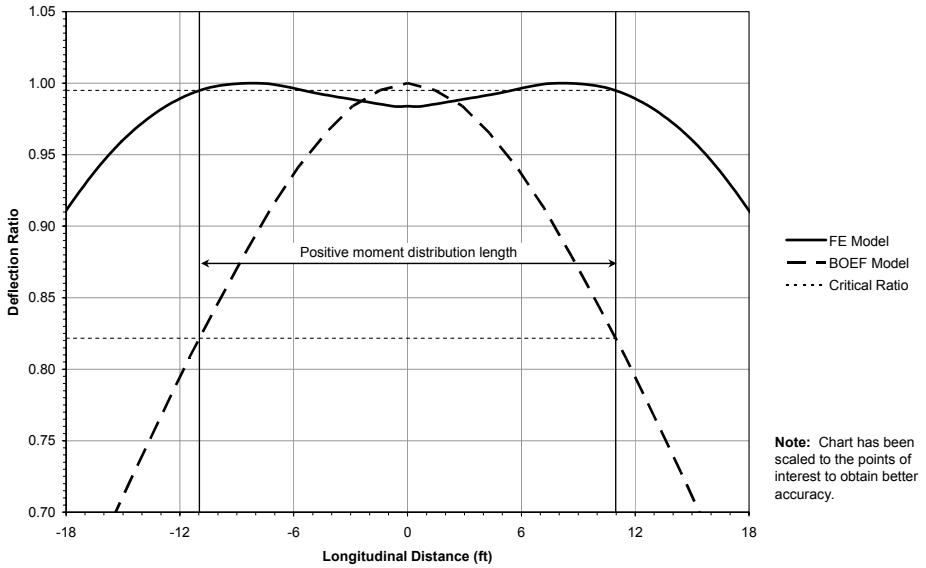

Figure D-3 – Deflection ratios for 24' span BOEF and FE models with five feet of fill

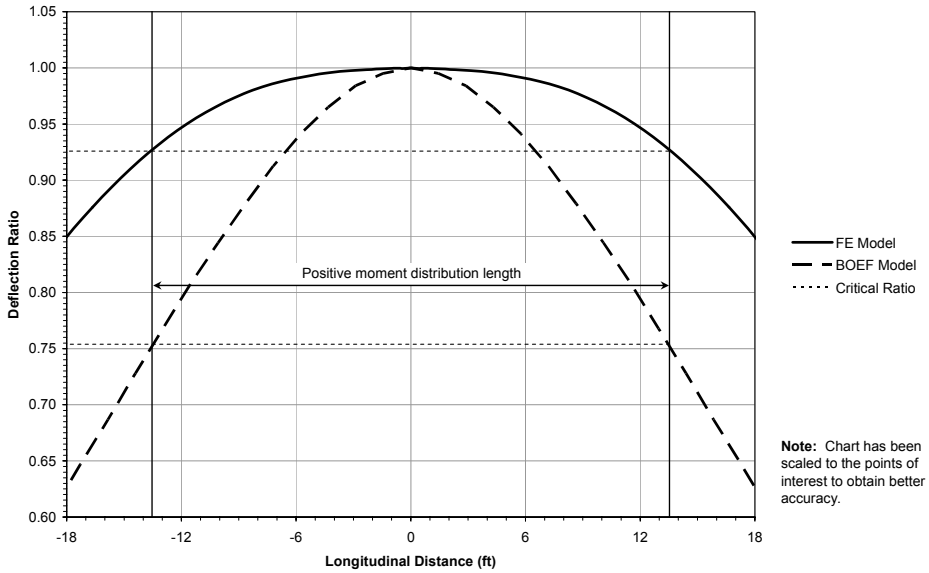

Figure D-4 – Deflection ratios for 24' span BOEF and FE models with ten feet of fill

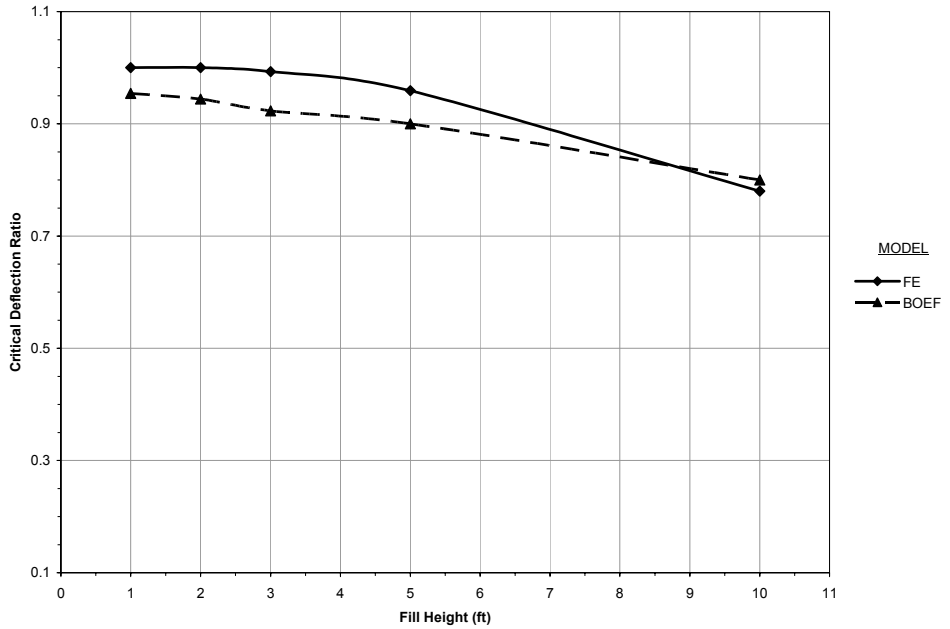

Figure D-5 – Critical deflection ratios for positive moment distribution lengths for 11' span BOEF and FE models as a function of fill height

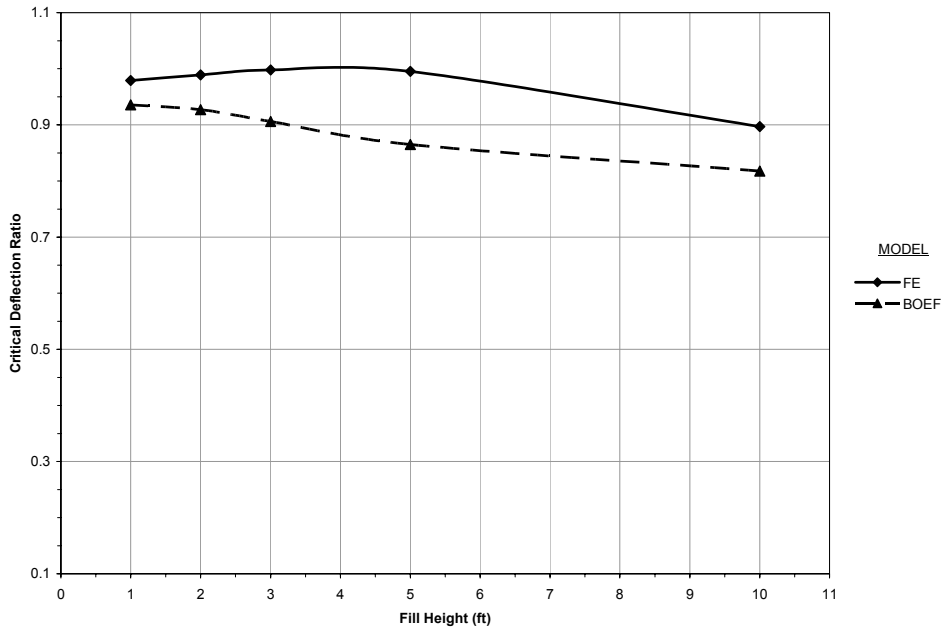

Figure D-6 – Critical deflection ratios for positive moment distribution lengths for 18' span BOEF and FE models as a function of fill height

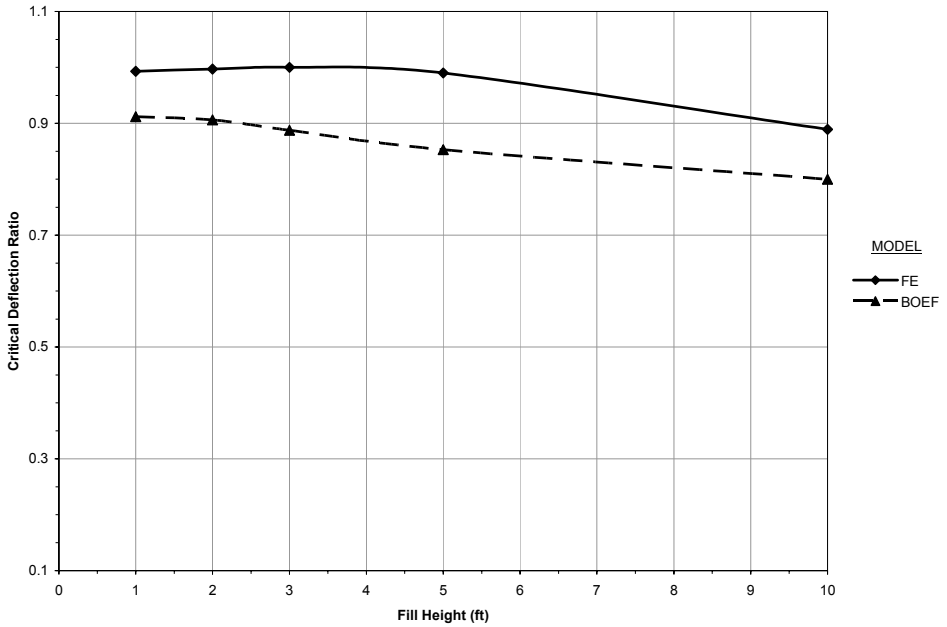

Figure D-7 – Critical deflection ratios for negative moment distribution lengths for 18' span BOEF and FE models as a function of fill height

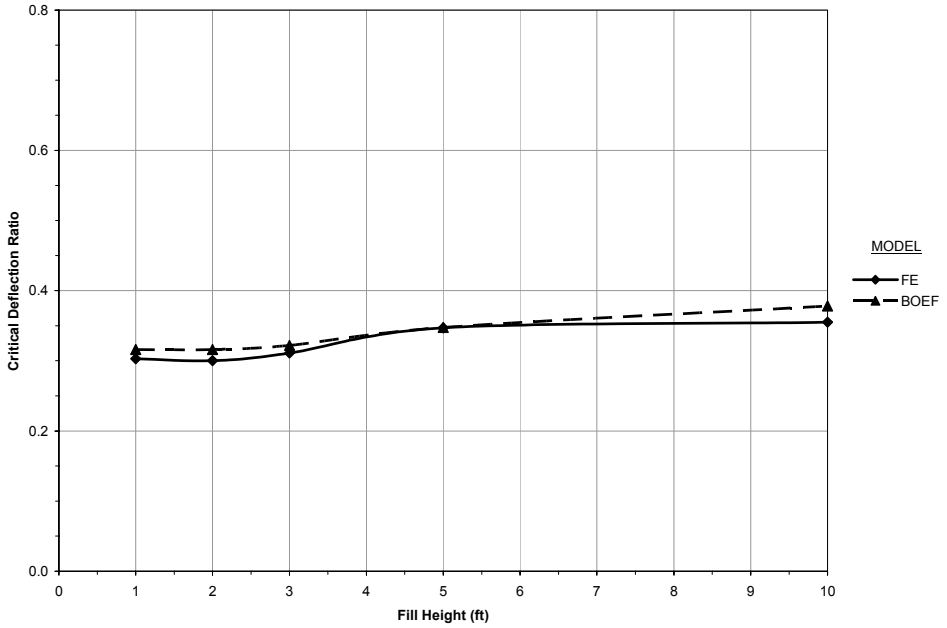

Figure D-8 – Critical deflection ratios for invert moment distribution lengths for 18' span BOEF and FE models as a function of fill height

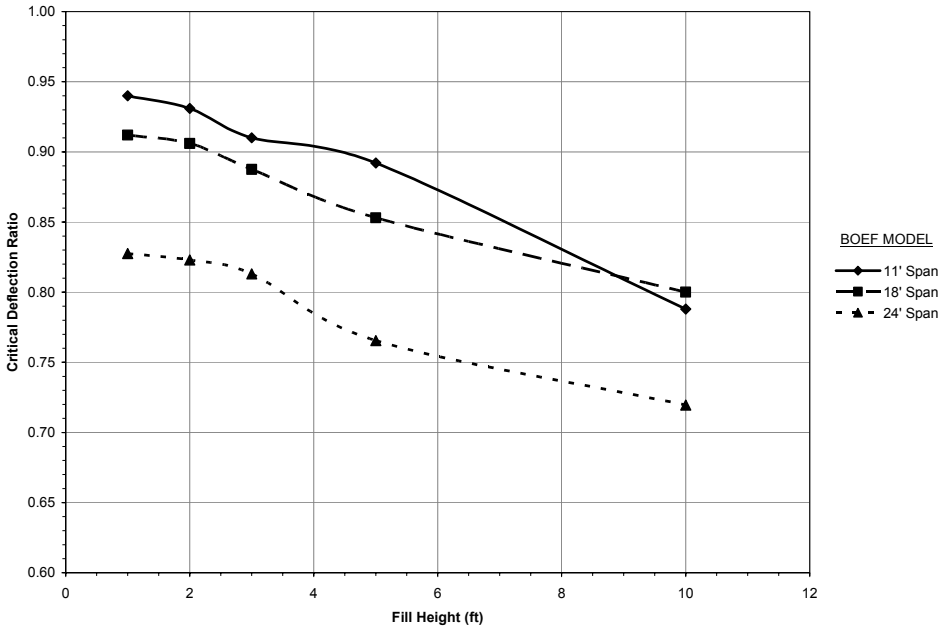

Figure D-9 – Critical deflection ratios for negative moment distribution lengths for BOEF models

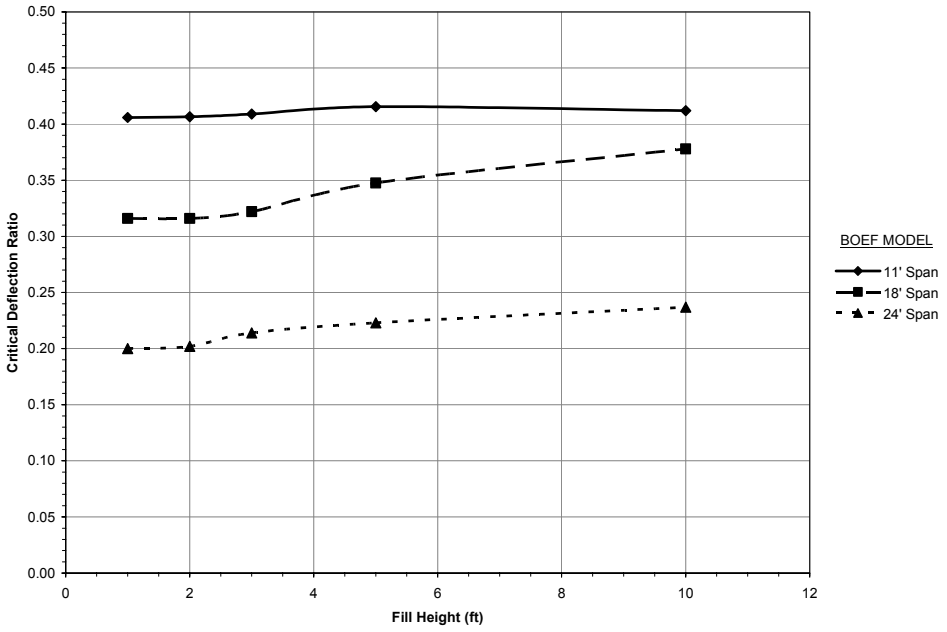

Figure D-10 – Critical deflection ratios for invert moment distribution lengths for BOEF models

Appendix E. Conservatism of Prediction Equations

The following appendix supplements Figure 5-22 and Figure 5-23.

Figure E-1 and Figure E-2 show the conservatism of the predicted distribution lengths for negative and invert moments as a function of fill height. The predictions have only about ten percent variation, and no bias. See also Figure 5-22.

Figure E-3 and Figure E-4 show the conservatism of the predicted distribution lengths for negative and invert moment as a function of span. From Figure E-3 it can be seen that there is a slight bias toward larger spans for prediction of distribution length for negative moment. Also, Figure E-4 shows that there is a slight bias toward smaller spans in the distribution length prediction equations for invert moment. See also Figure 5-23.

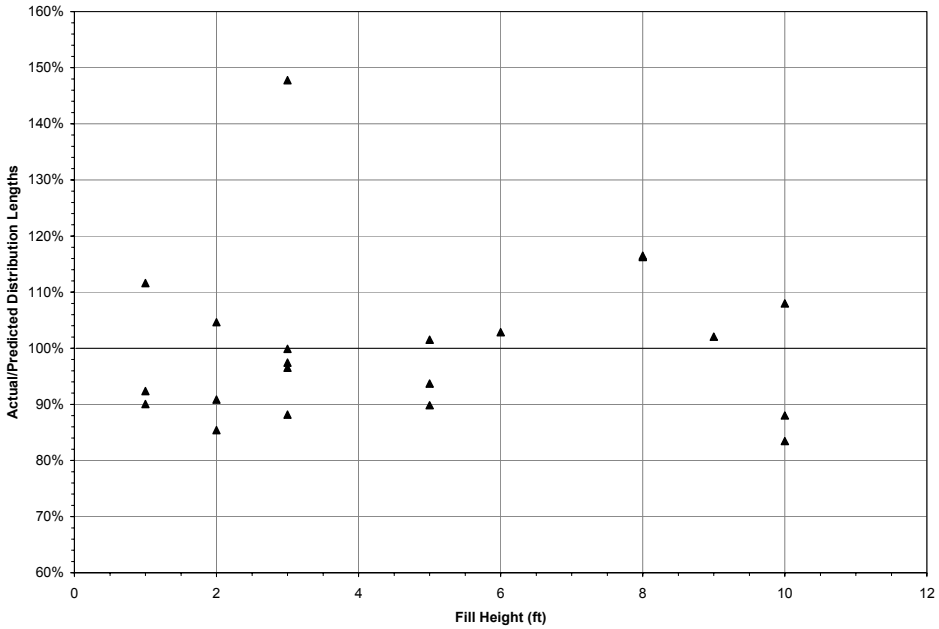

Figure E-1 – Conservatism of predicted to actual distribution length for negative moment as a function of fill height

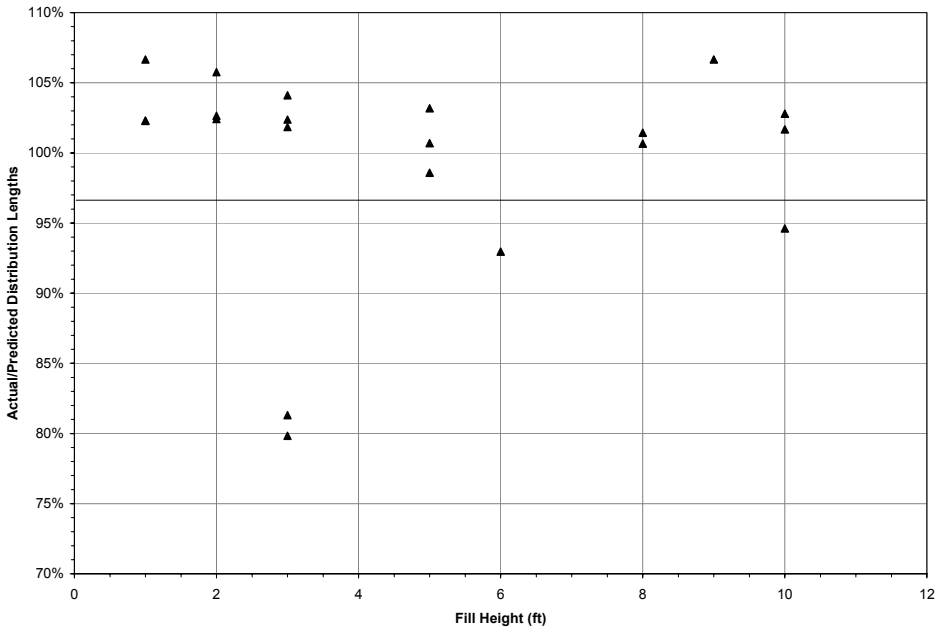

Figure E-2 – Conservatism of predicted to actual distribution length for invert moment as a function of fill height

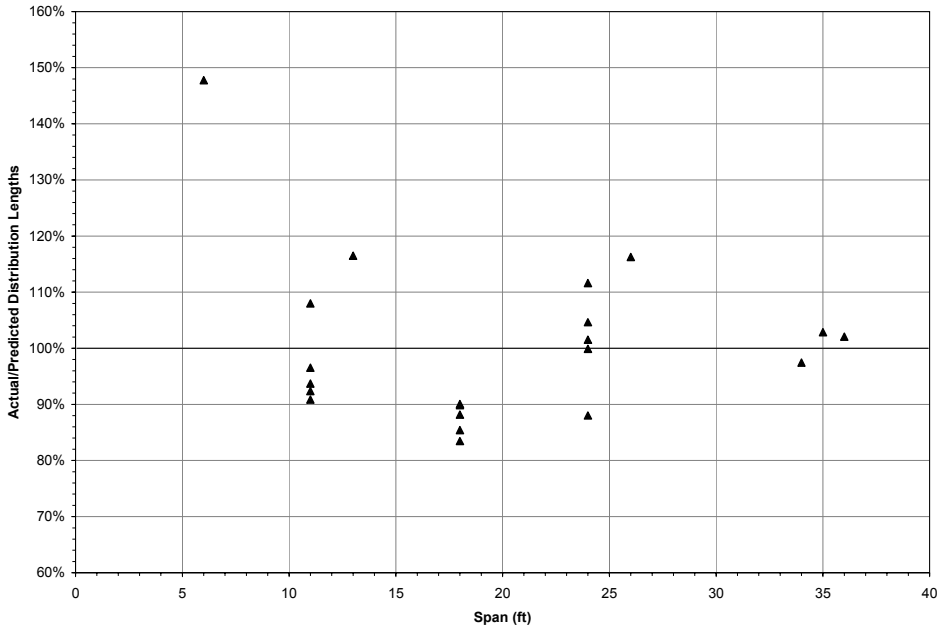

Figure E-3 – Conservatism of predicted to actual distribution length for negative moment as a function of span

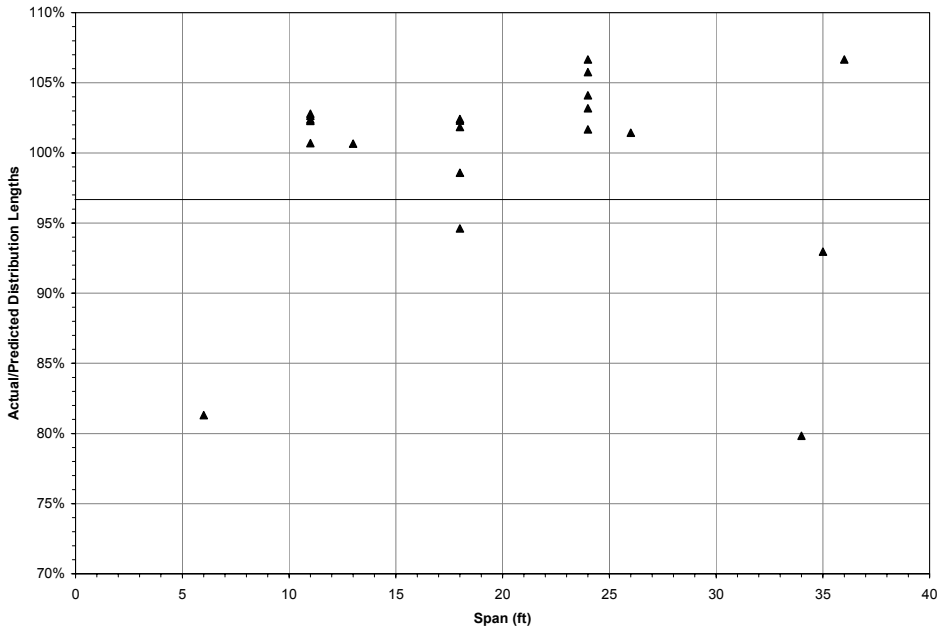

Figure E-4 – Conservatism of predicted to actual distribution length for invert moment as a function of span

Appendix F. Under-Prediction of Axial Forces

The following appendix supplements Figure 5-28.

Figure F-1 to Figure F-4 show that the predictions for axial force using the proposed method are generally less than or similar to those obtained by 3-D analysis under a discrete load. Such under-prediction results in slight design conservatism.

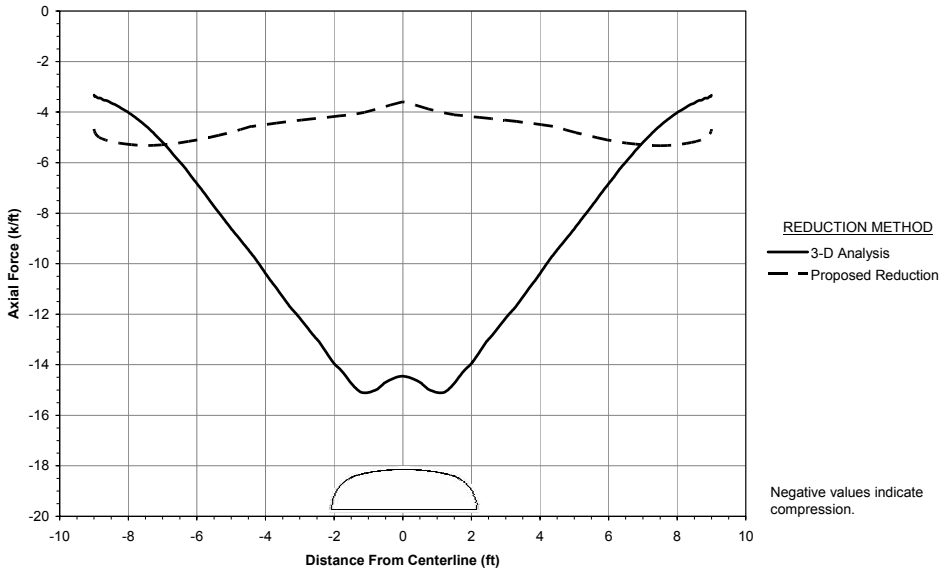

Figure F-1 – Axial force comparison for an 18' span arch ring with one foot of fill using proposed distribution length for positive moment and 3-D FE analysis

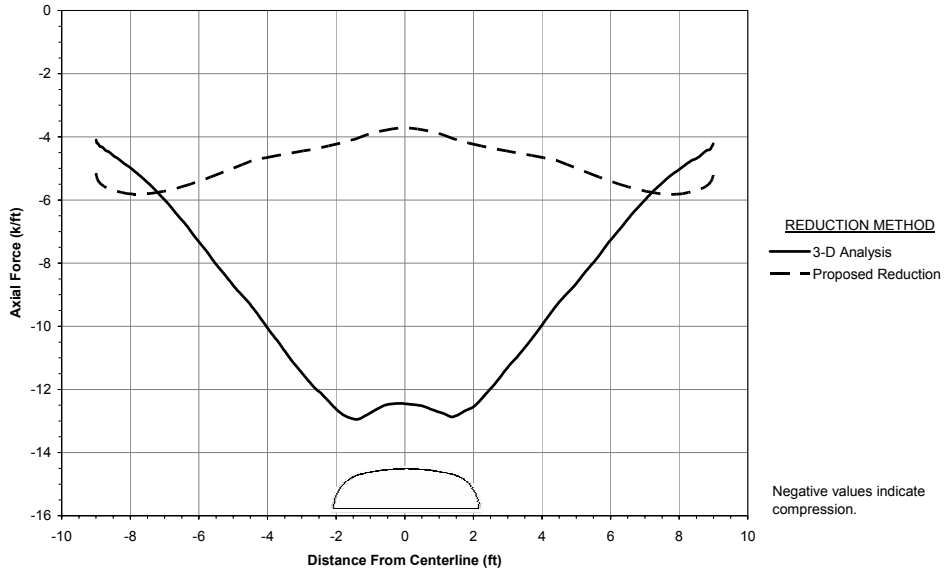

Figure F-2 – Axial force comparison for an 18' span arch ring with two feet of fill using proposed distribution length for positive moment and 3-D FE analysis

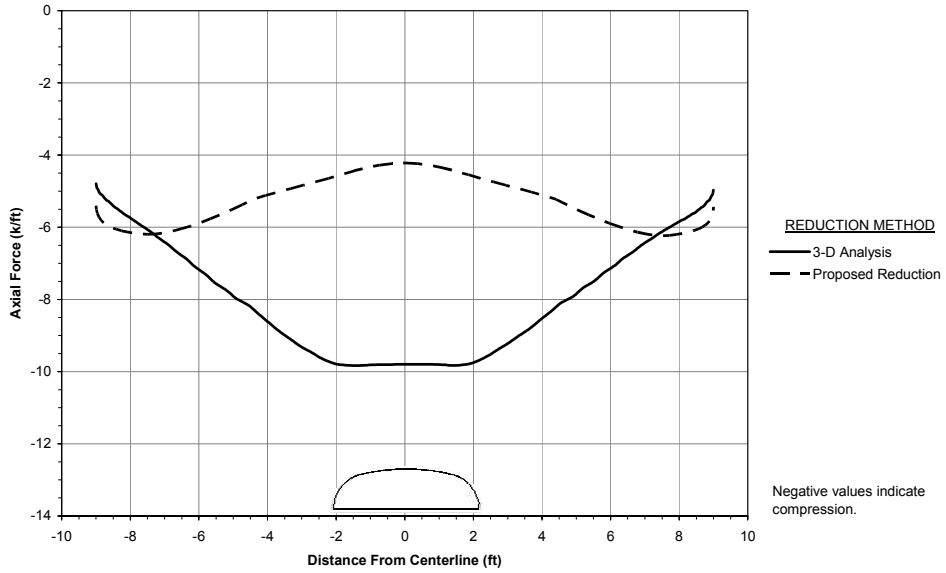

Figure F-3 – Axial force comparison for an 18' span arch ring with three feet of fill using proposed distribution length for positive moment and 3-D FE analysis

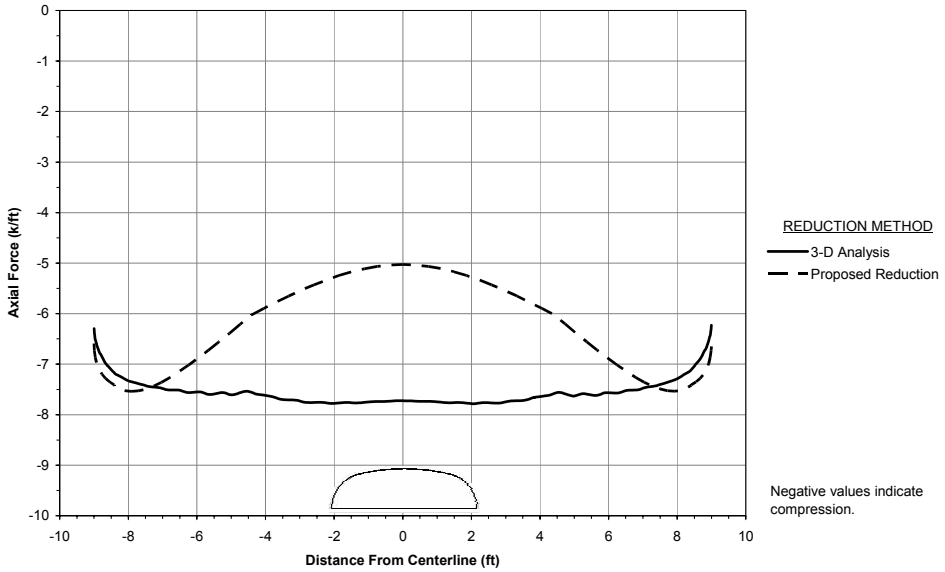

Figure F-4 – Axial force comparison for an 18' span arch ring with five feet of fill using proposed distribution length for positive moment and 3-D FE analysis

Appendix G. Design Examples Using Current and Proposed Methods

The following is a design example from Engineering System Solutions, for an 18' span arch culvert with one foot of fill cover. The arch has been designed once using current protocol ('96 AASHTO, Load Case 1) and again using the proposed design method (Load Case 2). Analysis was done using the finite element program I-DEAS. Table G-1 is a summary of the design requirements. Only the distribution length for positive moment was used to reduce the load in Load Case 2. Reinforcing could be further reduced in the invert by running the FE model a second time using the distribution length for invert moment to reduce the load. Total cost is calculated for concrete at $120.00 per cubic yard and #4 reinforcing at $0.34 per foot. The material savings for the proposed method are $18.00/*ft* (a 10% decrease). Labor savings would add substantially to this amount.

Table G-1 – Summary of design requirements using current and proposed methods

MEHTOD	ARCH RING		INVERT		Material Cost per foot
	Thickness (in)	Reinforcing	Thickness (in)	Reinforcing	
Current (Load Case 1)	8	Transverse #4 at 5" oc Longitudinal #4 at 12" oc	8	Transverse #4 at 8" oc Longitudinal #4 at 12" oc	Concrete $134.00 Rebar $52.50
Proposed (Load Case 2)	8	Transverse #4 at 12" oc Longitudinal #4 at 12" oc	8	Transverse #4 at 10" oc Longitudinal #4 at 12" oc	Concrete $134.00 Rebar $34.50

*The calculated costs do not include labor or splices of transverse or longitudinal reinforcing

AASHTO LOAD FACTOR DETERMINATION

LOAD COMBINATIONS - GROUPS 1 AND 10

* See tables and equations below for derivation. Reference AASHTO 3.22.

1.3*D + 2.17*(L + I)

1.3*D + 2.82 *L
1.3*D + 2.60 *L
1.3*D + 2.39 *L

Live Load Impact Factors, I (AASHTO 3.8.2.3)

for culvert with cover:

0" to 1'-0" I = 0.30*L
1'-1" to 2'-0" I = 0.20*L
2'-1" to 2'-11" I = 0.10*L
greater than 2'-11", no impact increase req'd.

$$\text{Group(N)} = \gamma [\beta_D*D + \beta_L(L + I) + \beta_{CF}*CF + \beta_E*E + \beta_B*B + \beta_{SF}*SF + \beta_W*W + \beta_{WL}*WL + \beta_{LF}*LF + \beta_R(R + S + T) + \beta_{EQ}*EQ + \beta_{ICE}*ICE]$$

where:

N = group number
γ = load factor
β = coefficients per table below
D = Dead Load
L = Live Load
I = Live Load Impact
E = Earth Pressure
B = Buoyancy
W = Wind Load on structure
WL = Wind Load on live load
LF = Longitudinal Force from live load
CF = Centrifugal Force
R = Rib Shortening
S = Shrinkage
T = Temperature
EQ = Earthquake
SF = Stream flow pressure
ICE= Ice pressure

Reference AASHTO Table 3.22.1A

GROUP	γ	β Factors											
		D	(L+ I)	CF	E	B	SF	W	WL	LF	R+S+T	EQ	ICE
1	1.3	1.0	1.67	1.0	1.0	1.0	1.0	0	0	0	0	0	0
10	1.3	1.0	1.67	0	1.0	0	0	0	0	0	0	0	0

Note: Since CF, B and SF forces equal zero for culverts, and E is accounted for in dead loads, the corresponding values equal zero and can be omitted. Groups 1 and 10 are equivalent.

Wheel Load Overlap Magnification

AASHTO 6.4.2

Unfactored Wheel Load (kips) : 16

Nodes distributed over : 2

Span (ft): 18

*Note the span is only used with 2' or less of fill

	Depth ft	Distrib Width ft.	Live Load Factor	Wheel Point Load, kips	Node Point Load, kips
NO OVERLAP	*1	5.1	2.82	8.88	4.44
	*2	5.1	2.6	8.19	4.09
	3	5.3	2.17	6.61	3.31
	3.5	6.1	2.17	5.67	2.83
OVERLAPPING PROJECTED AREAS	4	6.5	2.17	5.34	2.67
	5	7.4	2.17	4.71	2.35
	6	8.3	2.17	4.21	2.10
	7	9.1	2.17	3.80	1.90
	8	10.0	2.17	3.47	1.74
	9	10.9	2.17	3.19	1.60
	10	11.8	2.17	2.95	1.48
	11	12.6	2.17	2.75	1.38
	12	13.5	2.17	2.57	1.29
	13	14.4	2.17	2.42	1.21
	14	15.3	2.17	2.28	1.14
	15	16.1	2.17	2.15	1.08
	16	17.0	2.17	2.04	1.02
	17	17.9	2.17	1.94	0.97
	18	18.75	2.17	1.85	0.93

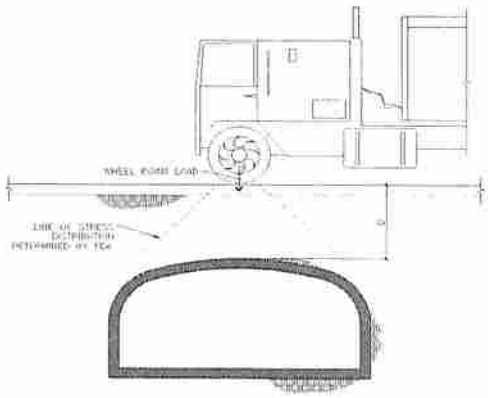

TRANSVERSE ARCH SECTION

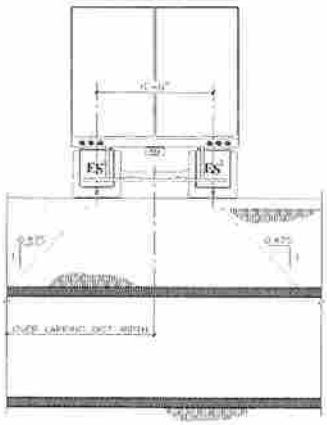

LONGITUDINAL ARCH SECTION (OUT-OF-PLANE TO FEA)

Wheel Load Overlap Magnification

Unfactored Wheel Load (kips) : 16 Span (ft): 18

Nodes distributed over : 2

	Depth ft	Distrib Width ft.	Live Load Factor	Wheel Point Load, kips	Node Point Load, kips
NO OVERLAP	*1	13.6	2.82	3.32	1.66
	*2	15.32	2.6	2.72	1.36
	3	16.89	2.17	2.06	1.03
	3.5	18.46	2.17	1.88	0.94
OVERLAPPING PROJECTED AREAS	4	20.01	2.17	1.74	0.87
	5	21.51	2.17	1.61	0.81
	6	22.95	2.17	1.51	0.76
	7	24.36	2.17	1.43	0.71
	8	25.74	2.17	1.35	0.67

DISTRIBUTION LENGTH CALCULATOR

DESCRIPTION: 18' MODEL - 1' COVER

BEAM DATA:

Width, W =	18.00	ft
Inertia, I =	935	ft^4
Modulus, E =	3605	ksi

SOIL DATA:

Modulus, E =	1100.00	ksi
Poisson's Ratio, μ =	0.33	
Subgrade, K =	1077	kcf

LOAD DATA:

Point Load, P =	34.72	k
Fill Height, H =	1.0	ft

DISTRIBUTION LENGTH:

+ Dist. Length, l^+ =	13.60	ft
- Dist. Length, l^- =	16.34	ft
Invert Dist. Length, l^I =	62.38	ft

Load Case #1: 1.3*DL + 2.17*LL*1.3(Impact)
18'x5'-9" with 1' of Cover Typical Live Load Analysis

The graphic below is a finite element mesh representing a 1-ft slice of the specified structure in the previously listed load case table. The scale of the elements is approximately 1ft square. Properties for the elements are as listed in the basis for design. Traffic live load locations are shown and their magnitude is noted previously under the load case table. Boundary conditions are represented by the following: Single arrow translation restraint, Double arrow rotation restraint, Triple arrow translation and rotation restraint.

Three critical design forces for this load case are shown in following calculation pages.

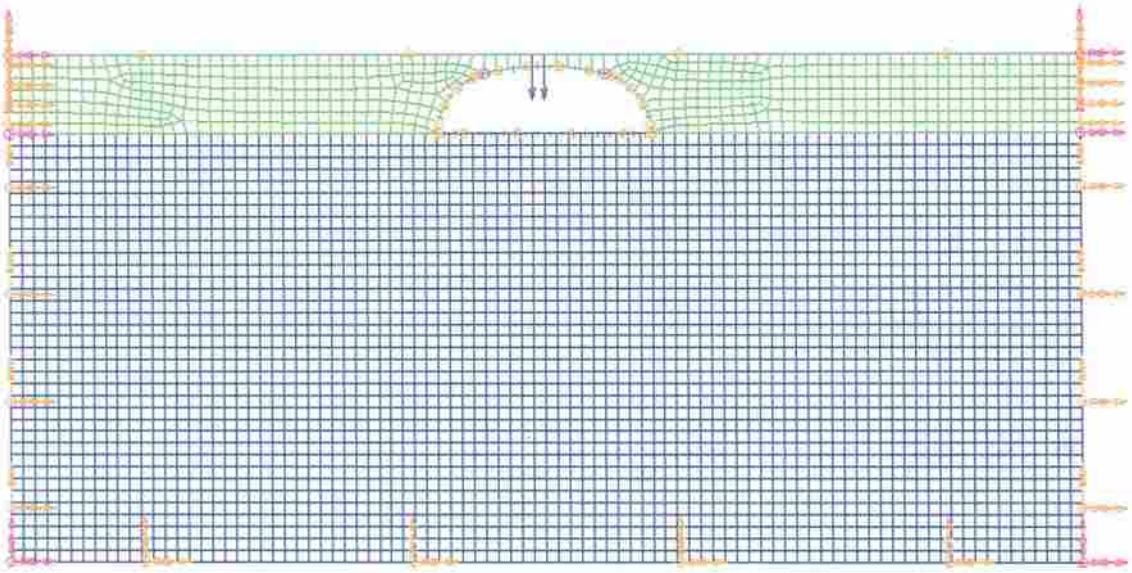

Bending Moments

Moments at critical design locations are penciled in. Reinforcing requirement calculations are shown following the load cases. The maximum moment for the given diagram is listed as part of the I-deas output and the moment diagram is to scale.

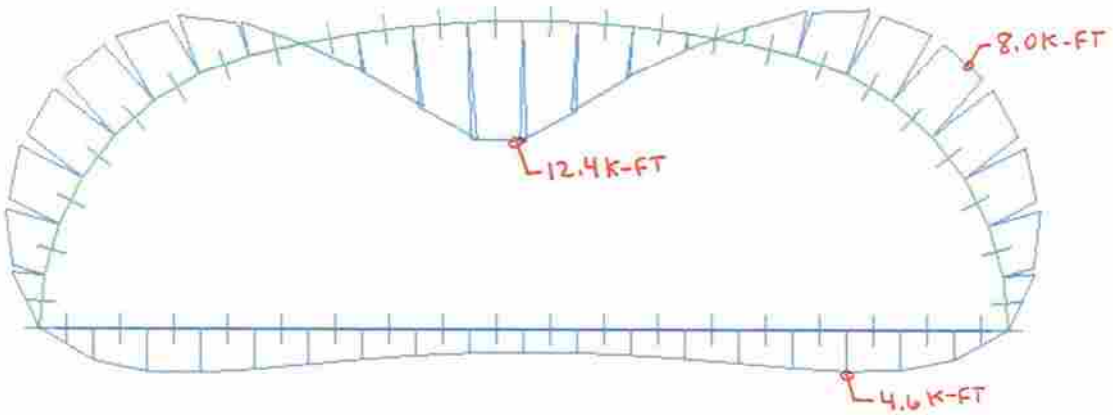

Shear

Shear forces at critical design locations are penciled in. Shear capacity calculations are shown following the load cases. The maximum shear for the given diagram is listed as part of the I-deas output and the shear diagram is to scale.

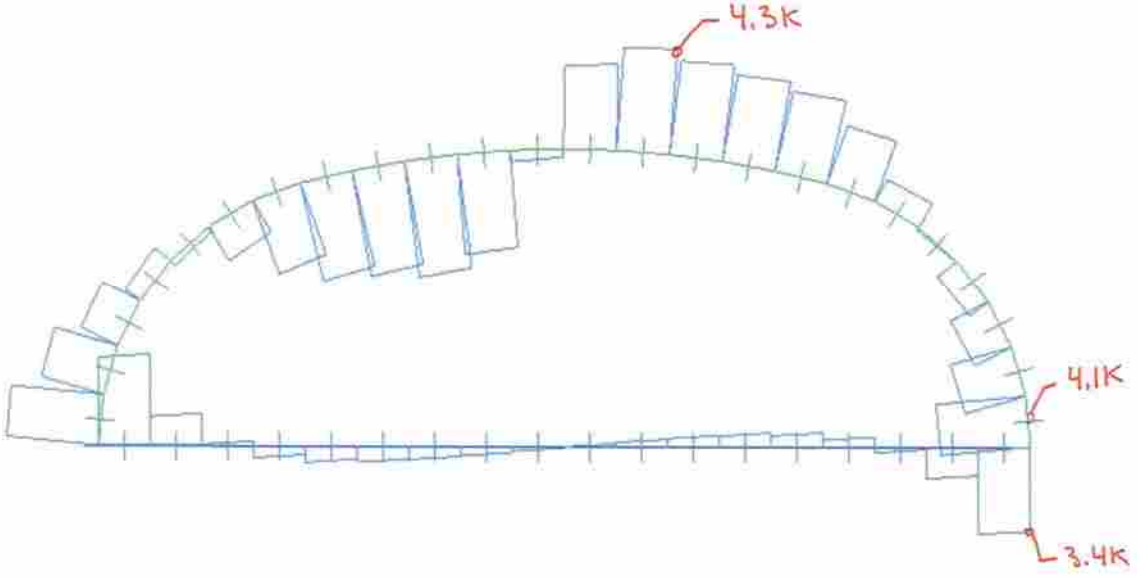

Axial Force

Axial forces at critical design locations are penciled in. The maximum axial force for the given diagram is listed as part of the I-deas output and the axial force diagram is to scale.

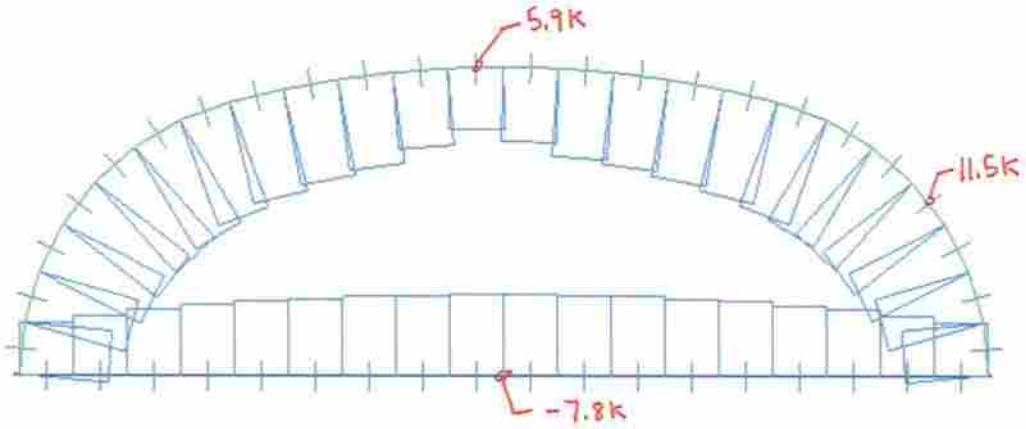

FINITE ELEMENT ANALYSIS RESULTS SUMMARY

LOAD CASE	ARCH GEOMETRY	COVER	SECTION FORCE LOCATION	*Pu (KIPS)	Mu (K-FT)	Vu (KIPS)
1	18' x 5'-9" CROWN	1'-0"	CROWN	5.9	12.4	4.3
			HAUNCH	11.5	8.0	4.1
			INVERT	-7.8	4.6	3.4

*NOTE: Pu IS SHOWN AS COMPRESSION BEING POSITIVE AND TENSION BEING NEGATIVE

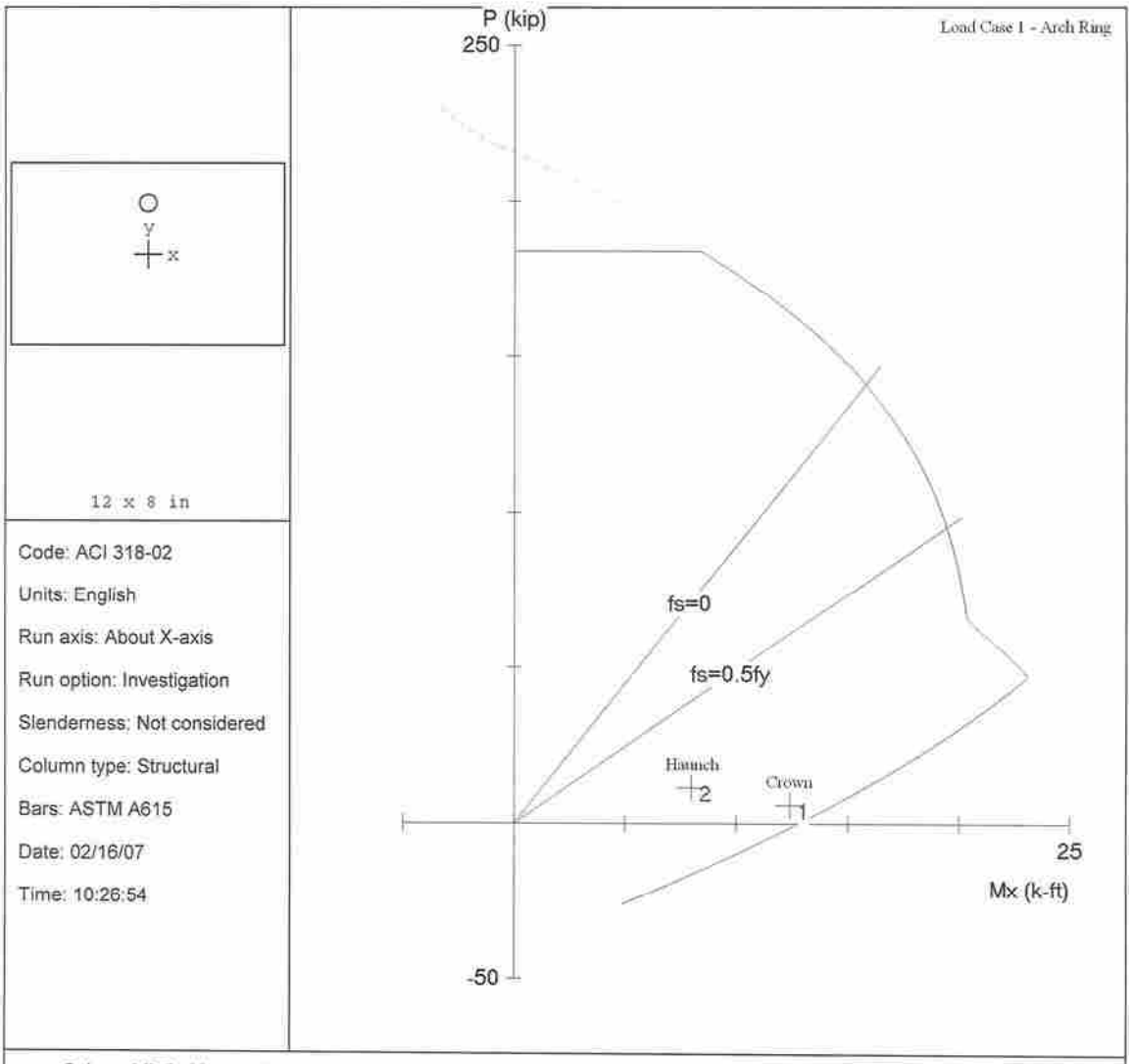

pcaColumn V3.5 - Licensed to: Es2

File: K:\Data2005\05318_PLAXISandCAnDe\Calculations\18x5ft9_arch w 1ft.col

Project: Thesis

Column: 18'x5'9"Arch		Engineer: jw	
f'c = 4 ksi	fy = 60 ksi	Ag = 96 in^2	1 bars
Ec = 3605 ksi	Es = 29000 ksi	As = 0.48 in^2 (#4 @ 5" oc)	Rho = 0.50%
fc = 3.4 ksi	e_rup = Infinity	Xo = 0.00 in	Ix = 512 in^4
e_u = 0.003 in/in		Yo = 0.00 in	Iy = 1152 in^4
Beta1 = 0.85		Clear spacing = 1.86 in	Clear cover = 1.36 in
Confinement: Tied	phi(a) = 0.8, phi(b) = 0.9, phi(c) = 0.65		

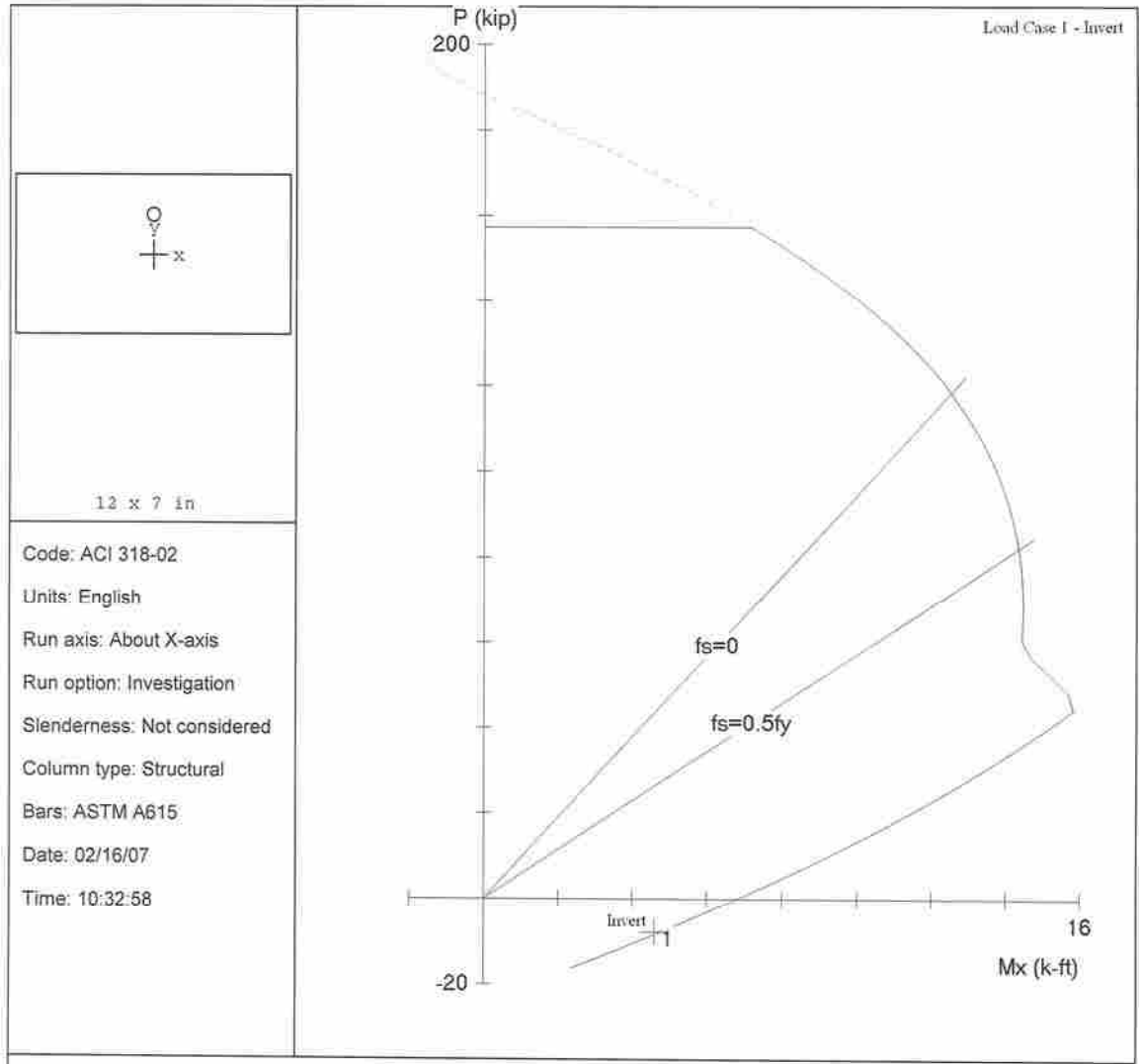

pcaColumn V3.5 - Licensed to: Es2

File: K:\Data2005\05318_PLAXISandCAnDe\Calculations\18x5ft9_Invert w 1ft.col

Project: Thesis

Column: 18'x5'9"Arch		Engineer: jw	
f'c = 4 ksi	fy = 60 ksi	Ag = 84 in^2	1 #5 bars
Ec = 3605 ksi	Es = 29000 ksi	As = 0.30 in^2 (#4 @ 8" oc)	Rho = 0.36%
fc = 3.4 ksi	e_rup = Infinity	Xo = 0.00 in	Ix = 343 in^4
e_u = 0.003 in/in		Yo = 0.00 in	Iy = 1008 in^4
Beta1 = 0.85		Clear spacing = 1.44 in	Clear cover = 1.44 in
Confinement: Tied	phi(a) = 0.8, phi(b) = 0.9, phi(c) = 0.65		

BUCKLING CALCULATION OF OPEN CYLINDER (ARCH)

ARCH ID : 18x5.75

f'c :	4000	psi		
E :	3,604,997	psi		
Span :	18	ft		
R :	20	ft		
t :	8	in		
L :	500	ft		
v :	0.3			
L/R :	25.00			
p :	6679898.8	psf	(Eq. 4 below)	2628.15
p :	5.3	psf	(Eq. 6 below)	
Soil unit wt :	120	pcf		

span to thickness ratio : **27** O.K.

Allowable External Pressure, p :	5282 psf	
Max allowed soil cover :	*44 ft.*	(Check against design cover depths)

Equation for allowable External Pressure from Concrete Shell Buckling,
ACI Publication SP-67, 1981, pp.49.

(The following text and figure was taken from the above referenced ACI publication.)

External Pressure

The effect of initial imperfections on the critical external pressure of cylindrical shells has been shown to be much less than for uniform axial compression (10). This theoretical result has been verified experimentally since the difference between theory and experiment are not so drastic as for axial compression. The theoretical critical pressure for moderately long simply supported cylinders is

$$p = \frac{\sqrt{6}\,\pi}{9(1-\nu^2)^{\frac{3}{4}}} \frac{E}{\frac{L}{R}\left(\frac{R}{t}\right)^{\frac{5}{2}}}$$

$$\approx \frac{0.92E}{\frac{L}{R}\left(\frac{R}{t}\right)^{\frac{5}{2}}} \qquad (\nu = 0.3) \qquad (4)$$

The correction factor by which the right side of Eq. (3) is multiplied is recommended in (42) as

$$C = 0.75 \qquad (5)$$

for all values of R/t. For long cylinders which buckle into an oval shape ($L/R > 3.35\sqrt{R/t}$) the critical pressure is given by

$$p = \frac{1}{4(1-\nu^2)} E \left(\frac{t}{R}\right)^3$$

$$= 0.27\, E \left(\frac{t}{R}\right)^3 \qquad (\nu = 0.3) \qquad (6)$$

with a recommended correction factor of 0.90. A comparison of the recommended design curve and experimental results for moderate length cylinders is shown in Fig. 8.

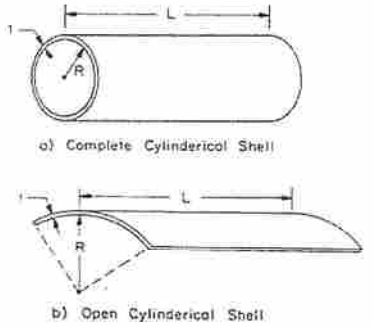

FIG. 1 CIRCULAR CYLINDRICAL SHELLS

Shear Capacity

18' SPAN ARCH

Arch

d =	6.25	d of section (in)
b =	12	1 foot effective width
fc =	4000	Concrete strength (psi)
Vc =	$\frac{(0.85 * 2\sqrt{fc})*b*d}{1000}$	ACI 11.12.3.1
Vc =	8.06	Concrete shear strength (kips) must be greater than values listed in shear diagrams in load cases.

Invert

d =	5.25	d of section (in)
b =	12	1 foot effective width
fc =	4000	Concrete strength (psi)
Vc =	$\frac{(0.85 * 2\sqrt{fc})*b*d}{1000}$	ACI 11.12.3.1
Vc =	6.77	Concrete shear strength (kips) must be greater than values listed in shear diagrams in load cases.

DISTRIBUTION OF FLEXURAL REINFORCEMENT

Load Case #1

AASHTO 8.16.8.4 and Caltrans 8.16.8.4

Applied Service Moment	$M := 9.4kip \cdot ft$
Applied Service Axial Force	$P := 4.5kip$
Member Thicknes	$t := 8in$
Concrete Compressive Strength	$f'_c := 4ksi$
Rebar Size	$Bar := 4$
Clear Cover	$clr := 1.5in$
spacing	$s := 5in$
Steel Yield Strength	$f_y := 60ksi$
Maximum Allowable Steel Stress	$f_s = 34.6\,ksi$
Maximum Service Steel Stress	$F_s = 36\,ksi$
Factor of Safety	$F = 1.04$

control = "Steel Stress OK"

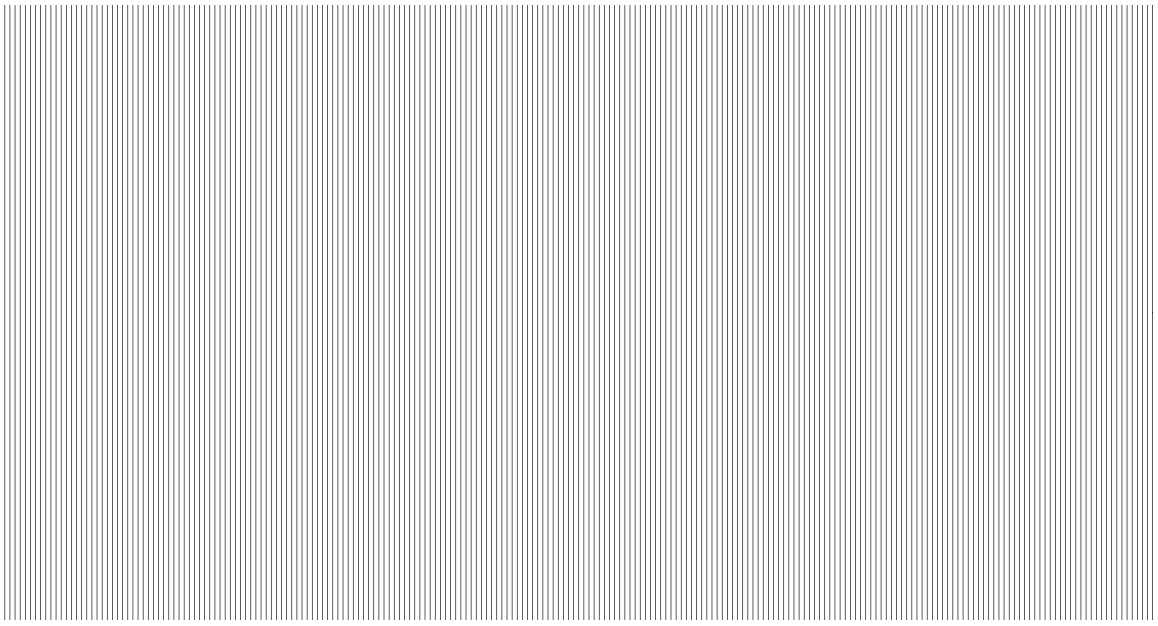

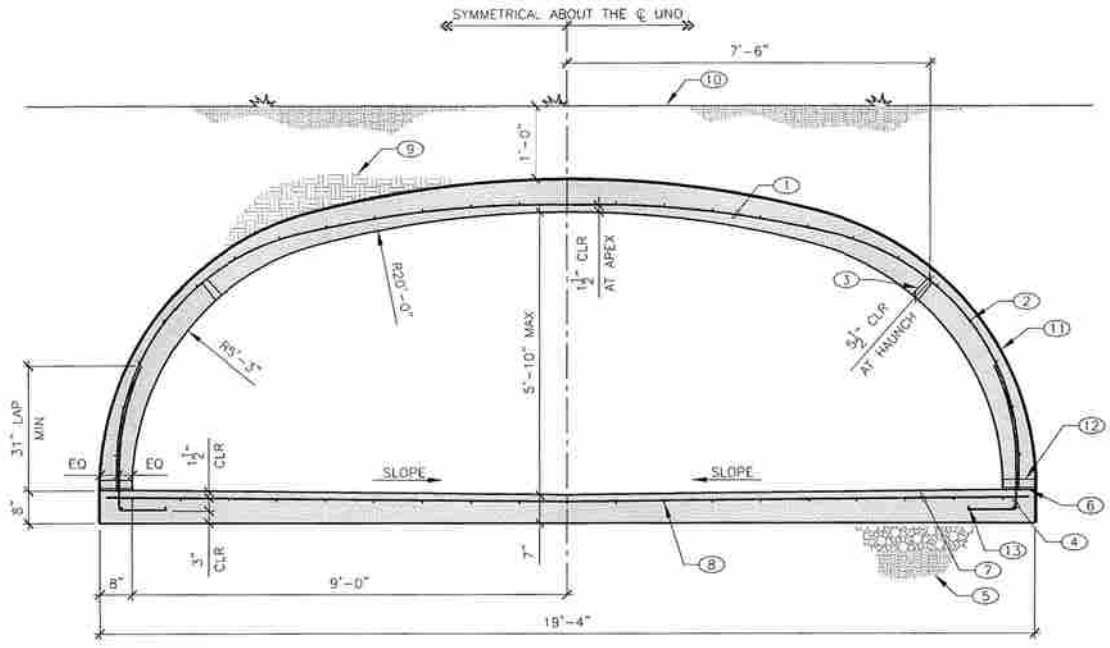

KEYNOTES:

1. #4 AT 5" O.C. TRANSVERSE
2. #4 LONGITUDINAL AT 12" O.C. LAP 18" MIN
3. REBAR CHAIR POINT
4. #4 DOWEL AT 5" O.C. W/ 12" HOOK AT BASE
5. BEDDING PER GSN
6. ROUGHEN CONSTRUCTION JOINT, PER GSN
7. #4 TRANSVERSE AT 8" O.C.
8. #4 LONGITUDINAL AT 12" O.C. LAP 18" MIN
9. BACKFILL PER GSN
10. FINAL GRADE
11. WATER PROOF MEMBRANE COVER ARCH AND WALL ONLY
12. 2"ø WEEP HOLE PER PLAN
13. (2) #4 CONT LONGITUDINAL LAP 18" MIN

1 TYPICAL CULVERT SECTION
NO SCALE

Load Case #2: 1.3*DL + 2.17*LL*1.3(Impact)
18'x5'-9" with 1' of Cover Typical Live Load Analysis

The graphic below is a finite element mesh representing a 1-ft slice of the specified structure in the previously listed load case table. The scale of the elements is approximately 1ft square. Properties for the elements are as listed in the basis for design. Traffic live load locations are shown and their magnitude is noted previously under the load case table. Boundary conditions are represented by the following: Single arrow translation restraint, Double arrow rotation restraint, Triple arrow translation and rotation restraint.

Three critical design forces for this load case are shown in following calculation pages.

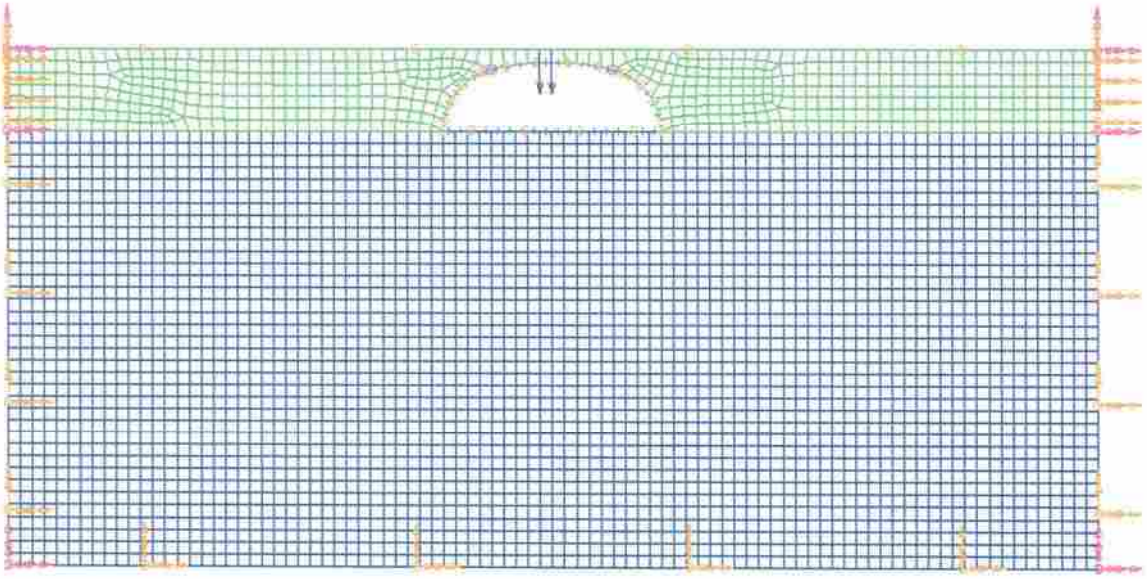

Bending Moments

Moments at critical design locations are penciled in. Reinforcing requirement calculations are shown following the load cases. The maximum moment for the given diagram is listed as part of the I-deas output and the moment diagram is to scale.

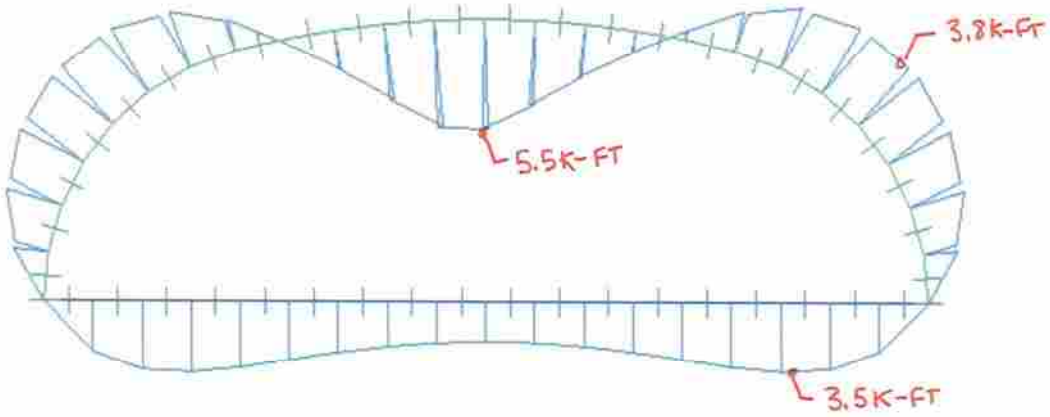

Shear

Shear forces at critical design locations are penciled in. Shear capacity calculations are shown following the load cases. The maximum shear for the given diagram is listed as part of the I-deas output and the shear diagram is to scale.

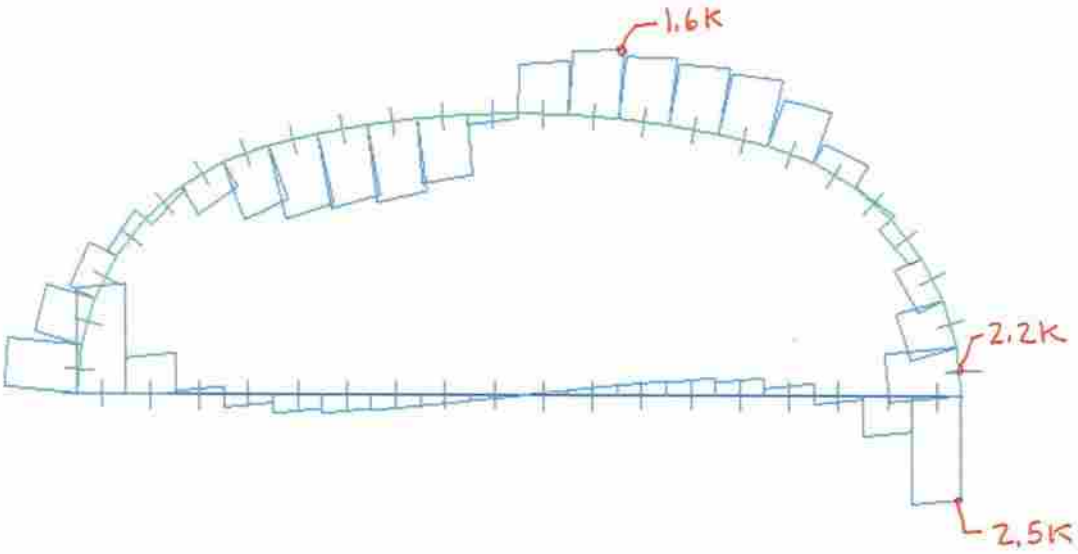

Axial Force

Axial forces at critical design locations are penciled in. The maximum axial force for the given diagram is listed as part of the I-deas output and the axial force diagram is to scale.

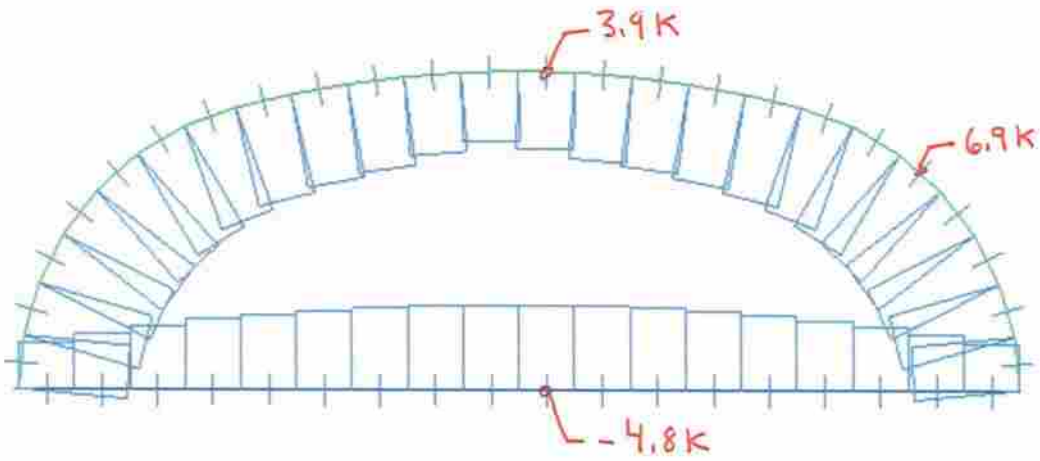

FINITE ELEMENT ANALYSIS RESULTS SUMMARY

LOAD CASE	ARCH GEOMETRY	COVER	SECTION FORCE LOCATION	*Pu (KIPS)	Mu (K-FT)	Vu (KIPS)
2	18' x 5'-9" CROWN	1'-0"	CROWN	3.9	5.5	1.6
			HAUNCH	6.9	3.8	2.2
			INVERT	-4.8	3.5	2.5

*NOTE: Pu IS SHOWN AS COMPRESSION BEING POSITIVE AND TENSION BEING NEGATIVE

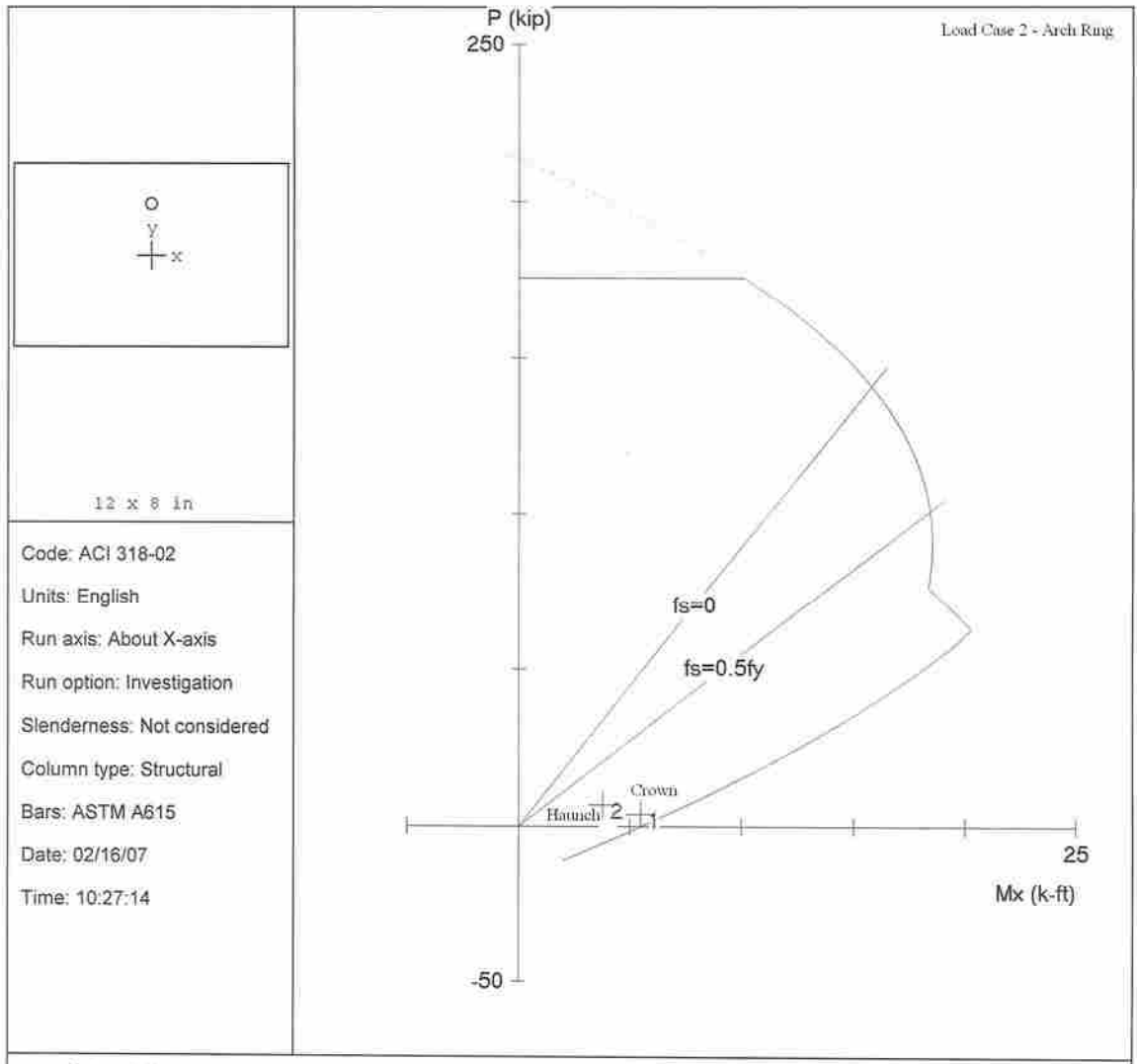

Code: ACI 318-02

Units: English

Run axis: About X-axis

Run option: Investigation

Slenderness: Not considered

Column type: Structural

Bars: ASTM A615

Date: 02/16/07

Time: 10:27:14

pcaColumn V3.5 - Licensed to: Es2

File: K:\Data2005\05318_PLAXISandCAnDe\Calculations\18x5ft9_arch w 1ft Revised.col

Project: Thesis

Column: 18'x5'9"Arch		Engineer: jw	
f'c = 4 ksi	fy = 60 ksi	Ag = 96 in^2	1 #4 bars
Ec = 3605 ksi	Es = 29000 ksi	As = 0.20 in^2 (#4 @ 12" oc)	Rho = 0.21%
fc = 3.4 ksi	e_rup = Infinity	Xo = 0.00 in	Ix = 512 in^4
e_u = 0.003 in/in		Yo = 0.00 in	Iy = 1152 in^4
Beta1 = 0.85		Clear spacing = 2.00 in	Clear cover = 1.50 in
Confinement: Tied	phi(a) = 0.8, phi(b) = 0.9, phi(c) = 0.65		

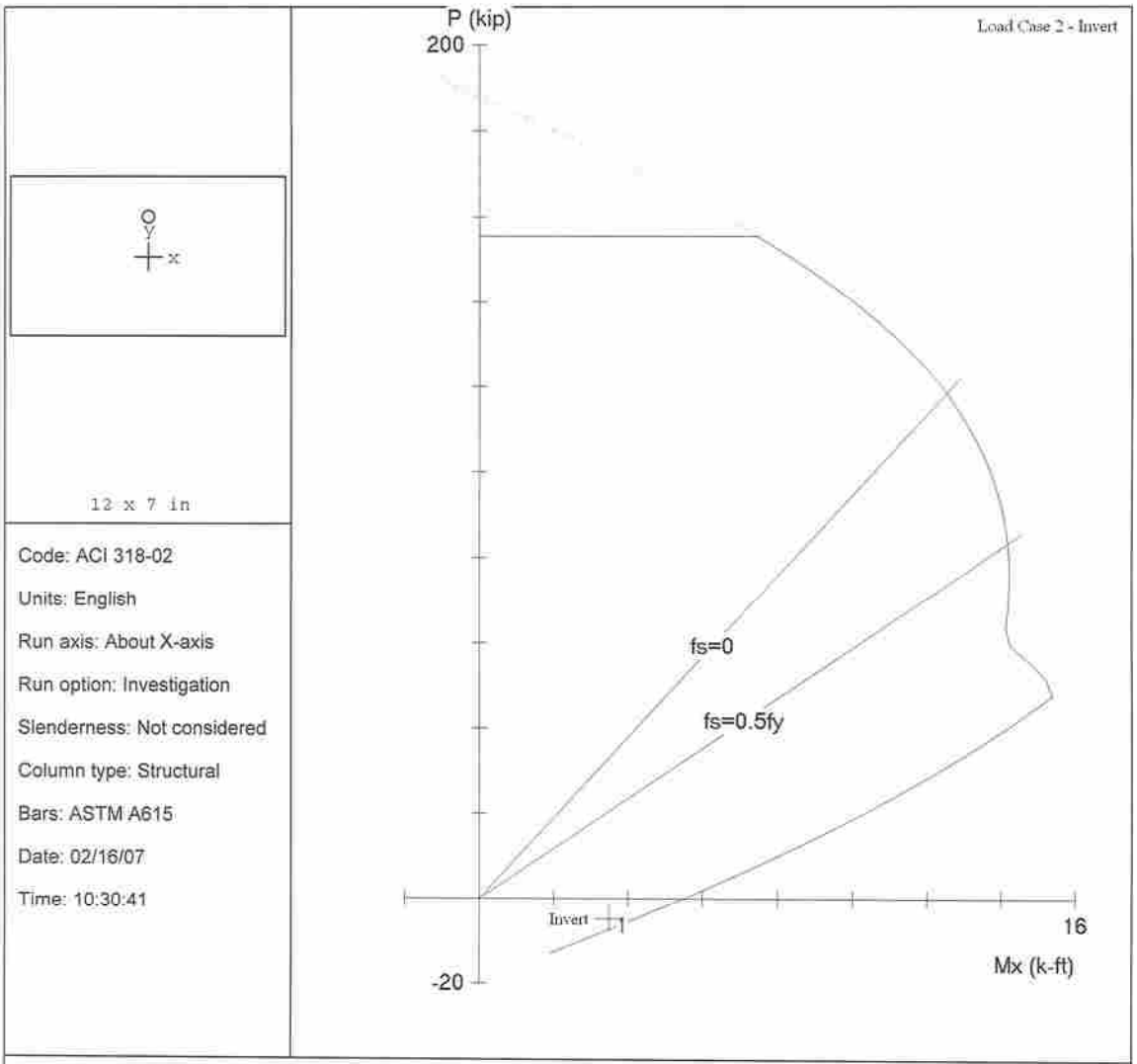

pcaColumn V3.5 - Licensed to: Es2

File: K:\Data2005\05318_PLAXISandCAnDe\Calculations\18x5ft9_Invert w 1ft Revised.col

Project: Thesis

Column: 18'x5'9"Arch		Engineer: jw	
f'c = 4 ksi	fy = 60 ksi	Ag = 84 in^2	1 bars
Ec = 3605 ksi	Es = 29000 ksi	As = 0.24 in^2 (#4 @ 10" oc)	Rho = 0.29%
fc = 3.4 ksi	e_rup = Infinity	Xo = 0.00 in	Ix = 343 in^4
e_u = 0.003 in/in		Yo = 0.00 in	Iy = 1008 in^4
Beta1 = 0.85		Clear spacing = 1.47 in	Clear cover = 1.47 in
Confinement: Tied	phi(a) = 0.8, phi(b) = 0.9, phi(c) = 0.65		

BUCKLING CALCULATION OF OPEN CYLINDER (ARCH)

ARCH ID : 18x5.75

f'c :	4000	psi		
E :	3,604,997	psi		
Span :	18	ft		
R :	20	ft		
t :	8	in		
L :	500	ft		
v :	0.3			
L/R :	25.00			
p :	6679898.8	psf	(Eq. 4 below)	2628.15
p :	5.3	psf	(Eq. 6 below)	
Soil unit wt :	120	pcf		

span to thickness ratio : **27** O.K.

Allowable External Pressure, p :	5282 psf
Max allowed soil cover :	*44 ft.* (Check against design cover depths)

Equation for allowable External Pressure from Concrete Shell Buckling,
ACI Publication SP-67, 1981, pp.49.

(The following text and figure was taken from the above referenced ACI publication.)

External Pressure

The effect of initial imperfections on the critical external pressure of cylindrical shells has been shown to be much less than for uniform axial compression (10). This theoretical result has been verified experimentally since the difference between theory and experiment are not so drastic as for axial compression. The theoretical critical pressure for moderately long simply supported cylinders is

$$p = \frac{\sqrt{6}\,\pi}{9(1-\nu^2)^{\frac{3}{4}}} \frac{E}{\frac{L}{R}\left(\frac{R}{t}\right)^{\frac{5}{2}}}$$

$$\simeq \frac{0.92E}{\frac{L}{R}\left(\frac{R}{t}\right)^{\frac{5}{2}}} \qquad (\nu = 0.3) \qquad (4)$$

The correction factor by which the right side of Eq. (3) is multiplied is recommended in (42) as

$$C = 0.75 \qquad (5)$$

for all values of R/t. For long cylinders which buckle into an oval shape ($L/R > 3.35\sqrt{R/t}$) the critical pressure is given by

$$p = \frac{1}{4(1-\nu^2)} E \left(\frac{t}{R}\right)^3$$

$$= 0.27\, E \left(\frac{t}{R}\right)^3 \qquad (\nu = 0.3) \qquad (6)$$

with a recommended correction factor of 0.90. A comparison of the recommended design curve and experimental results for moderate length cylinders is shown in Fig. 8.

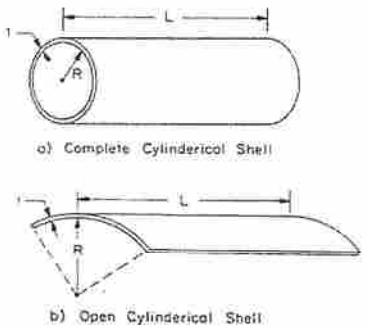

FIG. 1 CIRCULAR CYLINDRICAL SHELLS

Shear Capacity

18' SPAN ARCH

Arch

d =	6.25	d of section (in)
b =	12	1 foot effective width
fc =	4000	Concrete strength (psi)
Vc =	$\frac{(0.85 * 2\sqrt{fc})*b*d}{1000}$	ACI 11.12.3.1
Vc =	8.06	Concrete shear strength (kips) must be greater than values listed in shear diagrams in load cases.

Invert

d =	5.25	d of section (in)
b =	12	1 foot effective width
fc =	4000	Concrete strength (psi)
Vc =	$\frac{(0.85 * 2\sqrt{fc})*b*d}{1000}$	ACI 11.12.3.1
Vc =	6.77	Concrete shear strength (kips) must be greater than values listed in shear diagrams in load cases.

DISTRIBUTION OF FLEXURAL REINFORCEMENT

Load Case #2

AASHTO 8.16.8.4 and Caltrans 8.16.8.4

Applied Service Moment	$M := 9.4kip \cdot ft$
Applied Service Axial Force	$P := 4.5kip$
Member Thicknes	$t := 8in$
Concrete Compressive Strength	$f'_c := 4ksi$
Rebar Size	$Bar := 4$
Clear Cover	$clr := 1.5in$
spacing	$s := 5in$
Steel Yield Strength	$f_y := 60ksi$
Maximum Allowable Steel Stress	$f_s = 34.6\,ksi$
Maximum Service Steel Stress	$F_s = 36\,ksi$
Factor of Safety	$F = 1.04$

control = "Steel Stress OK"

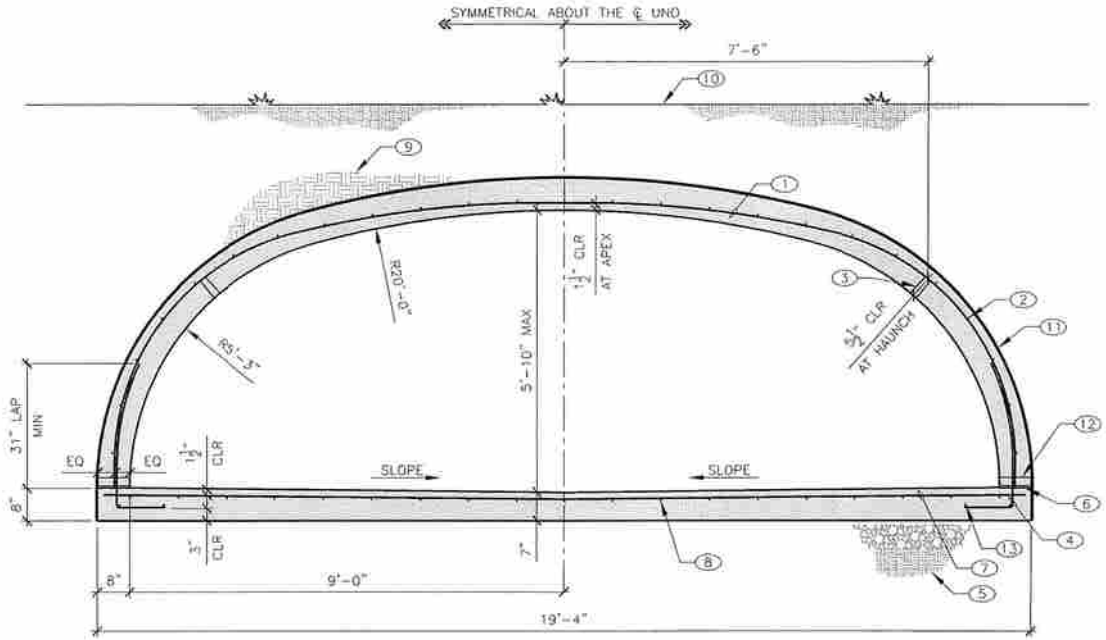

KEYNOTES:

1. #4 AT 12" O.C. TRANSVERSE
2. #4 LONGITUDINAL AT 12" O.C. LAP 18" MIN
3. REBAR CHAIR POINT
4. #4 DOWEL AT 12" O.C. W/ 12" HOOK AT BASE
5. BEDDING PER GSN
6. ROUGHEN CONSTRUCTION JOINT, PER GSN
7. #4 TRANSVERSE AT 10" O.C.
8. #4 LONGITUDINAL AT 12" O.C. LAP 18" MIN
9. BACKFILL PER GSN
10. FINAL GRADE
11. WATER PROOF MEMBRANE COVER ARCH AND WALL ONLY
12. 2"ø WEEP HOLE PER PLAN
13. (2) #4 CONT LONGITUDINAL LAP 18" MIN

2 REVISED CULVERT SECTION
NO SCALE